CO-GASIFICATION OF LOW-GRADE COAL AND BIOMASS IN A PRESSURIZED CIRCULATING FLUIDIZED BED GASIFIER

A Thesis

Submitted in Partial Fulfillment of the Requirements

for the Award of the Degree of

DOCTOR OF PHILOSOPHY

By

ABINASH MAHAPATRO

DEPARTMENT OF MECHANICAL ENGINEERING
INDIAN INSTITUTE OF TECHNOLOGY GUWAHATI
DECEMBER 2019

Dedicated to my grand parents

Late. Sobhabati Mahapatra,

Late. Sarat Chandra Mahapatra

and my dearest cousin, Late. Ansu

.

DECLARATION

I hereby certify that the work compiled in this dissertation is the outcome of the research work, performed by myself, else stated, under the guidance of **Prof. Pinakeswar Mahanta.**

Any part of this work has not been submitted for the award of any degree, diploma, associate-fellowship, fellowship or its equivalent to any university or institution.

Date: 23-12-2019

Abinash Mahapatro
Registration No. 146103025
Department of Mechanical Engineering
Indian Institute of Technology Guwahati

Department of Mechanical Engineering
Indian Institute of Technology Guwahati
Guwahati-781039
INDIA

Certificate

It is certified that the work contained in the thesis entitled **"Co-gasification of Low-grade Coal and Biomass in a Pressurized Circulating Fluidized Bed Gasifier"** submitted by **Mr. Abinash Mahapatro**, to the Indian Institute of Technology Guwahati for the award of the degree of Doctor of Philosophy has been carried out under my supervision in the Department of Mechanical Engineering, Indian Institute of Technology Guwahati. This work has not been submitted elsewhere for the award of any other degree or diploma.

Date: 23-12-2019

Prof. Pinakeswar Mahanta
Professor
Department of Mechanical Engineering
Indian Institute of Technology Guwahati
Guwahati-781039, India

ACKNOWLEDGEMENT

At first, I would like to express my heartfelt gratitude to my supervisor, Prof. Pinakeswar Mahanta, who have relentlessly supported me during the course of my research work with motivation, encouragement and colossal knowledge. His guidance has shaped my basic understanding in this domain up to a greater extent. Without his keen interest and help, I would not have been able to put forth the best foot forward during the current research work. I am also deeply obligated to the Director of Indian Institute of Technology Guwahati for providing such pleasing circumstances for the inception of my research career.

Besides my supervisor, I would like to acknowledge the doctoral committee members, Prof. Ujjwal K. Saha, Prof. Vinayak Kulkarni and Prof. Vimal Katiyar, for their valuable recommendations and insightful remarks throughout the course of research activities, which has constantly engaged me towards undertaking a meaningful thesis work. I would also like to thank Prof. Santosha Kumar Dwivedy, Head, Department of Mechanical Engineering , IIT Guwahati and also my Administrative Supervisor for his encouragement and support throughout the period of research. I also thank all the faculty members and staff of the department of Mechanical Engineering for their continued support during various issues like material procurement and others for my research.

Further, special appreciation for the senior technician and support staff of the Department of Mechanical Engineering and Central Workshop IIT Guwahati for their valuable help namely, Mr. N.K Das, Mr. Dilip Chetri and Mr. Nip Borah.

I would deeply thank all my fellow lab-mates in fluidized bed group: Dr. Mallick, Dr. Saikia, Mr. Hirakh, Mr. Plabon, Mr. Pavitra, Mr. Alok and, Mr. Dhananjay, Mr. Rishiraj for all the enriching and valuable discussions and sleepless nights we had to work together. Without this group, my journey perhaps would have been of less fun. I would like to thanks from bottom of my heart to Hotta & family, Soumya & family, Lula bhai & family, Saibal, Anil, Chita, Ankan, Binayak for their companion and for being a part of my small family making me feel like a home away from home. The journey would not have been so smooth without their whole hearted support during my tough times.

I would like to gratefully acknowledge Prof. Y. Itaya, Gifu University Japan for selecting me as a participant in the 2nd winter school at Department of Mechanical Engineering, Gifu University during December 03-23, 2016. I would also like to acknowledge Dr. P. Kalita, Prof. D. N. Thatoi, Prof. H. C. Das, Dr. S. S. Mohapatra, Dr. J. R. Pati, Dr. R. S. Patil, Dr. Shelke, Dr. Mishra for their guidance and support in my student life.

I would also like to thank all the cleaning staff of the hostel as well as Fluidized bed lab, staff of the mess of Brahmaputra hostel for providing day to day need during my stay at IIT Guwahati.

I would like to express my sincere thanks to Anita madam for her continuous support and encouragement, without her guidance the journey would not have been possible. I would also like to express my gratitude to Babai, Golide, Ting-Tong. Last but not the least; I owe my profound gratitude towards my parents Mr. Akshay kumar Mahapatro (Baba), Mrs. Sanjubala Mahapatro (Bou), Rajendra Kumar Mahapatro (Sana Mamu), Sana Main, Fukun, Leezu, Tiku, and Sonu for being the constant guiding, and supporting force throughout.

Abinash Mahapatro

ABSTRACT

Power generation and consumption is a major yardstick to determine the development of a nation. Spurred by the energy crisis and environmental pollution, researchers have paid attention to the use of alternative sources of energy for sustainable power production worldwide. In the present context, coal shares the maximum percentage as a primary source of energy for power generation in the world. Major share in power generation in India and China are reported to be obtained from coal. According to IEA 2019 report, China derives 72% of electricity from the combustion of coal, whereas the same is reported to be 58% in India. Similarly, Japan and USA have derived electricity by utilizing 32% and 40% of coal, respectively. To enhance the economic growth, there is a need to increase the energy utilization, where a substantial amount of energy is obtained from the secondary energy resources such as energy derived from biomass and other renewable energy sources. Biomass with 14% of the global share is stored in the unhygienic condition in a tropical country like India. In this context, the gasification process is one of the promising alternatives, that can be efficiently used for the production of cleaner energy. Fluidized bed gasification is one such technology for power generation that can be made assessable to a large section of the population even in rural and remote areas of our country. Pressurized circulation fluidized bed (PCFB) gasification is an advanced form of atmospheric circulating fluidized bed (ACFB) technology that has certain advantages like compactness and higher bed to wall heat transfer rate. However, this technology requires further study to thoroughly understand the complexities of flow behaviour and heat transfer during gasification process specially when used with various biomass blends and composite fuels. In the present work, the effect of various operating parameters such as bed inventory, particle size, superficial velocity, blends of coal with sawdust (percentage by weight) and operating pressure on bed hydrodynamics, i.e., bed voidage, suspension density, and solid circulation rate are studied experimentally in a PCFB gasifier. Further, an attempt is made to investigate the gasification process in a PCFB gasifier considering coal and locally available biomasses such as sawdust and rice husk and sugarcane bagasse as a feed material. A PCFB unit with a riser of 3 m height and 0.1 m inner diameter is fabricated for the investigation where the operating pressure is in the range of 1-4 bar.

Maximum decrement of 8.2% in bed voidage is observed as operating pressure varies from atmospheric to 4 bar. Further, the suspension density is found to increase with an increase in inventory weight. Peak increment of 28.3% in suspension density is perceived with an increase in inventory weights at a pressure of 4 bar. It is observed that the concentration of CH_4 increases with pressure for all the three feed materials. The concentration of CH_4 is found to be increasing from (3.65 to 4.86 vol%) and (2.98 to 3.46 vol%) for sawdust and rice husk, respectively. Similarly, the LHV is found to be increasing with pressure for coal and sawdust. There is a significant increase of 12% in LHV with an increase in pressure from 1 to 4 bar for both coal and sawdust. The CGE is found to increase by 34, 51, and 61% for rice husk, coal and sawdust, respectively with the increase in pressure from 1 to 4 bar.

Contents

Nomenclature

Notations

A_b	Cross sectional area of the bed/riser, (m^2)
A_D	Cross sectional area of the downcomer, (m^2)
A_d	Cross sectional area of the downcomer, (m^2)
A_R	Cross sectional area of the riser, (m^2)
C_D	Drag coefficient
C_{pg}	Specific heat capacity of gas
D_{ij}	Rate of strain tensor for solid phase
d_p	Particle size, (μm)
$D\overrightarrow{v_g}/Dt$	Substantial time derivative for gas velocity
$D\overrightarrow{v_s}/Dt$	Substantial time derivative for solids velocity
e_{ss}	Particle–particle restitution coefficient
$\overrightarrow{F_{dg}}$	Drag forces for gas phase
$\overrightarrow{F_{d,s}}$	Drag forces for solid phase
$\overrightarrow{F_{l,g}}$	Lift force for gas phase
$\overrightarrow{F_{l,s}}$	Lift force for solid phase
$\overrightarrow{F_{vm,g}}$	Virtual masses for gas phase
$\overrightarrow{F_{vm,s}}$	Virtual masses for solid phase
G_s	Solid circulation rate, (kg/m^3s)
g	Acceleration due to gravity, (m/s^2)
$g_{o,ss}$	Solid radial distribution function
ΔH	Difference of height in manometric fluid measured, (cm of water column)
Δh	Difference in pressure readings between two consecutive pressure tapping, (bar)
$h_{avg,pen}$	Average heat transfer coefficient according to penetration theory, (W/m^2- K)
h_s	Static bed height, (cm)
h_{sg}	Interphase heat transfer coefficient, (W/m^2- K)
I	Inventory, (kg)
I_{2D}	Second invariant of the deviatory stress tensor
k_g	Thermal conductivity of gas, (W/m-K)
k_g^{eff}	Effective thermal conductivity of gas, (W/m-K)
k_s	Thermal conductivity of solids, (W/m-K)
k_s^{eff}	Effective thermal conductivity of solids, (W/m-K)
L_a	Solid accumulation height in the downcomer, (m)
L_m	Distance between two consecutive pressure tappings, (m)

Nu_s	Solid-phase Nusselt number
P, Pr	Pressure, (pa, bar)
Pr	Prandtl number
P_{fr}	Frictional pressure, (Pa)
P_g	Gas-phase pressure, (Pa)
∇P_g	Gas-phase momentum equation
P_s	Solid-phase pressure, (Pa)
ΔP	Pressure drop, (Pa)
∇P_s	Solids phase momentum equation
Q_{sg}	Heat transfer between gas and solid phases, (J)
q	Heat flux, (W/m^2)
Re_s	Solid Reynold number
$\overline{S_s}$	Solid-phase source term
T_b	Bed temperature, (K)
T_g	Temperature of gas, (K)
T_s	Temperature of solids, (K)
T_w	Wall temperature, (K)
t	Time required for solid accumulation height of L_a after closing the ball valve,(s)
U_g	Velocity of gas, (m/s)
U_{sup}	Superficial velocity, (m/s)
v	Velocity vector
$\overrightarrow{v_g}$	Local velocity of the gas phase
$v_{r,s}$	Relative velocity of solid particles
$\vec{v}_s$	Local velocity of the solid phase
$v_s'^2$	Mean square velocity of particles
W	Weight of bed inventory, (g)
Y	Dry gas yield, (kg/Nm^3)

Greek symbol

β_{gs}	Drag coefficient between the gas and solid phase
ε	Bed voidage
ε_g	Voidage of gas
ε_{mf}	Bed voidage at minimum fluidization
ε_s	Volume fraction of the solid phase
$\varepsilon_{s,cr}$	Critical solid volume fraction
$\varepsilon_{s,max}$	Maximum solid volume fraction
ρ_s	Density of solid phase, (kg/m^3)
ρ_g	Density of gas phase, (kg/m^3)
ρ_{sus}	Suspension density, (kg/m^3)
ϕ	Angle of internal friction
ϕ_s	Sphericity of solid particle

μ_g	Viscosity of gas, (Pa-s)
μ_s	Solid viscosity, (Pa-s)
$\overline{\overline{\tau}}_g$	Gas-phase stress tensor
$\overline{\overline{\tau}}_s$	Solid-phase stress tensor
k_{Θ_s}	Diffusion coefficient
$k_{\Theta_s} \nabla \Theta_s$	The transport of energy due to diffusion
Θ_s	Granular temperature
γ_{Θ_s}	Dissipation of energy due to collision
γ_w	Collisional dissipation at the wall

Abbreviations

2D	Two-Dimensional
3D	Three-Dimensional
ACFB	Atmospheric Circulating Fluidized Bed
AFR	Air fuel ratio
B & W	Babcock and Wilcox
BFB	Bubbling Fluidized Bed
BHEL	Bharat Heavy Electricals Limited
Bt	Billion ton
BT	Bed temperature
CCE	Carbon Conversion Efficiency
CFB	Circulating Fluidized Bed
CFBC	Circulating Fluidized Bed Combustion
CFD	Computational Fluid Dynamics
CGE	Cold Gas Efficiency
CH_4	Methane
CIMFR	Central Institute of Mining and Fuel Research
CO	Carbon Monoxide
CO_2	Carbon Dioxide
DAQ	Data Acquisition
EMMS	Energy Minimization Multi-Scale
ER	Equivalence ratio
FC	Fixed Carbon
FCC	Fluid catalytic cracking
FCIL	Fertilizer Corporation of India Limited
GAIL	Gas Authority of India Limited
GCV	Gross calorific value
H	Height
H_2	Hydrogen Gas
HHV	Higher Heating Value, (kJ/kg)
ID	Internal Diameter
IEA	International Energy Agency
IGCC	Integrated Gasification Combined Cycle
KTGF	kinetic theory of granular flow
LHV	Lower Heating Value, (kJ/kg)
MBM	Meat and Bone Meal
MC	Moisture Content
MNRE	Ministry of New and Renewable Energy
Mt	Million ton
N_2	Nitrogen Gas
NTPC	National Thermal Power Corporation
OD	Outer Diameter
PBFB	Pressurized Bubbling Fluidized Bed
PCFB	Pressurized Circulating Fluidized Bed
PEDA	Punjab Energy Development Agency
PFBC	Pressurized fluidized bed combustion
RCF	Rashtriya Chemicals & Fertilizers
S/F	Steam to fuel ratio
UDF	User Defined Function
VM	Volatile Matter
WD	With dolomite
WoD	With out dolomite
wt	Weight

List of Figures

List of Tables

Chapter – 1

Introduction

1.1 Motivation

Coal is the primary source of energy for the production of power. The major share in power generation in India and China are reported to be obtained from coal. According to International Energy Agency (IEA) 2019 report, China derives 72% of electricity from the combustion of coal, whereas the same is reported to be 58% in India. Similarly, Japan and the USA have derived electricity by utilizing 32% and 40% of coal, respectively IEA, (2019). However, the natural reserves of fossil fuel with coal as a major share has been depleting fast. With the present rate of consumption, the oil and gas resources may not last for more than 50 to 60 years, whereas the coal may be available for another 200 years in India (Rawat 1993, B. P. Statistics 2016). Due to the high ash content (~ 40%) of Indian coal, the same is difficult to handle in the pulverized power plant through the combustion route. Moreover, emission of CO_2, oxides from nitrogen, oxides of sulfur, and particulate matter from coal-based power plants are increasing at an alarming rate. Power derived through combustion is well established but leads to an increased level of atmospheric pollution. On the other hand, biomass such as rice straw, rice husk, corn husk, sawdust, etc. are available in India and other developing countries abundantly. Many researchers have observed these biomasses as a potential source of energy through characterization and laboratory level studies. Mallick et al. (2018, 2019). These biomasses cause hygienic problems otherwise if dumped on the ground. The substitution of coal partially or fully with biomass has become popular amongst technologists to mitigate atmospheric pollution and to increase efficiency in power generation in several countries such as Polaniec Power Station, Poland, and Osaki CoolGen Corporation, Japan. However, generalized technology is yet to be developed in this direction.

Drawbacks of coal combustion also influenced the researchers to develop gasification processes for the last 2 (two) decades. Gasification occurs at relatively moderate temperatures reducing the exergy losses so as to improve the energy efficiency of the system. Moreover, water consumption in the gasification process is less than that of combustion. The attractive feature of the gasification is that air pollution is drastically reduced along with a reduction of particulate emission. Thus, the development of new generation gasifiers to handle multi-feed fuel got attention in recent years. The fluidized bed gasifier got importance under this context.

A fluidized bed gasifier (FBG) is one of the promising devices for sustainable gasification of solid feed materials as long as the same can be fluidized with sub-stoichiometric air. Low-grade coal, rice husk, corn husk, sawdust, sugarcane bagasse, etc. can be handled by this gasifier, significantly reducing the cost of grinding and ball milling of the same. More than 700 atmospheric circulating fluidized bed (ACFB) boilers are installed in the world for power generation from coal. In contrast, pressurized circulating fluidized bed (PCFB) is gaining importance from the late 90s' due to its compactness and high-power density. However, only a few studies on gasification of low-grade coal and biomass are reported in the literature using PCFB. Hence there is a call for a thorough investigation on gasification of low-grade coal and loose biomass in PCFB.

1.2 Coal and Biomass as Feed Material for Power Production

Coal is available in various forms such as peat, lignite, sub-bituminous, bituminous, and anthracite. Except for the peat coal, all the aforementioned coal is used for power generation (IEA, 2019). Table 1.1 presents the gross calorific value (GCV) and the mean random reflectance of vitrinite of various types of coal. The GCV is given based on a wet basis considering the coal to be ash-free.

Table 1.1 GCV and vitrinite standards of different types of coal (IEA, 2019)

	GCV in kJ/kg	Mean random reflectance of vitrinite
Anthracite	>24000	2.0>
Bituminous	>24000	0.6>
Sub-bituminous	20000-24000	<0.6
Lignite	<20000	--

Production and consumption of coal in selected countries, including India in a million tons (Mt) for the year 2016-2018, is presented in Table 1.2. It is observed from the table that India produces and utilizes its large share of coal in the form of sub-bituminous and bituminous ranks.

Table 1.2: Coal Production and consumption in Mt (2016-18), (IEA,2019)

	Coal Production			**Steam coal Consumption**			**Lignite Consumption**		
	2016	**2017**	**2018**	**2016**	**2017**	**2018**	**2016**	**2017**	**2018**
China	3268.2	3397.2	3550.1	3067.9	3125.4	3157.8	--	--	--
India	**703.1**	**725.5**	**770.9**	**740.2**	**799.5**	**842.3**	**43.1**	**45.9**	**45.3**
USA	660.8	702.7	685.4	576.1	561.5	545.4	67.2	64.4	52.4
World	7310.7	7562.9	7813.3	5706.6	5839.7	5935.6	810.8	816.9	793.5

However, the consumption of lignite is very low in comparison to the world average. Indonesia and Australia are the major coal exporters, while China and India are the major coal importers for the last few years. India imported 192.1, 209.4, and 240.2 Mt of coal in the years 2016, 2017, and 2018, respectively. India mainly imports two types of coal, steam coal for power production/ electricity generation and coking coal for the production of steel in the industrial application.

1.2.1 Coal reserves in India

According to the Geological Survey of India, a total inventory of 315.148 billion tons (BT) of coal is reserved in India. Jharkhand has the reserve with the highest share of 82.4 BT, while Odisha shares the second highest with 24.52% of the total reserve of the country. The state-wise coal reserve is presented in Table 1.3.

Table 1.3 State-wise coal reserves in India as on 01.04.2017
(http://www.mahanadicoal.in/Others/ecoalfields.php)

Name of the state	Reserves in billion tonne	% of total reserves
Jharkhand	82.440	26.16
Odisha	77.285	24.52
Chattishgarh	56.661	17.98
West Bengal	31.667	10.05
Madhya Pradesh	27.673	8.78
Telangana	21.464	6.81
Maharastra	12.259	3.89
Others	5.699	1.81
**Others – NE States, Andhra Pradesh, Uttar Pradesh, and Bihar*		

The rank of the coal is based on the GCV (coal India). The GCV of coal produced is in the range of (3100-4000 K. Cal./Kg). These coals are generally supplied to the power sectors like National thermal power corporation (NTPC), Jindal steel power, and state-owned power plants. The major complaint by these industries is the poor quality of coal, which affects the efficiency of the plant. From the quality taste conducted by the coalfields, it is also confirmed that 30% of the coal fails in passing the quality check. The use of high ash content coal in conventional powder-fed fired powerplants poses problems due to the wear and tear in the grinding machines and combustion equipment which inevitably leads to lower plant availability Iyengar and Haque (1991). In general, the primary quality requirements of the industries are coal with low ash content (less than 24%), good reliability, high ash fusion temperature, and medium volatile

content (CIMFR-Coal India). It is also worth mentioning that coal having ash content more than 35% is treated as low-grade coal (Iyengar and Haque 1991).

Presently, mined coals do have ash content in the range of 30-50% (Datta et al. 2015). However, coal that has only limited use because of undesirable characteristics, such as high mineral matter content, can also be categorized under low-grade coal. All low-rank coals (sub-bituminous coals and lignites) are generally categorized as 'low grade' due to the presence of high moisture content and low heating value. Such coals often require the application of specific technologies for their successful use in power generation and other industrial processes. Fortunately, most of the Indian coal ashes are refractory in nature and have very high melting temperature as indicated from ash fusion test. The major disadvantage of low-grade Indian coal is that it has a negative impact on the environment. During the combustion process, the low-grade coals create tremendous air and particulate emissions. Suitable technology is in demand to utilize the low-grade coal efficiently for power generation.

The biomasses such as sawdust, bamboo dust, rice husk, sugarcane bagasse, cotton stalk, forest residues are abundantly available in many parts of India having huge power potential. (Fig. 1.1). Similarly, the global biomass potential is explained by many researchers in terms of proximate analysis and calorific value of biomass (Table 1.4). From the table, it is observed that biomass containing high volatile matter and fixed carbon along with low to medium calorific value are good candidates for power generation.

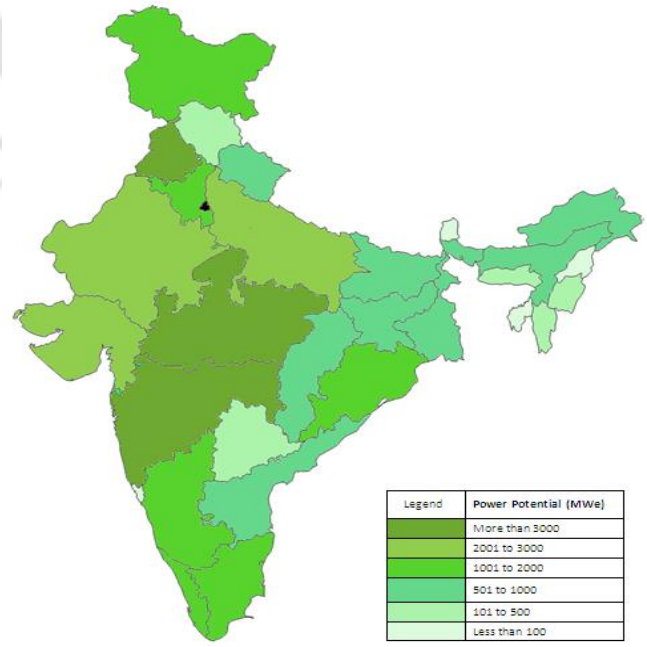

Fig. 1.1 State wise biomass potential in India (https://biomasspower.gov.in/biomass-info-asa-fuel-resources-map-001.php)

Table 1.4: Proximate analysis and calorific value of biomass

Author	Feed Stock		Proximate Analysis (% w/w)				Calorific Value MJ/kg
			MC	Ash	FC	VM	
Padban et al. (2000)	Bark		-	3.63	25.48	70.89	19.2
	Sawdust A		-	0.68	15.93	83.39	20.4
	Sawdust B		-	0.72	16.55	82.73	19.4
Garcia Ibanez et al. (2004)	Leached orujillo		8.9	8.5	17.1	74.4	18.5
Guan et al. (2007)	Corn stalk		2	6.94	14.38	76.68	15.84
Lapuerta et al. (2008)	Pinus pruning wastes		-	2.67	15.13	82.1	19.99
	Olive pruning wastes		-	3.67	13.98	82.35	19.99
	Grapevine pruning wastes		-	2.06	19.78	78.16	17.91
	Sawdust wastes		-	1.28	16.27	82.45	20.47
	Marc of grape		-	7.83	26.4	65.77	19.51
Srinivas et al.(2009)	Rice husk		-	22.2	-	-	22.98
	Sawdust		-	1.20	-	-	23.71
	Solid waste		-	0.37	-	-	25.02
	Manure		-	0.90	-	-	25.20
Seo et al. (2010)	Quercus acutissima sawdust		2.29	0.76	19.94	77.01	19.88
Fermoso et al. (2010)	Petcoke biomass	PC	0.3	-	-	9.6	35.1
		OP	7.6	-	-	71.9	21.6
		PS	1.4	-	-	86.5	20.2
Kitzler et al. (2011)	Woody biomass		-	-	-	-	4-6
Karmakar and Datta (2011)	Rice husk		9.95	19.52	14.99	55.54	15.68
Mayerhofer et al. (2012)	Wood pellet		4.84	0.12	14.3	85.58	20.6
Camacho Ardila et al. (2012)	Sugarcane bagasse		5.9	7.4	14	78.6	18.2
Berrueco et al.(2014a)	VW-ST		3.79	0.46	23.41	72.34	16.12
	GROT-ST		4.71	2.73	31.47	61.63	18.29
Sahoo and Ram (2015)	Sugarcane bagasse		-	-	-	-	17.73
Zeng et al. (2016)	Pine sawdust		1.44	1.5	16.28	80.78	18.33
Adeyemi et al. (2017)	Waste wood		8.95	0.28	21.88	68.89	18.70
Motta et al. (2019)	Sugarcane bagasse		9.4	2.3	17.5	80.2	-
			7.3	2	17.1	80.9	19.6
Suksuwan et al. (2018)	Palm kernel cake		6.12	5.6	17.67	70.61	-
Mallick et al. (2019)	Rice husk		8.7	19.7	12.01	60.21	14.1
	Bamboo dust		9.12	1.68	14.7	74.51	17.2
	Sawdust		9.43	1.1	15.63	73.84	17.52

It is interesting to note that some of the biomasses with low calorific value such as rice husk, rice straw, coconut shell, sawdust, etc. are abundantly available across the globe. The utilization of these biomasses for power production is a challenge.

1.3 Gasification Process

Gasification is a partial oxidation process of carbonaceous raw materials. The product of gasification is syngas consisting of CO, H_2, N_2, CH_4, having low to medium calorific value. Usually, one-fifth to one-third of the stoichiometric oxygen content is required for the complete gasification process. Though the amount of oxygen is less, it is still sufficient to generate adequate heat to gasify the remaining unoxidized fuel-producing synthetic gas (syngas) as an output. The entire gasification process is achieved through a series of chemical reactions inside a high temperature/pressure vessel known as a gasifier.

In this context, the gasification process can be an alternative solution due to many significant advantages over combustion. The process of gasification utilizes less amount of oxygen-producing CO, H_2, N_2, and H_2S as output where the useful content is the producer gas or syngas, which can later be utilized for many applications like power production in power plants, urea production in the fertilizer industry, etc. The output gases from the process of combustion and gasification are summarized in Table 1.5. The primary difference between gasification and the combustion process can be explained based on the composition of output gases.

Table 1.5 Difference between combustion and gasification based on the ultimate analysis

Gasification	versus	Combustion
	Ultimate analysis	
CO	C	CO_2
H_2	H	H_2O
N_2	N	NO_x
H_2S	S	SO_x
	O	O_2

As mentioned above, the gasification process takes place using limited oxygen in a closed container called a gasifier. However, many factors, such as temperature, pressure, airflow rate, affect the gasification process in a significant way. Therefore, different designs have been adopted by many researchers over the years. However, the gasification process is achieved through some specified chemical reactions.

1.3.1 Stages of gasification

The stages of the gasification process are drying, pyrolysis, partial combustion, cracking, and reduction. These stages are generally occurring with an increase in temperature inside the gasifier. The stages of the gasification process of different solid materials are presented in Fig. 1.2.

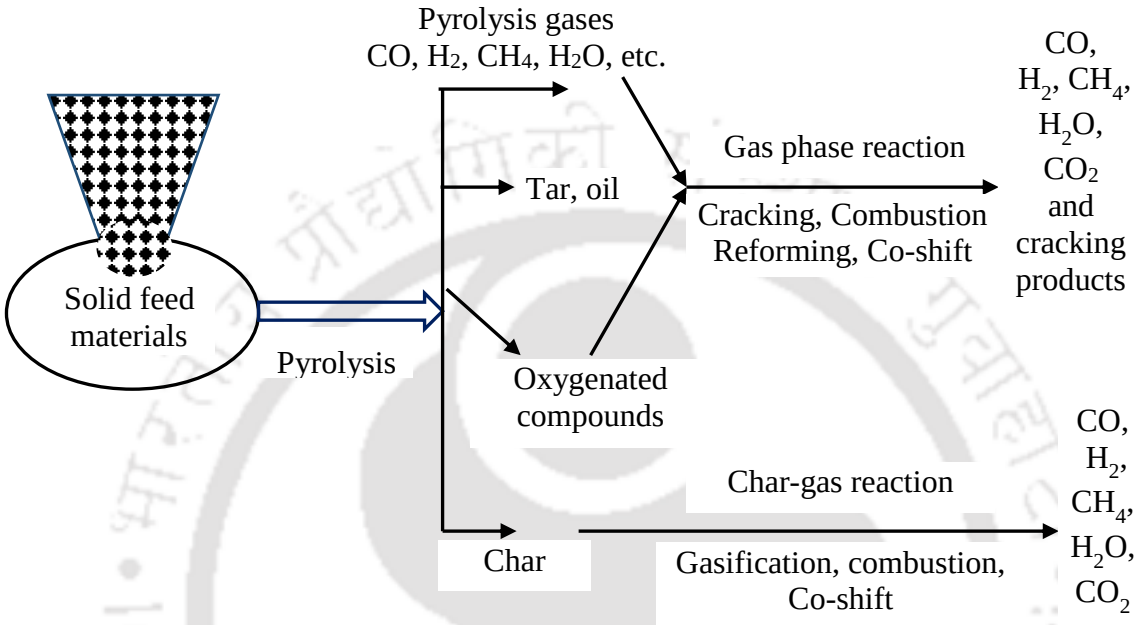

Fig. 1.2 Stages of gasification of solid feed material

The sequential chemical reactions for different stages of gasification is presented in Table 1.6.

Table 1.6. Chemical reactions during the gasification process, Basu (2006)

Reaction	Equation	Reaction Enthalpy (kJ/mol)	
Oxidation	$C + O_2 = CO_2$	-393	(1.1)
Partial oxidation	$C + 0.5O_2 = CO$	-111	(1.2)
CO Partial oxidation	$CO + 0.5O_2 = CO_2$	-283	(1.3)
Boudouard	$C + CO_2 = 2CO$	+172	(1.4)
Water-gas Primary	$C + H_2O = CO + H_2$		(1.5)
Secondary	$C + 2H_2O = CO_2 + 2H_2$	+131	(1.6)
Water gas shift	$CO + H_2O = CO_2 + H_2$	+77	(1.7)
Methanation	$C + 2H_2 = CH_4$	-41	(1.8)
Steam reforming	$CH_4 + H_2O = CO + 3H_2$	-75	(1.9)
Dry reforming	$CH_4 + CO_2 = 2CO + 2H_2$	+247	(1.10)
Shift conversion	$CO + H_2O = CO_2 + H_2$	-42	(1.11)

From the mentioned reactions in Table 1.6, all or a few of the reactions may co-occur simultaneously. These reactions occur within a few seconds of the gasification process. Further, these reactions are a strong function of pressure and temperature which leads to change the gas composition, thereby affecting the overall efficiency of the process.

1.3.2 Advantage and disadvantages

The power plant integrated with the gasifier provides some distinct applications such as decentralized electricity generation in remote locations. It offers a sustainable solution to electricity generation economically and affordably with the employment of semiskilled and skilled laborers. Significant advantages of the gasification process are enlisted below:

- Less particulate emission
- Relatively low-temperature requirement than the combustion process
- higher efficiency (~40%) as compared to combustion-based power plants
- lower NOx and SOx emission
- output gas is cleaner in nature
- producer gas can replace natural gas and oil due to its low production cost and capability of small-scale production

Challenges associated with the gasification process and gasifier are (1) control of agglomeration inside the gasifier because agglomerates lead to clogging of the gasifier (2) control of tar formation, (3) prevention of slagging occurring due to the handling of high ash content feed material. These problems are more pronounced in conventional gasifiers such as updraft, downdraft, and cross draft gasifiers.

Generally, in the gasification process, coal and biomass are fed into the gasifier, and hot gas is mixed with the feed materials. Syngas is generated after a series of chemical reactions inside the gasifier. The syngas has several applications such as power generation, chemical industries, fertilizer industries, transportation fuel, and power generation through integrated gasification combined cycle (IGCC) route. The significant applications obtained from syngas is shown in Fig. 1.3.

1.4 Types of Gasifiers

Basically, three types of gasifiers are used for gasifying the feed materials as mentioned in Fig. 1.4. These gasifiers are divided according to types of flow, the flow direction of air, and different operating conditions. Based on types of flow, the gasifiers are divided as a fixed bed,

fluidized bed, and entrained bed. According to operating pressure, fluidized bed gasifiers are operated on the atmospheric bed and pressurized bed.

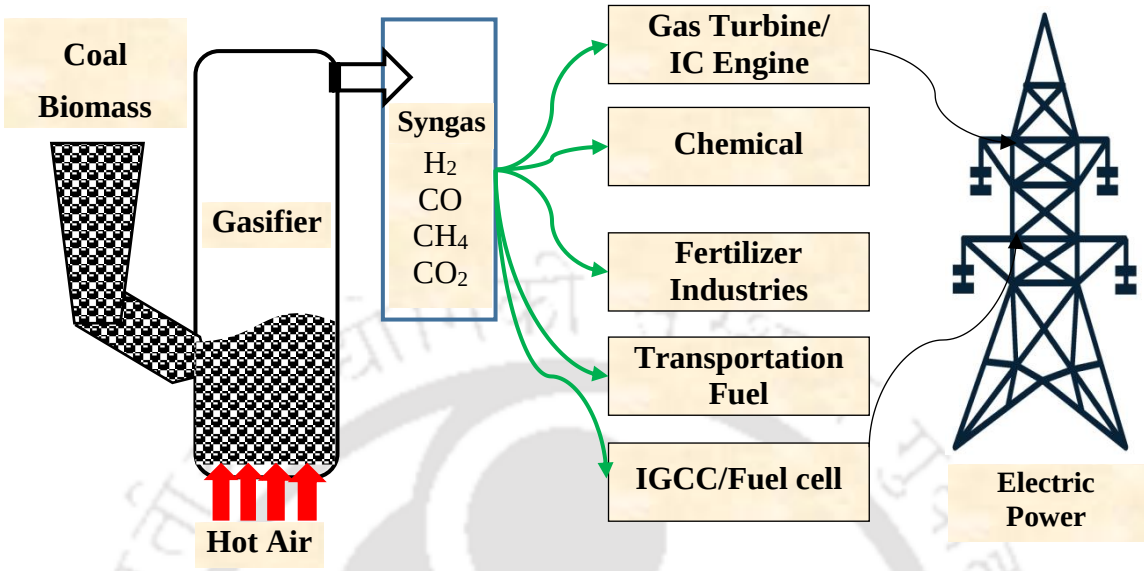

Fig. 1.3 Application of the gasification process

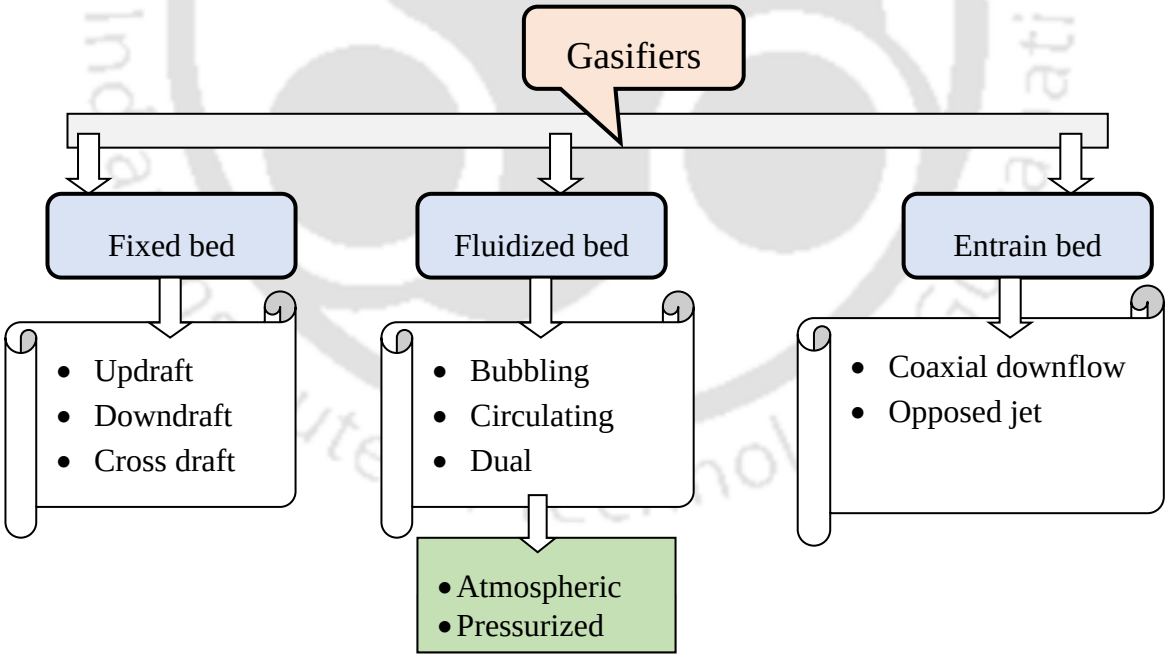

Fig. 1.4 Types of gasifiers

1.4.1 Fixed bed gasifiers

The fixed bed gasifier (Fig. 1.5a) is classified into three groups depending upon the airflow direction, such as updraft, downdraft, and cross-flow gasifier.

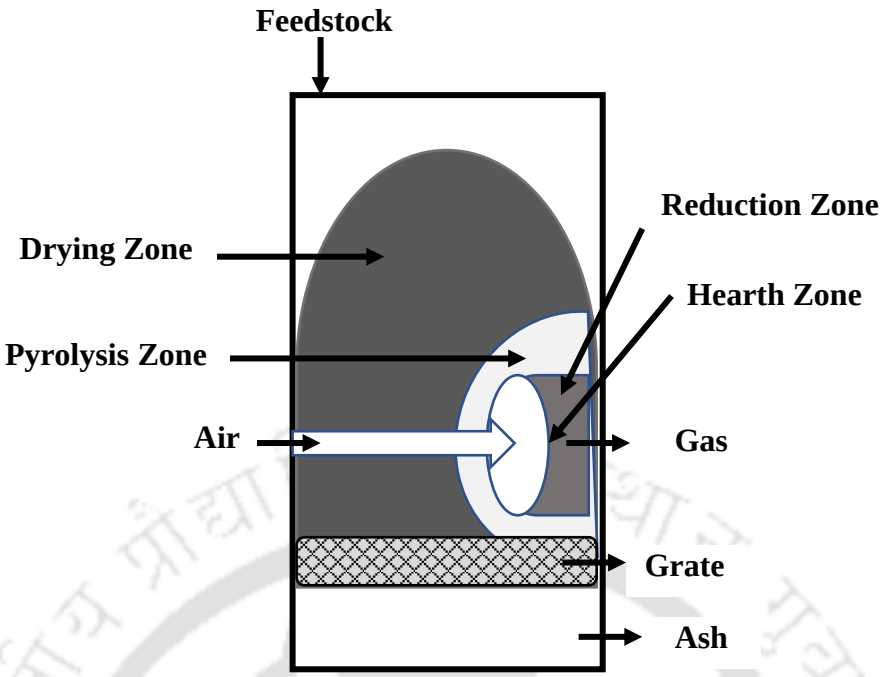

(a) Fixed bed, (Basu, 2006)

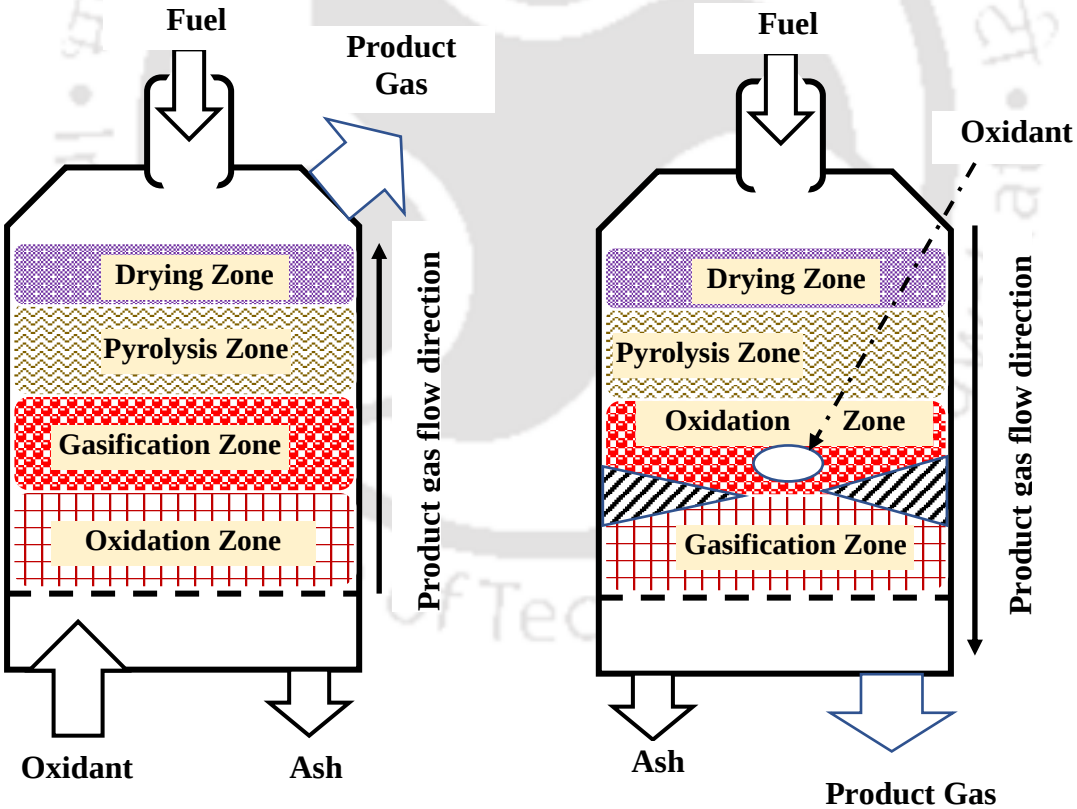

(b) Updraft (c) Downdraft

Fig. 1.5 Types of fixed bed gasifiers

As per the operating procedure, the fuel and the product gas flow in opposite directions in the updraft gasifier (Fig. 1.5b) whereas, the fuel and the product gas flow in the same direction in

the downdraft gasifier (Fig. 1.5c). These gasifiers are easy to operate, but the major disadvantage of a fixed bed gasifier is that the temperature profile is not uniform inside the gasifier. Another major problem with fixed bed gasifiers is the problems associated with tar content. The significant advantage associated with a fixed bed gasifier is its application for power generation in the small-scale power production unit, i.e., below 10 kW.

1.4.2 Entrained bed gasifiers

In the entrained bed gasifier (Fig. 1.6), a dry pulverized solid, an atomized liquid fuel, or a fuel slurry is gasified with oxygen. Air is a much less frequent gasification agent in co-current flow, and the gasification reactions take place in a dense cloud of very fine particles. The entrained flow gasifier requires a smaller particle size of the feedstock than the fluidized bed gasifier so that the feedstock can be conveyed pneumatically by the reactant gases; typically, the fuel must be pulverized. In this case, there is little or no mixing of the solids and gases, except when the gas initially meets the solids. These types of gasifiers result in high pressure and high temperature with extremely turbulent flow.

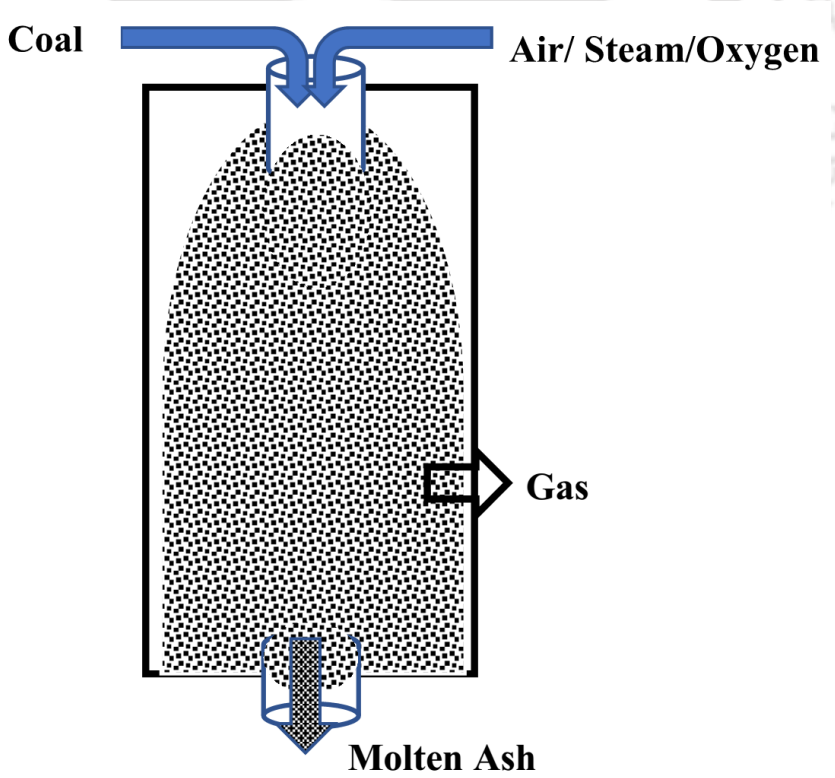

Fig. 1.6 Entrained bed gasifiers Basu (2006)

All the gasification reaction takes place at a higher rate with a residence time of a few seconds. The main advantages of such gasifiers are that higher carbon conversion efficiency (98-99.5%). There is no formation of tar, oil, and other types of liquids because these are decomposed into

syngas inside the gasifier. The syngas obtained from these types of the gasifier is free from tar, and the ash formed during the gasification process also melts inside the gasifier due to higher temperature. The major disadvantages of such gasifiers are that a wide range of fuel cannot be used in these types of gasifiers. Only dry coal (moisture-free) is used as feed material in these types of systems.

1.4.3 Fluidized bed gasifiers

In the fluidized bed gasifier (Fig. 1.7), the solid particles are transformed into a liquid-like state through the suspension of a gas or liquid. Fluidization is the process by which solid particles are transformed into a liquid-like state through suspension of a gas or liquid. This method of contacting between gas and solid has some unusual characteristics, and fluidization engineering puts them to good use. The fluid-like behavior of solids with its rapid and easy transport and intimate gas contacting is the most important property recommending fluidization for industrial applications.

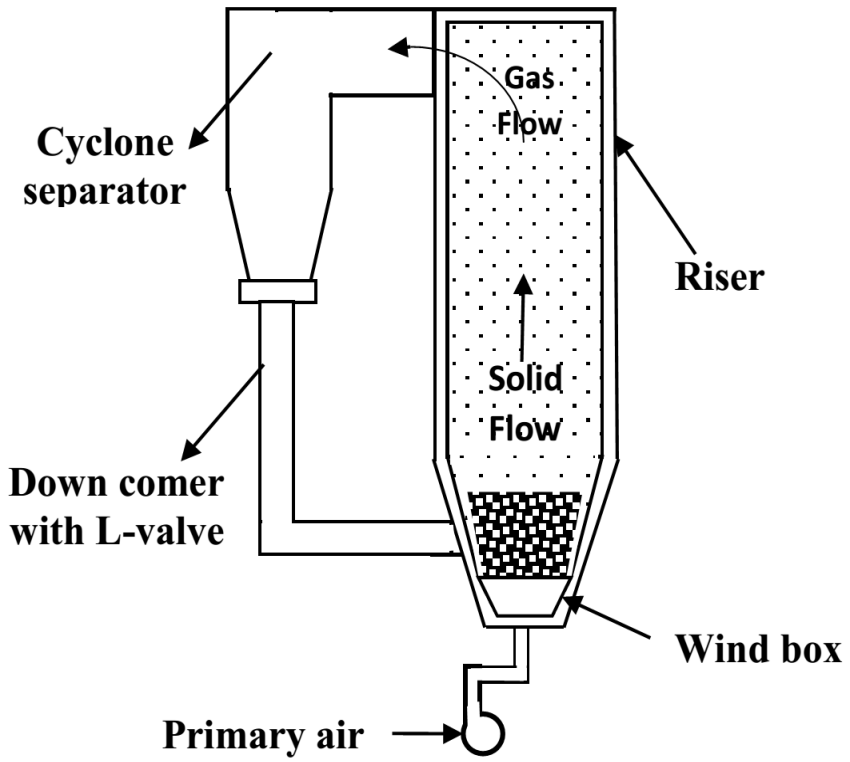

Fig. 1.7 Circulating fluidized bed gasifier Basu (2006)

The primary phase fluid is generally air/steam/carbon dioxide, and in the secondary phase, solid fuel such as coal, biomass is used. The advantages of fluidized bed gasifiers are the fuel flexibility in which a wide range of fuels can be used. The temperature profile is also uniform

in the combustor zone. The major disadvantages associated with fluidized bed gasifiers are its complex phenomenon and mixing of gas and solids inside the bed. A fluidized bed gasifier is feasible for moderate to large scale applications. The fluidized bed gasifiers are divided into three types, such as bubbling, circulating and dual bed gasifiers. The fluidized bed is preferred over other types of gasifiers due to better turndown ratio, start-up facility, control facility, scale-up potential, better handling of ash feed elasticity, sintering safety, blending of feed material.

The fluidized bed is divided into two sub-groups, such as bubbling fluidized bed and circulating fluidized bed. Circulating fluidized bed (CFB) mode is preferred over bubbling mode due to better solid handling inside the bed. In CFB, the un-brunt particles out of the riser and separated by the cyclone enter the riser through the downcomer. The particle circulation provides efficient heat transfer to the furnace walls and longer residence time for feed material. Similar to Pulverizing coal firing (PC firing), the controlling parameters in the CFB combustion process are temperature and pressure. Based on the operating pressure of the fluidizing medium, the fluidized bed gasifiers can further be classified as atmospheric fluidized beds or pressurized fluidized beds. Atmospheric fluidized beds (bubbling/circulating) are established technology, and several researchers have reported the gasification study of different types of feed material through the gasification route in laboratory scales as well as pilot type gasifiers. The major components of the CFB (Fig. 1.7) technology are riser, cyclone separator, and a downcomer. A typical circulating fluidized bed boiler is shown in Fig. 1.7. The CFB is more preferred than a bubbling fluidized bed due to better handling of fuel and can operate at more pressure and velocity.

The advantage of PCFB over ACFB is its compact boiler, which is $1/5^{th}$ the size of that used in an ACFB. PCFB boilers are capable of handling all types of coals including low-grade coal, high moisture, high ash, high sulfur, and low gross calorific value. The other advantages of PCFB are more uniform bed temperature, reduced size of boiler island components, lower bed surface area, reduced maintenance, and free lime formation. The other key benefits of PCFB over ACFB are less capital cost (due to higher specific power output), higher efficiency, (practically all the combustion takes place within the bed), negligible free-board combustion, facilitation of gas turbine operation, low SO_2 emissions and low NO_x formation than a pulverized coal-fired boiler.

In 2018, more than 4000 CFB boilers are installed in China. The highest capacity of the CFBC supercritical boiler is of 600 MWe. The advantage of CFB over pulverized boiler is that the

boiler efficiency is the same as pulverized bed whereas the cost is 5-10% cheaper. Another advantage of CFB is that heat flux is uniform in the reactor. The world's largest pressurized fluidized bed combuster (PFBC) with a capacity of 600 MWe is in Balma, China. CFB technology is stable, reliable, and uses a wide range of fuel. The future of this technology is the production of CO_2 in the plant by fluidizing oxygen instead of air. Another advantage of use biomass as a feed material is that it will reduce the CO_2 emission, which is a regulatory mandate in some countries like Netherland.

Table 1.7: Indian scenario of co-gasification

Year	Company	Place	Capacity/ Power output	Remarks
1959-60	Lurgi	Sindri	23470 tpy urea	Due to non-availability of raw materials in quality and quantity, the capacity of the plant was reduced in 1971-72
1965-75	Shell	Sindri	25 MW	To produce urea and captive power plant
1971	Koppers-Lurgi	Ramagundun	300 tpd NH_3	To produce ammonia and steam gasification
1977	Texaco	Bharuch	1350 tpd	NH_3 production and urea
1990s	BHEL			Pressurized fluidized bed gasification
1997	BHEL	Trichy	6.2 MWe	IGCC technology
--	NTPC	Auraiya	125MW	Jointly with BHEL
2013	Jindal Steel and Power limited	Odisha	5.7 million standard cubic meters per day	--
--	Coal India limited	Talcher	Production of ammonia syngas	Jointly with RCF, GAIL, and FCIL
2013	PEDA	Punjab	52.5 MW	It produces 25% of the country's cotton, 22% of wheat and 55% of rice. The power is generally derived from these biomasses.

There are some commercial plants based on gasification and co-gasification reported in India. The commercial plants are generally operated by Lurgi, shell, BHEL, Thermax, TBW, and Alstom/foster Wheeler. The industrial experiences by these commercial companies stated that

power production through gasification and the co-gasification process is a promising technology due to increasing efficiency. The R&D department of India stated that IGCC is not feasible in the Indian Scenario due to low-rank and high ash content of coal. Therefore, air blown pressurized fluidized bed gasification based IGCC technology holds a great potential to produce power and energy in a cleaner way. The application based on co-gasification in the Indian scenario is limited. Some of the applications are shown in Table 1.7.

1.5 Present Objective and Roadmap

From the preceding sections, it is observed that the ACFB gasifier can handle a wide range of fuels such as low-grade coal and different types of biomass. Many authors have used such feed materials in their experimental units and performed the hydrodynamic and heat transfer studies. Moreover, very limited studies are available on gasification and co-gasification in CFB under high operating pressure. Following the aim and objectives for the present study are proposed.

Aim: The aim of the present work is to investigate hydrodynamics, heat transfer, and gasification characteristics of low-grade coal, biomass, and blends of coal and sawdust in a PCFB unit.

The following are the scope of the work:

- Development of a PCFB gasifier and study of hydrodynamic and heat transfer characteristics under different operating parameters. It is proposed to conduct both the numerical as well as experimental investigations for a thorough understating of the hydrodynamics and heat transfer of the PCFB.
- Performance evaluation of the PCFB gasifier to study the effect of feed material, superficial velocity, and operating pressure on bed voidage, suspension density, solid circulation rate, and temperature distribution.
- Gasification study of the PCFB unit with coal and biomass as feed material.
- Performance evaluation of the gasifier in terms of gas composition, LHV, gas yield, cold gas, and carbon conversion efficiency, etc.
- Performance evaluation of co-gasification with blends of low-grade coal and sawdust in various proportions with and without the in-situ catalyst.

The road map of the present study is shown in Fig 1.8

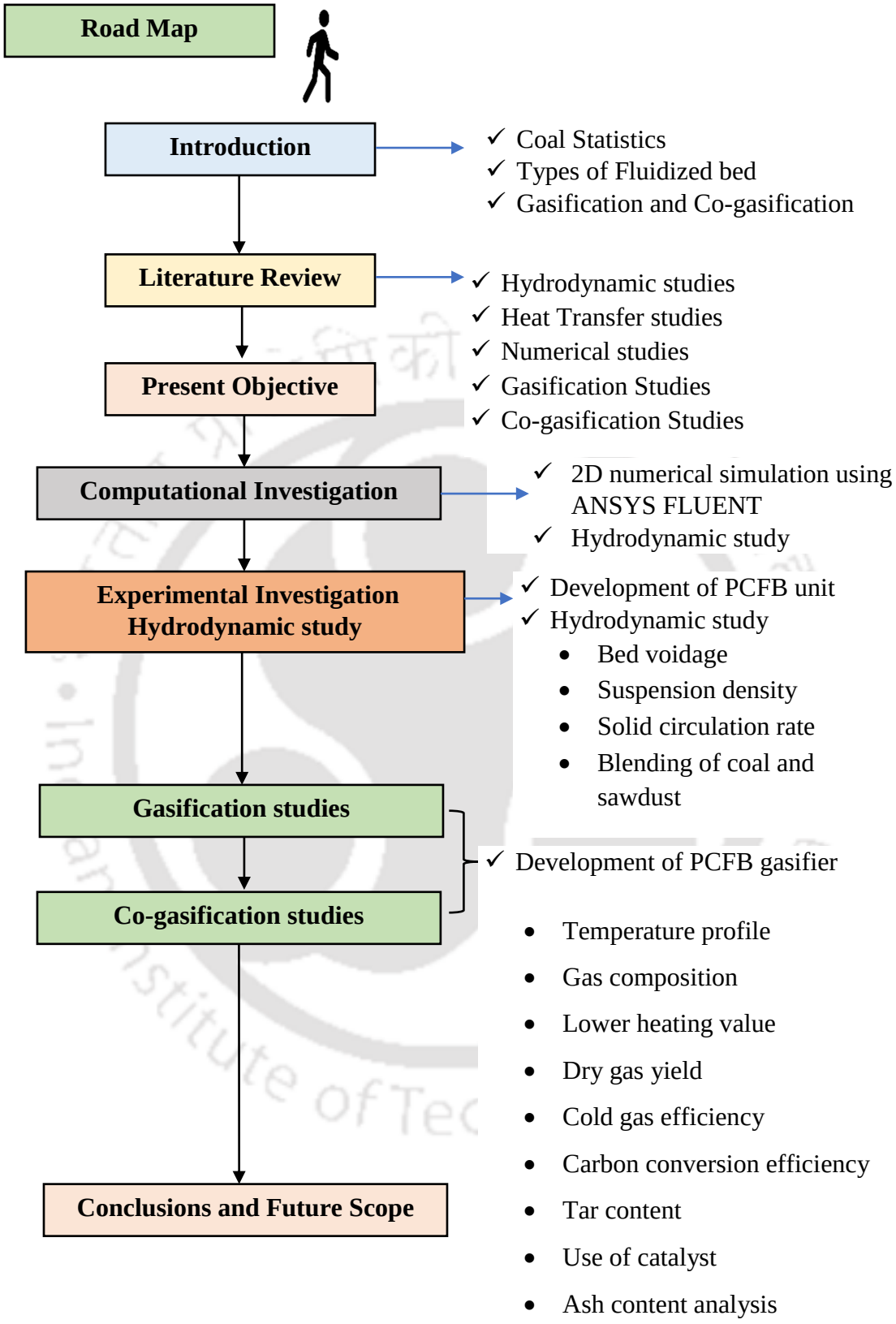

Fig 1.8 Road map for present work

1.6 Organization of Thesis

The thesis consists of eight chapters. Chapter 2 reports a brief open literature review for different papers for hydrodynamic, heat transfer, and gasification studies in a fluidized bed. Chapter 3 reports the computational investigation of a PCFB riser under hydrodynamics studies. Chapter 4 describes the cold and hot-bed experimental setup and procedures with working formulas. Chapter 5 details the hydrodynamic studies of the PCFB riser under different operating conditions. The gasification studies of low-grade coal and biomass are reported in Chapter 6, while Chapter 7 represents the co-gasification studies under coal-sawdust blends in the PCFB gasifier. Chapter 8 details the conclusions and future scope of the present work.

Chapter – 2

Literature Review

2.1 Introduction

Present chapter elaborates state of the art review pertaining to gasification. The literature review is presented in 4 (four) key sections, such as bed hydrodynamics, followed by heat transfer, gasification, and co-gasification studies in the CFB gasifiers. Research-based on experimental as well as numerical simulations are also discussed. Finally, the research gap based on the literature review is highlighted.

2.2 Bed Hydrodynamic study in ACFB and PCFB

The bed hydrodynamic study in a CFB unit based on the fluidization process and the effect of different operating parameters such as superficial velocity, operating pressure, types of inventory, particle size, etc. are discussed in the following sub-sections.

2.2.1Fluidization regimes and particle size distribution

Kunii and Levenspiel (1991) have classified the regimes of fluidization as (1) fixed bed, (2) bubbling, (3) slugging, (4) turbulent, (5) fast fluidization and (6) pneumatic conveying based on increase in superficial gas velocity. Figure 2.1 presents the various regimes with solid-fluid patterns of fluidization (Basu 2006, Davidson et al. 1985). A fixed bed is characterized by the percolation of gas through the bed material at a relatively low superficial velocity where bed material remains stationary.

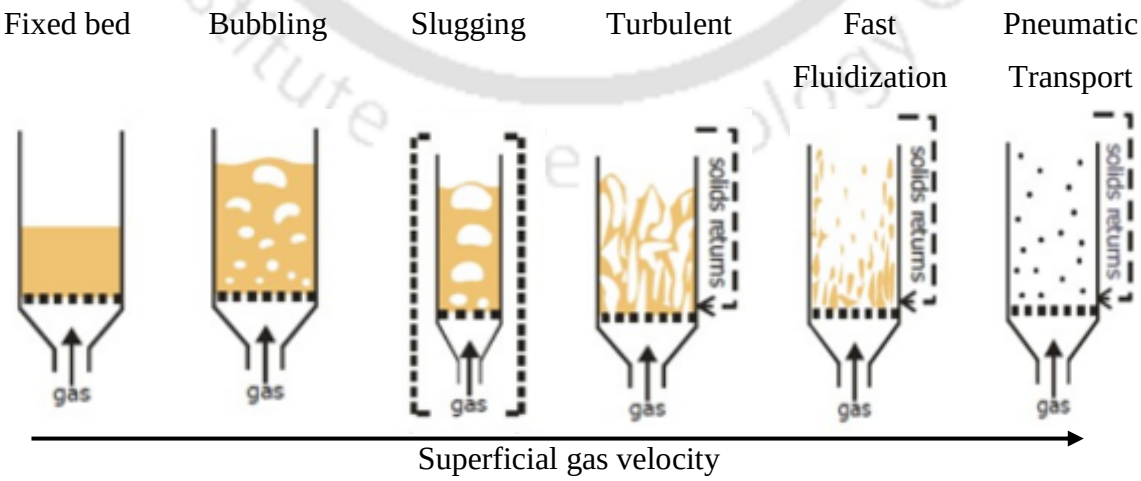

Fig.2.1: Regime of fluidization for a solid-gas mixture with superficial gas velocity Barletta (2009)

With further increase in velocity, the solid particles move apart, vibrating and even entering into the restricted regions known as the expanded bed. At still higher superficial velocity, the particles get just suspended by upward-flowing gas. This is the situation when the frictional force counterbalances the weight of particles. The pressure drop through any section of the bed equals the weight of fluids and particles in that section. This is called incipient or minimum fluidization.

Gas-solid systems show large instabilities with bubbling and gas channeling, with the rise in flow rate beyond minimum fluidization (Grace 1986, Barletta 2009). At a high flow rate, vigorous agitation of particles is seen. Such a bed is called an aggregative or heterogeneous or bubbling fluidized bed. In both lean and turbulent phase fluidization, there is large particle entrainment. For steady-state operation, entrained particles have to be collected by cyclones and returned to bed. For the turbulent fluidized bed, inner cyclones are sufficing, as entrainment is moderate. The rate of entrainment is much larger in lean phase fluidized beds and large cyclone collectors are required outside the bed. This is a fast-fluidized bed. If a dip leg or other solid trapping device is used for fast-fluidized beds, it is called a circulating fluidized bed.

However, the effect of particle size of inventory is an important parameter in the hydrodynamic study. Geldart (1973) proposed the criteria based on the density of the inventory. The Geldart particle size distribution is shown in Table 2.1.

Table: 2.1 Geldart particle size distribution

Type	Properties and examples
Group C	Cohesive, or very fine powders Example: Face powder, flour, and starch are typical of these solids
Group A	Areable, or materials heaving a small mean particle size Example: FCC catalysis is representative of these solids
Group B	Sand-like structure Example: Sand
Group D	Spoutable, or large and or dense particles Example: coffee bins

Several alternative classifications have been published in the literature, among which Grace's (1986) deserved to be singled out. Grace uses two-dimensional parameters (a dimensionless number $D_p^* = Ar^{1/3}$ and a dimensionless velocity $u^* = u[\rho^2 / (\rho_p - \rho_g) g \mu]^{1/3}$ to represent the map of flow regimes encountered in gas-particle fluidization. Grace's map represented in Fig. 2.2 draws in a broader database than Geldart's (including gases other than air and temperatures and pressures other than atmospheric) and proposes new boundaries between groups A-B and

B-D based on the additional data. Flow regime maps are presented in Fig.2.2. This diagram is useful for selecting the size of the feed material (particle) required for sustaining the fluidization process.

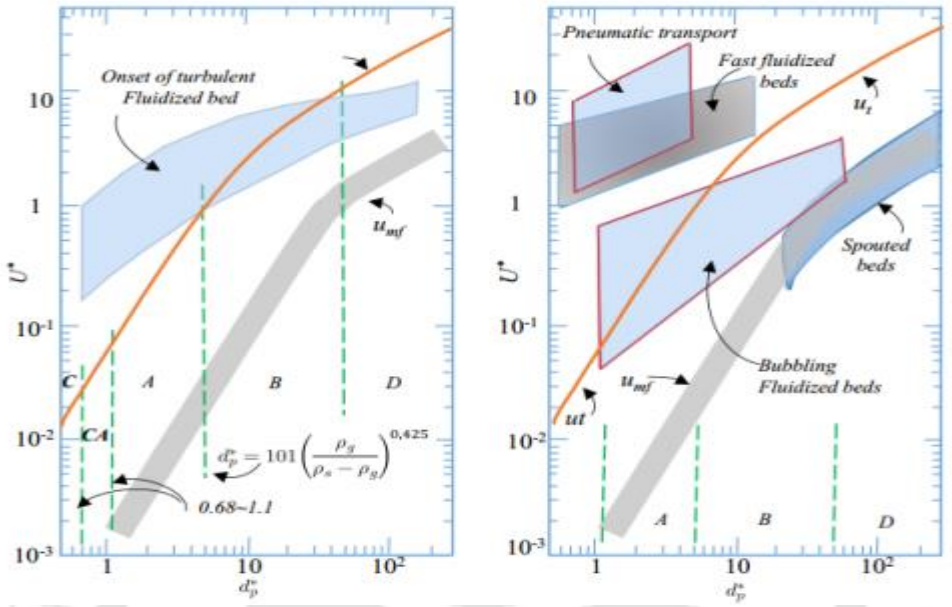

Fig.2.2: Flow-regime map Grace (1986)

2.2.2 Pressure drop along the riser of fluidized bed

The hydrodynamic behaviour of the circulating fluidized bed is characterized by the pressure drop that exists along the fluidized bed riser and cyclone separator. There exists a strong correlation between the pressure drop and the superficial velocity in the case of ACFB Basu and Nag (1996). During experimentation, depending on the air velocity, pressure drop occurs along the riser height. The pressure drop is typically measured with the help of a differential U-tube manometer (Patil et al. 2011, Kalita et al. 2013a, Das et al. 2008). In some of the cases, especially for ensuring higher accuracy, differential pressure gauges are used to measure the pressure drop (Saikia and Mahanta 2017). In ACFB, the frictional drag mostly contributes towards pressure drop whereas, in PCFB, both frictional, as well as pressure drags lead to pressure variation (Kalita et al., 2013a). The relationship between pressure drop and superficial air velocity determines the quality of fluidization. Many researchers studied the relationship between pressure loss and gas velocity (Ergun and Orning 1949, Gibilaro 2001). The empirical relation developed by Ergun and Orning (1949) gives the pressure drop as expressed in Eq. (2.3)

Reynolds Number $$\mathrm{Re} = \frac{d_p u_g \rho_g}{\mu} \qquad (2.1)$$

where Re= Reynolds number, d_p is the diameter of the particle, u_g is the velocity of the gas, ρ_g density of the gas, μ is the dynamic viscosity, ρ_s is the density of the solid.

The minimum fluidization velocity is a basic required value for designing and developing a fluidized bed.

$$\Delta P = 150.\frac{\mu_f LU}{d_p^2}.\frac{\left(1-\varepsilon^2\right)}{\varepsilon^3}+1.75\frac{\rho_f LU^2}{d_p}.\frac{\left(1-\varepsilon\right)}{\varepsilon^3} \tag{2.2}$$

On rearranging,

$$\begin{aligned}&\frac{1.75\left(1-\varepsilon_{mf}\right)}{\phi\varepsilon_{mf}^3}\left(\frac{d_p u_{mf}\rho_g}{\mu}\right)^2+150\frac{1-\varepsilon_{mf}}{\phi_s^2\varepsilon_{mf}^3}\left(\frac{d_p u_{mf}\rho_g}{\mu}\right)=\frac{gd_p^3\rho_g\left(\rho_p-\rho_g\right)}{\mu^2}\\ &\text{or, }\frac{1.75}{\phi\varepsilon_{mf}^3}\left(\mathrm{Re}_{mf}\right)^2+150\frac{1-\varepsilon_{mf}}{\phi_s^2\varepsilon_{mf}^3}\left(\mathrm{Re}_{mf}\right)=\frac{gd_p^3\rho_g\left(\rho_p-\rho_g\right)}{\mu^2}\end{aligned} \tag{2.3}$$

Thus, it is observed that for laminar flow region ($\mathrm{Re}_{mf}<2$) and for small/light particles ($d_p<100\mu m$), the loss of viscosity is more compared to the loss of kinetic energy; and the minimum fluidization velocity (u_{mf}) has an inverse relation to the gas viscosity as seen from the second left term of Eq. (2.3). The minimum fluidization velocity (u_{mf})is therefore expected to decrease with an increasing temperature that results in an increased value of μ.

$$u_{mf}\propto\frac{d_p^2\left(\rho_p-\rho_g\right)}{\mu^2} \tag{2.4}$$

For turbulent flow ($\mathrm{Re}_{mf}>1000$) and larger particles, where the kinetic loss predominates, the minimum fluidization velocity is inversely proportional to the square root of the gas density or pressure, and therefore, it decreases with pressure.

$$u_{mf}\propto\sqrt{\frac{d_p\left(\rho_p-\rho_g\right)}{\rho_g}} \tag{2.5}$$

Eq. (2.3) may be rewritten as,

$$\begin{aligned}&\frac{gd_p^3\rho_g\left(\rho_p-\rho_g\right)}{\mu^2}=\frac{1.75}{\phi\varepsilon_{mf}^3}\left(\mathrm{Re}_{mf}\right)^2+150\frac{1-\varepsilon_{mf}}{\phi_s^2\varepsilon_{mf}^3}\left(\mathrm{Re}_{mf}\right)\\ &or,\ Ar=\frac{1.75}{\phi\varepsilon_{mf}^3}\left(\mathrm{Re}_{mf}\right)^2+150\frac{1-\varepsilon_{mf}}{\phi_s^2\varepsilon_{mf}^3}\left(\mathrm{Re}_{mf}\right)\end{aligned} \tag{2.6}$$

The calculation of particle Reynolds number (Re_{mf}) at the onset of fluidization based on shape, size and pressure has been done by many researchers and various correlations are available.

The generic expression of the particle Reynolds number (Re_{mf}) at the onset of fluidization, is given by,

$$\mathrm{Re}_{mf} = \sqrt{C_1^2 + C_2 Ar} - C_1 \tag{2.7}$$

$$Ar = \frac{d_p^3 g \rho_g \left(\rho_p - \rho_g\right)}{\mu^2} \tag{2.8}$$

As reported in literature, Ergun equation (Eq. 2.3) is an appropriate correlation for spherical particles whereas Wen and Yu (1966) correlations are a better one for irregular solids. The correlation constants C_1 and C_2 developed by various researchers for prediction of the minimum fluidization velocity at elevated pressures are shown in Table 2.2.

Table-2.2 Comparison of correlation constants

Correlation	**Pressure range** (kPa)	**Bed Material**	**Constant** C_1	**Constant** C_2	$\frac{1-\varepsilon_{mf}}{\phi_s^2 \varepsilon_{mf}^3}$	$\frac{1}{\phi_s \varepsilon_{mf}^3}$
Wen and Yu (1966)	Atmospheric	Fine powders	33.70	0.0408	11	14
Saxena and Vogel (1977)	179-834	Core dolomite particles	25.28	0.0571	---	---
Borodulya *et al.* (1982)	8000	Quartz and glass ballotini	16.00	0.0370	---	---
Chitester*et al.* (1984)	2169, 4238 and 6306	Ballotini particles	28.70	0.0494	7.94	11.57
Nakamura *et al.* (1985)	4900	Geldart B and D Glass beads	33.95	0.0465	---	---
Basu (2006)	High pressure	---	25.25	0.0651	5.19	8.81

Gas solid fluidization is highly influenced by pressure and temperature in both bubbling and circulating fluidized bed Yates (1996) for Geldart A and Geldart B particles. An increase of operating pressure results in a decrease in the minimum fluidization velocity, the bubbling velocity, and the terminal velocity. As gas density increases with pressure, high pressure may cause the appearance of more homogenous fluidization conditions than at atmospheric pressure. Similar findings reported by Yates (1996) were also observed by Sidorenko and Rhodes (2003) relating to the effect of pressure on gas-solid fluidized bed behaviour.

As observed in the literature, the pressure drop is also greatly influenced by the operating pressure, particle size, solid circulation rate other than superficial gas velocity (Kunii and Levenspiel, 1991). Yin et al. (2014) carried out an experiment on high-flux PCFB for analyzing the hydrodynamic behaviour of gas and solid. Quartz sand having d_p of 137 µm was used for the experiment and it was found that with an increase in pressure, the pressure drop along with the height of riser increases. A similar study of pressure drop in PCFB with alteration in two of the operating parameters such as superficial air velocity and particle size was studied by

Sarbassov et al. (2015). Silica sand particles were used as a dispersed phase whereas air was used as the dispersing medium. They observed that the pressure drop increases with an increase in superficial gas velocity and particle size at high pressure. Khurram et al. (2016) suggested that there exists a linear relationship between solid circulation rate and pressure drop for glass bead in PCFB riser. It has been reported that the pressure drop in the riser section increases with the enhancement of pressure, gas velocity, solid circulation rate, and particle size.

2.2.3 Bed voidage and solid volume fraction

The bed voidage (ε) represents the volume fraction of space occupied by the air/gas phase inside the fluidized bed. It can be determined experimentally by measuring the bulk density and relating it to the gas and particle densities (Kunni and Levenspiel 1991). In every section of the fluidized bed, void fraction and solid fraction (ε_s) magnitude cumulatively turn out to be 1 (one). Bed voidage is typically calculated by measuring pressure drops along with the riser height. Bed voidage, calculated from pressure drop data as given Kunni and Levenspiel (1991). is shown in Eq. 2.9.

$$\varepsilon = 1 - \frac{\rho_L \times \Delta h}{\rho_s \times L_m} \tag{2.9}$$

where, Δh is the difference of liquid levels in the manometer. L_m is the difference in height between two successive tappings.

Many authors have used differential U-tube manometer for measurement of pressure drop in laboratory-scale fluidized bed units (Patil et al. 2011, Kalita et al. 2013a, Das et al. 2008, Kolar and Sundaresan 2002, Basu et al. 1996, and Gupta and Nag 2002). The major difficulty in the U-tube differential manometer is that the level of accuracy is low at higher pressure. Saikia and Mahanta (2017) have used piezo-electric pressure gauges for finding the pressure drop in the PCFB unit to capture the transient pressure variation along the riser.

Various sophisticated measuring instruments have been incorporated previously to measure the voidage along the riser. Tuzla et al. (1998) used a more sophisticated instrument like capacitance probes. Optical fibers are used by Sobrino et al. (2009) for measurement of bed voidage, while X-ray and $\gamma-$rays attenuation and capacitance tomographic imaging are used by Yates (1997), Louge et al. (1999), and Sidorenko and Rhodes (2004). Casleton et al. (2010) integrated the image analysis technique while Mahmoudi et al. (2011) used the single

radioactive particle tracking technique for measuring the bed voidgae in the fluidized bed systems.

Kalita et al. (2013a) observed that bed voidage is found to be decreasing with operating pressure at the lower part of the riser (Fig. 2.3). Rongtao et al. (2019) reported increment in solid fraction with an increase in the operating pressure (Fig. 2.4).

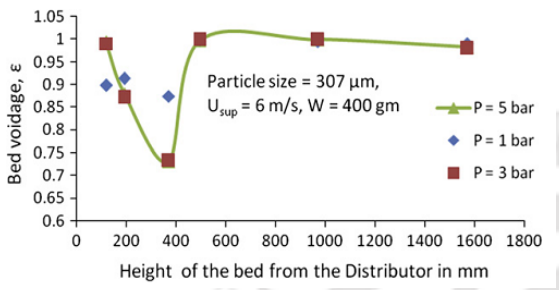

Fig. 2.3: Variation of bed voidage with operating pressure Kalita et al. (2013 a)

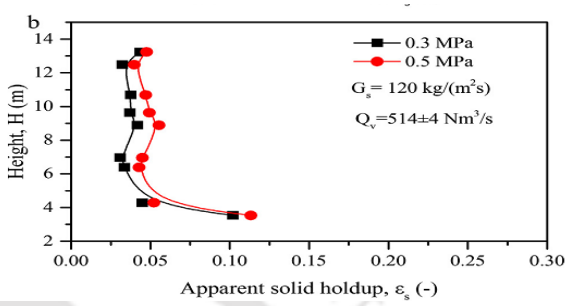

Fig. 2.4: Effect of operating pressure on solids holdup Rongtao et al. (2019)

Transient hydrodynamic behaviour in a PCFB considering sand as a bed inventory has been carried out by Saikia and Mahanta (2017). They observed that the voidage increases in the upper region with a sudden decrease in airflow rate, whereas the effect seems to have diminished in the lower region. They have also reported that the reverse effect is observed as the airflow rate increases.

Gupta and Nag (2002) studied the voidage profile along the riser of a ACFB by considering the effect of pressure, superficial air velocity, and bed inventory. The voidage in the axial direction was found to be minimum at the bottom zone and increases along with the riser height. However, the converse trend was perceived as the system pressure is increased. A similar result was observed upon the increase in the superficial velocity. They also reported that the bed voidage decreases with an increase in bed inventory. Jin et al. (2012) experimentally investigated the solid concentration inside a spouted bed. They found that with an increase in pressure, the solid holdup increases. A similar result was also observed by Yin et al. (2014) for quartz sand of d_p 137 µm as bed material. However, contradictory results for the solid hold up was observed with enhancement of superficial velocity. The axial solid distribution was found to be non-uniform for higher solid mass flux. Moreover, enhancement of pressure in the riser section resulted in inhomogeneous solid distribution. Investigation of axial voidage in PCFB with air as the primary phase was also carried out by Kalita et al. (2013a). The results indicated that bed voidage decreases with an increase in pressure and weight of inventory. Sarbassov et al. (2015) also observed similar results when atmospheric O_2 was taken as a primary phase.

Monazam et al. (2016) reported the effect of solid flux in the formation of axial voidage. They found that with an increase in solid flux, the voidage profile deviates from homogeneity. The attributed reason for the same was cited as the higher solid flux, which accumulates at the bottom of the flash region of the fluidized bed riser before accelerating to the fully developed region.

2.2.4 Suspension density

The suspension density represents the density of the multiphase fluid at each section of the riser. The mathematical expression for suspension density has been derived by Kunni and Lavenspiel (1991) as in Eq. 2.10.

$$\rho_{sus} = (1-\varepsilon)\rho_s + \varepsilon\rho_g \tag{2.10}$$

It is calculated based on the bed voidage magnitude in each section of the riser. The suspension density is a strong function of both gas and solid densities. It is also dependent upon the bed voidage which in turn gets altered by the particle size, bed inventory, superficial air velocity, and operating pressure. Few researchers have investigated the suspension density along with the height of the riser of ACFB by considering the effect of the aforementioned parameters. Gupta and Berruti (1999) compared the profile of experimentally obtained suspension density between pilot, laboratory and industrial scales. Gupta and Nag (2002) studied the variation of suspension density of sand particles in PCFB and reported that the suspension density decreases with an increase in the superficial velocity. They have also reported that, an increase in bed inventory and operating pressure, increases the suspension density at all sections in the riser column. Similar results have also been observed by Kalita et al. (2013a) and Basu et al. (1996). Apart from the study of the effect of pressure on suspension density, they have also investigated the effect of particle size on the suspension density. Suspension density is reported to increase with the decrease in particle size. Similar results are also reported by Miao et al. (2011) with 100% sawdust as bed inventory in the case of ACFB. Cheng and Basu (1999) also observed similar trends during the analysis of the effect of particle size. The effect of particle size and bed inventory on suspension density in a CFB furnace was reported by Basu (2006). The suspension density was found to be increasing with an increase in bed inventory. Yue et al. (2005) demonstrated the exponential relationship between suspension density profile and bed inventory. It was proposed that the suspension density is greatly influenced by bed inventory in a CFB boiler. Ersoy et al. (2004) emphasized the effect of secondary air injection on suspension density. The same suspension density profile was observed across the secondary

air injection point, i.e., the dense region at the bottom flash region and dilute region in the upper zone. Patil et al. (2011) reported the effect of scale-up on the variation of suspension density in CFB riser through correlating area of cross-section. They affirmed that for the same static pressure across the bed cross-section, the suspension density increases with an increase in the cross-sectional area. Besides the parameters mentioned above, it is also influenced by solid mass flux, as reported by Yin et al. (2014). It was found that the suspension density increases when the solid mass flux is increased. As reported from the open literature maximum works are reported on lab-scale considering sand as an inventory. The details of the research carried out for estimating variation in suspension density during lab-scale experiments are reported in Table 2.3.

Table 2.3 Comparison of suspension density with other operating conditions

Investigators	**Riser dimension**		U_{sup} **(m/s)**	**Pr (bar)**	**I**	ρ_s **(kg/m^3)**	d_p (μm)	ρ_{sus} **(kg/m^3)**
	D (m)	H (m)						
Basu and Nag (1987)	0.102	5.5	3-5	1	Sand	2650	87, 227	21.5-96.7
Basu et al. (1996)	0.0525	2.02	3.6-4.8	1- 7	Sand	2818	232,507	600
Cheng and Basu(1999)	0.026	0.33	0.15-0.25	1-8	Sand	2365 2730 2818	90, 232, 503	--
Gupta and Berruti (2000)	0.04 -0.41	3 - 15.1	1.5 -18.3	1	--	660 5200	40 -520	--
Gupta and Nag (2002)	0.0375	1.94	0.25-1.25	2-6	Sand	--	264	160
Kolar and Sundaresan(2002)	0.1×0.1	5.5	4.5-7.3	1	Sand	2740	363	330
Ersoy et al. (2004)	0.23	7.62	3-5	1	Sand, FCC	2600 1600	300, 60	--
Das et al. (2008)	0.1016	5.62	2.01	1	Coal	1150	215	138
Patil et al. (2011)	0.15×0.15 0.20×0.20 0.25×0.25	2.85	2.5-4	1	Sand	2600	460	7.2-288
Kalita et al. (2013a)	0.054	2	5-7	1-5	Sand Sawdust	2300	278, 307, 469	11-800
Yin et al. (2014)	0.068	5.2	6-40	1-5	Quartz sand	2490	137	--

d_p = particle size; ρ_s = density of the solid particle; ρ_{sus} = suspension density;
U_{sup} = superficial velocity; Pr = operating pressure; I= Inventory

2.2.5 Numerical simulations on hydrodynamic study

In addition to the lab-scale experiments, numerical simulations using various algorithms have been attempted for better representation of the actual experiments, thereby enhancing the capability to predict the bed hydrodynamic profile efficiently. In view of the numerical simulation of hydrodynamic behaviour in CFB, the Eulerian-Eulerian model is frequently used.

In the Eulerian-Eulerian model, a set of governing equations are solved for each phase. However, for modeling the dynamics of solid particles, the Kinetic Theory of Granular Flow (KTGF) is implemented. The integration of the KTGF model enables us to determine the solid particulate pressure, particle particulate viscosity, the granular temperature of particles, etc. In fluidized bed simulation, apart from this model, the Euler-Lagrange approach is also incorporated for tracking particle trajectories.

Adamczyk et al. (2014) compared the experimental results with numerical results by using the commercial software ANSYS FLUENT 14.0. They used both Euler-Euler and hybrid Euler-Lagrange approaches for determining the transport of particles in the 3D CFB reactor. They found that using Euler-Euler model, there was a huge difference between experimental and numerical results. Almuttahar and Taghipour (2008) developed a numerical model based on a 2-D Eulerian-Granular approach for modeling hydrodynamics of gas-solid in high-density CFB reactors. In view of determining the effect of solid wall modeling on solid particle concentration, different drag models like Arastoopour, Gidaspow and "Syamlal and O'Brien" were integrated to model no-slip, free slip, and high slip wall conditions. The Syamlal and O'Brien drag model were reported to be a better choice for predicting the solid volume fraction profile. The Syamlal-O'Brien drag model was also found to be best suited for the prediction of solid velocity apart from the solid volume fraction during the investigation of the flow behaviour of high flux CFB riser (Wang et al. 2010). However, Yin et al. (2014) observed that the Gidaspow drag model could predict the pressure drop and radial solid volume profile accurately than other drag models. The experimental results were found to have a good agreement with the numerical results with the use of the Gidaspow drag model in the case of high-flux PCFB riser. Li et al. (2009) also compared the different Eulerian-Eulerian CFD drag models like Syamlal-O'Brien, modified Syamlal-O'Brien, Gidaspow, and modified Gidaspow. They have proposed a four-zone drag model that gives a satisfactory agreement between predicted and experimental results. Zhou et al. (2013) have also incorporated the Gidaspow drag model for analyzing the homogeneous flow structure of fluid catalytic cracking (FCC) particles in the CFB unit. It was observed that with the inclusion of this model, the solid-phase wall boundary condition seems to have less effect on the axial voidage profile.

Shah et al. (2012) studied the effect of mesh size for the numerical simulation of gas-solid drag model based on the Eulerian approach in the CFB riser. They found that the flow of gas-solid was heterogeneous in the fluidized bed, and to have an accurate estimate of the heterogeneous gas-solid flow very fine mesh along with a short time step size is essential. Contrarily, the use

of coarse mesh results in an overestimation of the drag force. Therefore, in order to solve the heterogeneous flow structure in a fluidized bed, energy-minimization multi-scale (EMMS) based drag model is used (Zhou et al. 2013, and Shah et al. 2015). Zhang et al. (2018) investigated the two-fluid (gas-solid) model coupled with the EMMS-based drag model in a PCFB riser having a pressure range from 1-10 bar. With an increase in pressure and axial velocity, uniformity in the radial profile was reported to be decreasing. They also observed that temperature affects the gas density as well as the viscosity of gas and with the increase in gas viscosity axial velocity of solid increases in core zone while it slightly reduces in near the wall regime.

Chalermsinsuwan et al. (2010) compared the hydrodynamics and chemical reaction in 2D CFB riser by considering three different geometries. They observed that tapered-out riser is a suitable configuration for enhancing turbulence inside the system. However, with the use of tapered-in riser, the residence time of the solid was found to be improved. Peng et al. (2011a, b) numerically studied and compared the two-phase gas-solid flow in CFB riser, modeled using the k-ε turbulence scheme with the experimental results. They have studied the effect of distributor design on the radial distribution of solid particles. They proposed that for the gas distributor, center-sparse and side-dense configuration improves the entraining ability of air jets and thereby results in uniformity of radial flow structure. However, for the solid distributor, the side-cover arrangement is recommended as it flattened the core-annulus structure and improves the flow structure. Khongprom et al. (2012) also numerically investigated the gas-solid behaviour in the downflow CFB reactor. The 2-D Eulerian-Eulerian model with the k-ε turbulent model was used for the CFD simulation. They observed that an increase in superficial velocity, particle diameter, and particle density results in increment in axial peclet number. However, peclet number decreases with an increase in solid circulation rate. Kong et al. (2014) studied the simulation of CFB riser for gas-solid flow and used the kinetic theory of granular flow. They observe that the enhancement of solid flux or declination of gas velocity leads to an increase in the solid volume fraction in the riser.

Zhang et al. (2010) presented the 3D CFD simulation of 150 MWe full-loop CFB boiler hydrodynamics with the help of the Eulerian granular multiphase model. They found that using two cyclone separators, non-uniform distribution of solid flux was observed. Luo et al. (2015) carried out a 3D full-loop simulation using CFD discrete element method to study the gas-solid flow in CFB. The results demonstrated that the flow of solid in the riser follows S rising path while in cyclone it follows spirally falling behaviour. Zou et al. (2019) also performed a 3D

simulation of the hydrodynamic property of dual fluidized bed using the Eulerian granular multiphase model. They found that the structure-based drag model gives accurate flow behaviour and precise prediction of a dual fluidized bed under different operating conditions.

2.3 Heat Transfer Studies in ACFB and PCFB

Bed hydrodynamics accompanied by the heat transfer phenomenon plays an important role in designing the fluidized bed unit (Cheng and Basu 1999, Kolar and Sundaresan 2002, Patil et al. 2011). The heat transfer of particle mixtures in a swirling fluidized bed is investigated by Tawfik et al. (2020). With an increase in bed height, the heat transfer coefficient is found to be decreasing for all the blends of the mass fraction. The bed to wall heat transfer coefficient in a BFB considering silica sand, ilmenite and ground steel converter slag as a bed material have been studied by Stenberg et al. (2019). They have compared their bed to wall heat transfer coefficient with the available research data under the temperature range of 400 °C. The heat transfer coefficient is found to be increased with an increase in temperature and a decrease in particle size. Moon et al. (2017) investigated the bed to wall heat transfer coefficient in a ACFB unit. They have analyzed a relationship between bed to wall heat transfer coefficient and particle behavior in ACFB. The instability of the particles in the CFB was determined by fluctuating the operating pressure in the riser and it was also found to depend on the fluidization regime.

The bed to wall heat transfer in a PCFB was studied by Basu et al. (1996), and Kalita et al. (2014). They have investigated the effect of operating pressure and suspension density on the convective heat transfer coefficient, which turns out to be a direct relationship between them. They have also reported that fine particles enhance the heat transfer coefficient. However, the effect of superficial velocity on the heat transfer coefficient was found to be negligible. Wiman and Almstedt (1997) also observed similar results for superficial velocity, particle size, and operating pressure. On the contrary, Gupta and Nag (2002) claimed that the heat transfer coefficient is inevitably influenced by the superficial velocity in the CFB reactor. With an increase in superficial velocity along with pressure, suspension density, and temperature, the heat transfer coefficient was found to be increasing. Similar results were also observed by Reddy and Basu (2001) in their experimental and numerical investigations. They have correlated the enhancement in heat transfer coefficient with an increase in suspension density. As suspension density increases, it tends to form more clusters and concentration of solid

particle which thereby leads to a higher heat transfer coefficient. Ersoy et al. (2004) have also verified that the suspension density affects heat transfer between bed and wall.

The study of heat transfer in PCFB combustor at high-temperature conditions was studied by Winaya and Basu (2001)**.** They have investigated the effect of pressure and CO_2 concentration on the heat transfer coefficient. The enhancement of the heat transfer coefficient was found with the addition of limestone as a catalyst. The heat transfer coefficient was also found to increase with the increase in operating pressure of the system, bed temperature, and concentration of CO_2. However, the effect of CO_2 concentration on radiative heat transfer was found to be negligible during the experimental investigation carried out by Reddy and Basu (2002). The radiative heat transfer coefficient found to be increasing with an increase in operating pressure. Gupta and Reddy (2006) compared results of bed to wall heat transfer in PCFB riser experimentally and numerically. They have observed that with an enhancement of pressure and bed temperature, the thermal conductivity of the particle cluster increases. They have also noticed that the heat transfer between particle and dispersed phase increases with an increase in pressure.

The wall to bed heat transfer coefficient in the upper flash regime of PCFB was studied by Kalita et al. (2013a, 2014). They have witnessed an increase in axial heat transfer coefficient with the increment of pressure, suspension density as well as superficial gas velocity. Nevertheless, the heat transfer coefficient was found to be decreasing with an increase in particle size. Similarly, the variation of the radial heat transfer coefficient was reported to be reducing from wall to core region. Besides, the effect of twisted tape on the bed to wall heat transfer in the upper splash zone of PCFB was also investigated. They have noticed that an optimum twist ratio of four in the twisted tape helps in enhancing the heat transfer coefficient. The increase in the average heat transfer coefficient with twisted tape was found to be 2 to 2.9 times compared to without twisted tap. Kalita et al. (2013b) have reviewed the effect of biomass blending in the wall to bed heat transfer in PCFB riser. It was observed that an increase in the blending of sawdust in sand results in the enhancement of the heat transfer coefficient. Saikia and Mahanta (2017) attempted to describe the transient behaviour of heat transfer in PCFB riser. They have perceived more heat transfer in the near-wall region rather than the core of the riser. They have also noticed that abrupt decrement in fluidized air flow rate results in an instantaneous decrement of heat transfer, which becomes steady at later stages.

2.4 Gasification Studies in ACFB and PCFB

Fluidized bed gasification is one of the promising technologies for the conversion of carbonaceous content in feedstock into syngas. This process eventually occurs inside the reactor of the fluidized bed, where hot air is directly mixed with the feed materials such as coal and different types of biomasses resulting in a series of chemical reactions to produce syngas (Basu 2006). The syngas typically comprises different flammable gases such as CO, CH_4, H_2, and CO_2. To analyze the composition in a more qualitative way and to couple these with the effectiveness of the experimental facility, usually, various parameters such as lower heating value (LHV), dry gas yield (Y), carbon conversion efficiency (CCE) and cold gas efficiency (CGE) are estimated by Mallick et al. (2019). The significant input parameters associated with the operation of gasifiers are equivalence ratio, operating pressure, temperature, feed material, and steam to fuel ratio (Pinto et al. 2010, Seo et al. 2010). The ash formed during the gasification process is also one of the important parameters. It is, in fact, the by-product of this process which can further be used as a marketable solid. The gasification process may be enhanced by using different types of catalysts such as dolomite which absorbs the oxides formed from sulfur. In this section, a brief discussion of available literature incorporating the important input as well as output parameters in regard to gasification studies is presented.

Padban et al. (2000) investigated the tar formation of different sawdust in pressurized bubbling fluidized bed (PBFB) at a pressure of 12 bar. They used the recalcined magnesite as bed material and observed that an increment in pressure gives rise to a reduction in devolatilization and thereby decreasing the tar formation. Mayerhofer et al. (2012) also studied the various parameters like pressure, temperature, and steam on tar production which affect the fluidized bed gasification. Olivine having an average particle size of 0.25 mm was used as bed material. They have carried out experiments at an elevated pressure of 2.5 bar and two different temperature 750°C and 790°C. The analysis indicated that the concentration of H_2 and CO content increases with an increase in temperature. However, the concentration of CH_4 and CO_2 was found to be decreasing. Abdoulmoumine et al. (2014) investigated the gasification characteristics of pine wood sawdust in the BFB gasifier. The effect of equivalence ratio (ER) and temperature on syngas composition along with concentration of tar in the syngas were investigated. They observed that with an enhancement of temperature, Gas yield increases while concentration of tar decreases in the syngas. Berrueco et al. (2014a) also analyzed the formation of tar during the gasification of biomass in PBFB gasifier at an elevated pressure of

5 bar by considering the effect of dolomite for two different ranges of temperature 750°C and 850°C. They used sand and dolomite sieved of particle size 150-200 µm as the bed material. The use of dolomite in place of sand helps the concentration of CO and CO_2 to increase with an increase in temperature. By increasing the operating pressure up to 10 bar, Berrueco et al. (2014b) studied the gasification characteristics and tar formation of torrefied woody biomass in a lab-scale PBFB reactor at an operating temperature of 850°C. They observed that with an increase in pressure, the tar formation increases. Sahoo and Ram (2015) investigated the biomass characteristics in the BFB gasifier for sugarcane bagasse and used different parameters to calculate the effect on syngas production. They had used dolomite, sand, and red mud as a bed material and found that when the mixture of sand and red mud was used in the ratio of 1:1 (wt/wt), H_2 yield was maximum as compared to other contemporary bed materials. They have also observed that with an increase in temperature from 500°C to 850°C, the concentration of H_2 yield enhances, whereas the concentration of CO, CO_2, and CH_4 reduces. Zeng et al. (2016) also investigated the gasification of pine sawdust in a dual fluidized bed having two separate reactors (fuel reactor and steam reactor) for gasification of sawdust. They found that in fuel reactor with an increase in temperature from 700-800°C composition of H_2, CO, and CH_4 increases while CO_2 composition in syngas decreases. The CGE was found to be maximum viz. 77.2% for riser temperature of 820°C. However, in the steam reactor with an increase in temperature from 700-970°C, concentration of H_2 increases while CO, CO_2, and CH_4 decrease. CGE in the steam reactor was reported to have a decreasing trend from 81 to 77% with an increase in temperature. Nevertheless, in the near past, many researchers have been involved with analysing the gasification characteristics in BFB and PBFB reactors by considering different biomasses, bed materials and operating parameters (Jaimes Figueroa et al. 2014, Long et al. 2013, Suksuwan et al. 2018, Kitzler et al. 2011). However, similar studies related to BFB or PBFB along with coal as inventory, have not been explored too much extent.

Huang et al. (2003) analysed the characteristic of Chinese Fugu Coal with an air-steam mixture in BFB at a temperature of 880-980°C and pressure range from 5-14 bar. Xiao et al. (2006) focused on high-temperature gasification of coal in the pressurized spout gasifier. During the gasification, they varied different parameters like pressure (1-5 bar), gasifying agent temperature (300-700°C), ER (0.28-0.48), and steam flow rate (1.1-3.8 kg/hr). They have reported that with an increase in pressure, the concentration of H_2 and CO increases while CO_2 and CH_4 remain almost constant. Analysis of HHV, cold gas efficiency and carbon conversion efficiency reveals an increment of values from pressure 1 to 3 bar. A similar trend was also

perceived by Qin et al. (2007). Termel et al. (2012) examined the gasification of coal in both BFB and PBFB reactors. They noticed that the conversion of coal into syngas increases with temperature and residence time for both BFB and PBFB reactors. Gasification characteristics of underground coal in the BFB gasifier was studied by Konstantinou and Marsh (2015)**.** They surveyed the effect of reactant gas pressure on the syngas composition. They found that the concentration of H_2 is maximum at 9 bar and 16.5 bar pressure respectively. Sanchez et al. (2016) also studied the gasification characteristics of coal and developed a model for coal gasification in the PFB reactor having pressure range 1-6 bar and temperature range 920-1075°C. Gul et al. (2018) described the PBFB reactor gasification for Turkish lignite coal where the operating temperature of the gasifier was varied between 870-880°C and pressure from 2.4-2.7 bar. They have used silica sand as a bed material and mixture of oxygen, steam, CO_2, and air as a gasifying agent.

Unlike the comprehensive investigation of PBFB gasifiers, PCFB has been less explored by the researchers. Li et al. (2001) have investigated the equilibrium modelling for a PCFB gasifier, considering coal as bed inventory and operating pressure in the range of 1 to 1.6 bar. The decrement in CO content along with increment in concentration of hydrocarbon and CO_2 has been reported with an increase in pressure. Garcia Ibanez et al. (2004) experimented on the CFB pilot plant of 300 kW capacity and used olive oil waste as feed material and silica sand as bed material. They observed that with an increase in ER concentration of H_2, CO, and CH_4 decreased while concentration of CO_2 is enhanced due to shifting of gasification to combustion at higher ER. Gas yield and CCE showed an increasing trend whereas LHV decreases with an increase in ER. Srinivas et al. (2008) have performed experiments on a coal-based combined cycle power generation in a PCFB gasifier. Gasifier temperature was reported to increase from 920°C to 980°C with an increase in pressure from 4 to 32 bar. Similarly, the gasifier irreversibility and mole fraction of CO_2 was found to decrease with an increase in gasifier pressure. Srinivas et al. (2009) analyzed the thermodynamic equilibrium model of biomass gasification in the PCFB gasifier. They have considered different biomass like rice husk, sawdust, solid waste, and manure and thereby studied the effect of air-fuel ratio (AFR), steam to fuel ratio (SFR), and gasifier pressure on the syngas production. Duan et al. (2010) have carried out experimentation for the gasification of bituminous coal in a lab-scale PCFB gasifier for the range of pressure 1 to 5 bar. They have reported that with an increase in pressure, the mass flow rate of oxygen increases, which results in an increase in temperature and gasification rate up to ER of 0.39. However, for subsequent ER, combustion plays a significant role. The

LHV of syngas was observed to have maximum value for the stoichiometric ratio of 0.35. The gasification efficiency was found to have a direct relationship with temperature. They have also identified that the syngas concentration of H_2 and CO increases, whereas N_2 and CO_2 decrease with an increase in temperature. Guan et al. (2007) investigated the impact of reaction pressure based on the thermodynamic equilibrium analysis of biomass. They observed that the fraction of syngas composition remains constant under the pressure range 0.1 MPa to 0.6 MPa. Above 0.6 MPa the concentration of H_2 increased rapidly and achieved the maximum value at a pressure of 1.3 MPa, and thereafter the concentration of H_2 starts decreasing slowly with an increase in pressure because at elevated pressure methanation reaction takes place. The mole fraction of CO and CO_2 decreases with the increase in pressure, while the concentration of CH_4 continuously increases with the increase in pressure. Long et al. (2013) examined the production of H_2 rich syngas through PBFB gasification of sawdust and used silica sand as bed material. They observed that the fraction of H_2 and CH_4 increases while the fraction of CO and CO_2 decreases with an increase in pressure. The increase in the fraction of CH_4 is due to water gas shift reaction which enhanced during high pressure. Figueroa et al. (2014) studied the gasification of sugarcane bagasse in the BFB gasifier and found that with an increase in ER, reaction temperature of gasifier increases which ultimately leads to increase in production of syngas. They observed that at ER of 0.28, the production of syngas was 95 wt%. Kitzler et al. (2011) experimented on wood pellet gasification with the use of air, steam, oxygen and CO_2 as gasification agents and olivine as bed material. For their experimental observation, they have varied different parameters like temperature, pressure and air ratio. They realize that the concentration of H_2 is higher in syngas when the temperature is above 820°C and at a pressure lower than 4 bar. They also noticed that the concentration of CH_4 and CO_2 increases with pressure while the concentration of CO follows the opposite trends to CO_2. Li et al. (2018) have examined the co-gasification of coal and meat bone meal in the PCFB gasifier for the range of pressure from 1 to 26 bar. They reported that with an increase in pressure, gasification rate, fuel throughput increases while the formation of slag decreases. They also found that the CCE increases with an increase in pressure. Seo et al. (2010) investigated the gasification and co-gasification of Indonesian Tinto sub-bituminous coal and sawdust in a dual circulating fluidized bed reactor. They observe that at 900°C, temperature gas yield increases with an increase in biomass ratio. They also noticed that the concentration of H_2 and CO were maximum for biomass ratio of 0.5 at 900°C. CGE and calorific value was found to be maximum for 50% blend ratio which was higher than individual gasification of coal and biomass.

In conjunction with the experimental assessment, some of the earlier research works have also been diverted towards numerically simulating these gasifiers. Investigation of gasification characteristics of sugarcane bagasse was studied numerically by Pellegrini and Oliveira Jr. (2007). The numerical investigation was based on the exergy analysis. They observed that an increase in ER concentration of CO decreases, and CO_2 increases due to higher ER gasification converts in the combustion reaction. At ER of 0.25, the concentration of H_2 was found to be maximum and it reaches up to 22%, and at the same point, LHV and CGE were also found to be maximum. They have also noticed that with an increase in moisture content, the concentration of CO decreases while concentration of CO_2 and H_2 increases. On the other hand, the LHV of syngas was found to be decreasing. Li et al. (2009) developed a numerical model for coal gasification of pressurized spout-fluid bed and simulation were done at 1, 3, and 5 bar pressure and a steam temperature of 350°C. Camacho Ardila et al. (2012) numerically examined the numerical model of sugarcane bagasse gasification in the ACFB reactor with the help of Aspen Plus. Zogola et al. (2014) modelled a coal gasifier and tried to simulate the effect of various factors like pressure, temperature, and gasifying agent on the composition of the syngas. They have considered temperature ranging from 500-1500°C and pressure from 1-35 bar for their simulation and used steam and oxygen as a gasifying agent. They have reported that with an increase in pressure, the mole fraction of H_2, CO, LHV as well as CGE decreases while mole fraction of CH_4 and CO_2 increases. However, with an increase in temperature, the LHV, CGE as well as the mole fraction of H_2 and CO increases whereas mole fraction of CO_2 decreases. Adeyemi et al. (2017) compared the experimental results of gasification analysis for Kentucky coal and woody biomass with numerical simulation. The numerical simulation was carried out using ANSYS FLUENT for 2D and 3D geometry, and results were compared. The Eulerian-Lagrangian model was used as the viscous model. Effect of fuel type, pressure, temperature and ER on syngas composition was studied. The numerical results were found to be accorded with the experimental results. Karmakar and Datta (2018) also compared the numerical results with the experimental results of rice husk gasification in BFB. They noticed that the concentration of H_2 and CO increases while CO_2 and CH_4 decreases with an enhancement of temperature. On the other hand, it was found that with an increase in steam to biomass ratio, the concentration of H_2 and CO_2 improved while CO and CH_4 concentration reduces. Both temperature and steam to biomass ratio favored the CCE and CGE. Klimanek and Bigda (2018) developed a CFD modelling of coal gasification in the PCFB gasifier for the range of pressure 1 to 15 bar using both Barracuda and Fluent simulation tool. The simulation

results were compared with the experimental data obtained from a small scale PCFB coal gasifier. Motta et al. (2019) analysed the gasification of sugarcane bagasse in Aspen Plus™ and used different operating parameters like temperature (750-950°C), pressure (1-15 bar), steam to biomass ratio (0.5-1.5), and moisture content (10-30%) to obtain syngas composition. Table 2.4 highlights the summary of literature related to gasification studies by various authors.

Table 2.4 Gasifier specifications

Investigators	Gasifier Specification	Operating conditions	Optimum results
de Jong et al. (1999)	BFB ID: 0.4 m H: 4 m	Air Coal and Biomass, Sand P: 1 MPa, T: 700-900°C	The concentration of CO, CH_4 and C_2H_2 are a function of air/fuel ratio.
Sjöström et al. (1999)	BFB ID: 144 mm H: 600 mm	Oxygen Birch wood-1-3 mm Bituminous coal: 1-1.35 mm Silver sand and olivine sand P: 0.4 MPa, T: 700-900°C	Char production decreases while gas production increases with biomass ratio.
Padban et al. (2000)	BFB ID:102 mm H: 3.3 m	Air, Woody biomass Pre-calcined magnesite d_p: 180 µm P: 0.5-2 MPa, T: 850-950°C	Increasing the pressure reduced the devolatization and decrease tar production.
Li et al. (2001)	ACFB Modelling ID: 100 mm H: 6.3 m	Air Coal d_p< 6 mm P :0.1-0.16 MPa, T:750-900°C	Hydrocarbon and CO_2 increase while CO decreases with an increase in pressure.
Huang et al. (2003)	BFB ID: 200 mm	Air - Steam Chinese Fugu Coal d_p: 0.86-3 mm, V_S: 0.8-1 m/s P: 0.53-1.4 MPa;T: 880-980 °C	H_2: 14.57-18.08% CO: 13.88-14.30% CO_2: 15.9-13.89% CH_4: 2.91-2.55%
Kurkela et al. (2004)	ACFB ID: 154 mm H: 7.9 m	Air, Steam, CO_2 Different biomass Al_2O_3, Silica sand, Limestone, Dolomite, MgO P:0.1-0.13 MPa,T: 600-1000°C U_{mf} : 1-5 m/s	
Xiao et al. (2006)	Spout fluid bed ID: 80 mm H: 1.45 m	Air - Steam Chinese Xuzhou coal d_p: 0.68 µm Silica sand- d_p: 0.75 µm P: 0.1-2.6 MPa,T: 870- 1030°C ER: 0.36-0.42	H_2: 10.6 - 15.2 (vol%) CO: 10.5 - 12.2 (vol%) CO_2: 15.3 - 13.5 (vol%) CH_4: 2.3 - 2.4 (vol%)
Guan et al. (2007)	ACFB	Steam Biomass, corn stalk P: 0.1-3 MPa T: 650-1200°C	Above 6 bar H_2 increases rapidly up to 13 bar and then decreases while CH_4 continuously increases with pressure.

Qin et al. (2007)	BFB ID: 34 mm H: 500 mm	Air - Steam,Sawdust d_p: 80-124 µm P: 0.5-2 MPa, T: 700-900°C	With an increase in pressure, CO and H_2 increases.
Fermoso et al. (2009)	BFB ID: 13 mm H: 305 mm	Steam - Oxygen Coal, biomass, petroleum coke P: 0.5-2 MPa,T: 850-1000°C O/C: 0.15-1.3	The concentration of H_2 and CO increases with the increase in temperature.
Li et al. (2009)	Simulation of Pressurized Spout-fluid bed	Steam - Air Chinese bituminous coal and Xuzhou coal P: 0.1-0.5MPa, T: 270-350°C A/C: 1.65-1.82	With the increase in pressure-volume fraction of H_2, CO and CH_4 increases while CO_2 remains constant.
Srinivas et al. (2009)	ACFB	Air - Steam Rice husk, Sawdust, Solid waste P: 1 – 2 MPa, T: 750-900°C	The concentration of H_2, CO_2 and CH_4 increases while CO decreases with an increase in S/F ratio.
Valin et al. (2010)	BFB ID: 124 mm H: 2.5 m	N_2, Steam Sawdust d_p: 1-2 mm P: 0.2-0.4 MPa,T : 800°C	With an increase in pressure H_2, CO_2, CH_4 and dry gas yield increases while CO content decreases.
Duan et al. (2010)	ACFB ID: 70 mm H: 6.8 m	Air - Steam Chinese bituminous coal d_p: 0.5 mm P: 0.1-0.5 MPa, T: 400-700°C	H_2: 10.55-13.62 vol% CO: 9.57-13.12 vol% CO_2: 16.14-13.7 vol%
Kitzler et al. (2011)	PBFB ID: 80 mm H: 500 mm	Air – Steam – Oxygen Olivine d_p: 500 µm P: 0.1-0.6 MPa T: 750-920 °C	The concentration of H_2 found maximum for 3 bar at above 850ºC. For CH_4 production, higher pressure required while higher CO content requires high temperature and low pressure.
Mayerhofer et al. (2012)	BFB ID:154 mm H: 1500 mm	Steam Wood pellets of 8 mm dia Olivine - d_p: 0.25 mm P: 0.1- 0.25MPa,T: 750-840°C	The concentration of H_2 and CO increases while CH_4 and CO_2 decrease with an increase in temperature.
Han et al. (2013)	BFB ID: 56 mm H: 2300 mm	Cao, Steam Sawdust- d_p: 0.15-0.23 µm Silica sand d_p: 0.23 -0.38 mm P: 0.1-0.4 MPa, T: 530-760°C	H_2: 50.2-62.4% CH_4: 12.5-14.2% CO: 25.6-15.1% CO_2: 5.79-1.21%
Berrueco et al. (2014a)	BFB ID: 23.8 mm H: 404 mm	Steam - Oxygen Torrefied biomass (250-500µm P: 0.1 - 1 MPa, T: 850°C	H_2 yield and CO decreases while content of CH_4 and CO_2 increases with increase in pressure

Berrueco et al. (2014b)	BFB ID: 23.8 mm H: 404mm	Air - Steam Torrefied Biomass 250-550 µm Sand and Dolomite 150-200 µm P: 0.5 MPa, T: 750-850°C	H_2, CH_4 and dry concentration of gas increases with an increase in temperature.
Zogola et al. (2014)	Simulation	Air, Oxygen, Steam Coal P: 0.1-3.5 MPa,T : 500-1500°C	H_2 and CO decreases while CH_4 and CO_2 increases with the increase in pressure.
Sanchez et al. (2016)	BFB Simulation	Air-Steam coal P: 1-5 MPa, T: 650-800°C	Effect of pr. variation for H_2 and CH_4 was very negligible
Adeyemi et al. (2017)	BFB ID: 66 mm H: 1540 mm	Air Kentucky coal woody waste d_p: 100 µm P: 1-3 bar; T: 650-1100°C	Formation of CO and H_2 increases while CO_2 decreases with temperature enhancement.
Gül et al. (2018)	BFB ID: 300 mm H: 3500 mm	Air, Oxygen, Steam and CO_2 Coal- d_p: 0.5-1 mm Silica sand- d_p: 644 µm P: 2.4-2.7 bar,T: 850-930°C	H_2: 31.5-34.2% CO_2: 33.7-37.8% CO: 18.6-22% CH_4: 4-4.6%
Klimanek and bigda (2018)	ACFB Modelling ID: 80 mm	Air - Steam Coal P: 0.1-1.5 MPa, T: 1000°C	The concentration of H_2 is less in analysed system compare to conventional reactor.
Li et al. (2018)	ACFB L: 300 mm W: 30 mm H: 1.45 m	Oxygen - Steam JCA coal and MBM d_p< 6mm Polystyrene- d_p: 1.32µm P: 0.1-2.6 MPa, T: 900-1400°C	The rate of gasification increases with an increase in pressure.
Mallick et al. (2019)	ACFB ID: 153 mm H: 3.5 m	Air Coal, Sawdust, Bamboo dust, Rice husk T: 500-850°C ER: 0.19-0.35	With increase in ER, CO, H_2 and CH^4 is found to be decreases. Optimum condition for 60:40 coal-biomass (wt/wt) ratio at ER 0.29.

From the ongoing discussion trend of gas composition with operating parameters is given in the tabular form (Table 2.5). From the table, it is observed that with an increase in operating parameters such as equivalence ratio (ER), temperature (T), steam to fuel ratio (S/F), pressure (P), it is difficult to distinguish the trends of the syngas. There are no particular trends of syngas is observed and the trend is difficult for different operating conditions. The trends are also a function of gasifier specifications. Hence, it is more important to investigate the gasification study under a pressurized condition.

Table 2.5 Effect of operating parameters on gas composition

Investigators	Operating parameters (↑)	Gas composition			
		H_2	CO	CH_4	CO_2
Li et al. (2001)	ER	↓	-	↑↓	↑
	T	↑	↑	↓	↓
Huang et al. (2003)	T	↑↓	↑	↑	↓↑
	P	↑	↑↓	↑↓	↓
Garcia Ibanez et al. (2004)	ER	↑↓	↓	↓	↓↑
	T	↑	↑	↓	↓
Xiao et al. (2006)	ER	↑↓	↑↓	↓	↑
	T	↑	↑	↑	↓
	P	↑≈	↑	≈	↓
Qin et al. (2007)	T	↓↑	↓↑	--	↓
Guan et al. (2007)	T	↑↓	↑	↓≈	↑↓
	P	≈↑	≈↓	≈↑	≈↓
	S/F	↑	≈	↓	↑
Pellegrini and Oliveira Jr. (2007)	ER	↑↓	↓	↓	↓↑
Srinivas et al. (2008)	T	--	--	--	↑
	P	--	--	--	↓
	S/F	--	--	--	↑
Srinivas et al. (2009)	ER	↓	↓	↓	↓
	P	↓	↑	↑	↓
	S/F	↑	↓	↑	↑
Li et al. (2009)	ER	↓	↑↓	↓	↑
	P	↑	↑	↑	↑
Duan et al. (2010)	ER	↑	↑	↓	↑
	T	↑	↑	↓	↓
	P	↑	↑	↑	↑↓
	S/F	↑	↑↓	↓	↓
Seo et al. (2010)	T	↑	↑	↑	≈
	S/F	↑	↓	↓	↑
Kitzler et al. (2011)	ER	↓	↓	↓	↑
	S/F	↑	↓	↑	↓
Karmakar and Datta (2011)	T	↑	↑	↓	↓
	S/F	↑	↓	↑	↑
Mayerhofer et al. (2012)	T	↑	↑	↓	↓
	P	--	↓	↑	↑
	S/F	↑	↓	↓	↑
Camacho Ardila et al. (2012)	ER	↓	↓	--	↑
	T	↓	↑	--	↓
	S/F	↑	↓	--	↑
Long et al. (2013)	T	↑	↓	↓	↓
	P	↑	↓	↑	↓
	S/F	↑	↑	↓	≈
Zogola et al. (2014)	ER	↑	↑	--	↑
	T	↑≈	↑≈	↓	↓

	P	↓	↓	↑	↑
	S/F	↑	↑	↑	↑
Abdoulmoumine et al. (2014)	ER	↓	↓	↓	↑
	T	↑	↑	↓	↓
Berrueco et al. (2014 a)	T	--	↑	↑	↑
Berrueco et al. (2014 b)	P	↓	↓	↑	↑
Jaimes Figueroa et al. (2014)	ER	↑	↑	↑	↓
	T	↑	↑	↑	↓
Konstantinou and Marsh (2015)	P	↑↓	↑↓	↑	--
Sahoo and Ram (2015)	T	↑	--	--	--
Sanchez et al. (2016)	ER	↓	↓	↓	↑
	T	↑	↑	↓	↓
	P	↓	↓	↑	↑
	S/F	↑	↓	↓	↑
Zeng et al. (2016)	T	↑	↓↑	↑	↓
	S/F	↑	↓	↑	↓≈
Adeyemi et al. (2017)	ER	↑	↑	--	↓
	T	↑	↑	--	↓
	P	↑	↑	--	↓
Motta et al. (2019)	T	↑	↑	↓	↓
	P	↓	↓	↑	↑
	S/F	↑	↓	↓	↑

2.5 Co-gasification studies in ACFB and PCFB

Jong et al. (1999) experimented on the co-gasification of biomass in PBFB at a pressure of 10 bar while temperature varies in the range of 700-900°C. Sand was used as bed material, while limestone was used as an additive. The use of limestone as an additive has a synergistic effect on gasification characteristics. They have reported that CGE increases with ER due to the higher reactivity of biomass during the devolatilization and gasification reaction. Similarly, Pan et al. (2000) investigated the co-gasification of low-grade coal with biomass and reported the effect of blending on the performance of fluidized bed co-gasification. They found that the composition of syngas was directly dependent on the blending ratio. They observed that concentration of $CH_4 + C_2H_2$ enhanced from 0.92 to 2.22% and 1.59 to 3.2% as blending of pine chip ratio increases in black coal and sabero coal, respectively. The percentage of CO concentration in syngas and LHV was reported to be increased as the proportion of pine chip increases. Pinto et al. (2002) studied the co-gasification of pinewood with plastic waste in a fluidized bed with air and steam as the gasifying medium. An increase in bed temperature seems to have resulted in an enhancement in the concentration of H_2 and gas yield while the concentration of C_nH_m, CO and CO_2 decreases. They have also observed that upon plastic waste addition to pine wood, the concentration of H_2 increases up to 50%, while the content of CO

decreases. Aznar et al. (2006) focused on the elimination of plastic waste produced in the BFB reactor with the help of coal and sawdust. For the co-gasification purpose, coal, biomass, and plastic waste were used in the ratio of 60:20:20 (wt%) and the experiments were carried out within a temperature range of 750 - 880°C. They noticed that with an increase in temperature, the concentration of H_2 increases from 12-15%, CO increases from 7.5-12%, and gas yield increase from 1.7-4 Nm^3/kg while the concentration of CO_2 decreases due to Bouduard reaction. They also observed that the concentration of CH_4 and LHV increases whereas tar content decreases due to enhancement of bed temperature. Kumabe et al. (2007) studied the co-gasification of coal and woody biomass at a temperature of 900°C on a fixed bed gasifier. With an increase in biomass ratio, conversion of tar and H_2 decreases whereas the concentration of CO_2 in product gas increases. However, the concentration of CO was found to be independent of biomass. Fermoso et al. (2009) also investigated the co-gasification of bituminous coal with a different type of biomass in the PFB reactor at a pressure range of 0.5-2 MPa and temperature varying between 800-1000°C. They have observed that higher temperature improvises the gasification process and due to the enhancement of endothermic reaction associated with gasification, H_2 and CO concentration increase with an increase in temperature. Co-gasification of coal and biomass in the BFB reactor was also studied experimentally by Li et al. (2010)**.** Chinese bituminous coal was used as a coal inventory along with rice straw and pine sawdust as biomass. Apart from that, co-gasification involving coal and biomass in bubbling fluidized bed was studied by many researchers (Sjostrom et al. 1999, Velez et al. 2009, Fermoso et al. 2010, Masnadi et al. 2015).

However, studies related to co-gasification characteristics in ACFB and PCFB are limited. Only a few literatures have reported the same on PCFB. Lapuerta et al. (2008) examined the co-gasification and gasification of coal and biomass in the ACFB gasifier. They have reported a significant effect of blending ratio characteristics on syngas production as compared to temperature variation. As the biomass content increases, the concentration of H_2, CO and CH_4 increases in syngas, and also the gasification efficiency increases exponentially. Seo et al. (2010) investigated the gasification and co-gasification of Indonesian Tinto sub-bituminous coal and sawdust in a dual circulating fluidized bed reactor. They have perceived that at 900°C of bed temperature, gas yield increases from 0.4-0.8 m^3/kg with an increase in biomass ratio. They have also noticed that the concentration of H_2 and CO were maximum for biomass ratio of 0.5. CGE and calorific value were also reported to have the same trend having a maximum value of 0.5 and 14.39 MJ/m^3 respectively for 50% blend ratio which was higher than individual gasification of coal and biomass independently. Aigner et al. (2011) also examined

the co-gasification of coal and biomass in the dual fluidized bed reactor. The biomass material was considered to be wood chips whereas olivine was used as bed material. Experimental results indicated that as the amount of coal in the blending ratio is increased, the concentration of H_2 increases while the content of CO decreases. However, the CGE increases from 48-62% as biomass was varied from 0-100%. Due to the higher volatiles content of wood, CCE was found to be higher than coal and with the enhancement of biomass ratio, the CCE of co-gasification also increases. Li et al. (2018) analysed the gasification and co-gasification of Jincheng Anthracite (JCA) along with meat and bone meal (MBM) in pressurized fluidized bed gasifier having a pressure range of 0.1 to 2.6 MPa and temperature varying from 900-1000°C. With an increase in pressure, the gasification rate was observed to be accelerating and the fuel throughput is increased in the gasifier. Due to the activation of more exothermic reaction with an increased in pressure, enhancement of gasification rate is observed. They have also observed that with the increase in pressure, the slag formation decreases. Mallick et al. (2019) investigated the co-gasification of coal sawdust in the ACFB reactor. They have varied the parameters like temperature (700-900°C), ER (0.19-0.35), and blending ratio (80:20, 60:40, 40:60, and 20:80) for their observations. They have noticed that with an increase in ER, the concentration of H_2, CO, and CH_4 decreases while the concentration of CO_2 increases in produced gas. With the increment in ER, LHV of syngas was found to be decreasing while CGE and CCE of syngas increases. They have found the maximum value of CGE and CCE as 56 and 99%, respectively, for ER of 0.35. They have also reported that dolomite as a gasifying agent, increases the gas yield of produced gas, whereas tar yield decreases. Peng et al. (2017) have also performed similar studies and have investigated the effect of co-gasification on coal-biomass blends in a PCFB gasifier for the range of pressure up to 20 bar considering different catalytic agents such as $NaHCO_3$, $KHCO_3$, and K_2CO_3. They found that the gas composition of H_2 and CO is higher for K_2CO_3 as a catalytic agent among all the considered variants, which further results in higher heating value. The inclusion of different catalyst results in the decrement of CO_2 and increment of H_2. They have also studied the tar content and reported that the tar yield decreases with an increase in catalyst mass ratio.

After a comprehensive review of the literature, it has been observed that the gasification characteristics are a strong function of gas compositions, which is further used for the calculation of LHV of gas. Apart from this, the dry gas yields, CCE and CGE are also subject of interest of the present study. This section presents the literature review consisting of the relationship between different input parameters to the syngas production and other significance output conditions.

2.6 Research Gap

It is observed from the literature review that both the numerical and experimental studies on bed hydrodynamic have been conducted by the large number of researchers in ACFB. The majority of the numerical study addresses the flow regimes and validation of different drag models, such as Symalal-Oberyan, Gidspow, modified Gidspow, EMMS, etc. The effect of the restitution coefficient and spirituality coefficient on bed voidage and axial velocity are also reported in numerical studies. However, the results of numerical studies deviate from real ACFB problems due to a large number of assumptions and simplified 2D studies. On the other hand, most of the experimental studies are reported on laboratory-scale ACFB units where flow and heat transfer characteristics widely differ from industrial ACFB units. Further, many of the papers are published with sand as bed inventory (Basu and Nag 1987, Patil et al. 2011, Kalita et al. 2013a), and the air is used as the fluidizing medium. But in real practice coal is used as inventory in the power plants. Since the density of coal is half of the density of the sand, the bed hydrodynamics and subsequently heat transfer vary widely in practical conditions. Some authors have studied the effect of blending by using mixtures of sand and sawdust as inventory. Again, it is worth mentioning that hydrodynamics is a strong function of particle densities. The effect of pressure on the ACFB unit is reported by a few researchers and the effect of pressure on blends of coal and biomass is limited.

Many authors have successfully conducted the gasification study both in the laboratory and pilot-scale gasifiers. Coal and different available biomasses have been used as a feed material. To avoid the problem of density difference of these biomasses and to properly fluidize these materials, sand is used as bed material. After continuous running of these gasifiers chocking near the nozzle area is observed in actual practice but due to limited run on a laboratory scale, the same is not reported on literature. Some modern plants replace sand as bed material with different catalyst and the ash formed during gasification also acts as bed material. It is also observed from the literature that with an increase in operating parameters such as equivalence ratio, temperature and steam flow rate it is difficult to distinguish the trends of the syngas production. Syngas production is also related to the geometry and operating pressure of the gasifier. Such investigations are important from the industrial design point of view but limited in academic research.

In the co-gasification study, many authors have reported the effect of the blending of coal and biomass at different percentages by weight. The effect of particle size is limited in open

literature but getting biomass at a constant particle size is also difficult in practice. The use of catalysts like dolomite is available in the literature under atmospheric conditions. The effect of pressure on co-gasification under the above operating conditions is limited. The co-gasification studies under low-grade coal and biomass without using biomass are hardly reported in the literature. Hence, a detailed study is required under pressurized conditions using blends of coal and biomass in a circulating fluidized bed unit.

2.7 Aim and Objectives

The aim of the present work is to investigate hydrodynamics, heat transfer, and gasification characteristics of low-grade coal, biomass, and blends of coal and sawdust in a PCFB unit.

The scope of the present work includes:

- Development of a PCFB gasifier and study of hydrodynamic and heat transfer characteristics under different operating parameters. It is proposed to conduct both the numerical as well as experimental investigations for a thorough understating of the hydrodynamics and heat transfer of the PCFB.
- Performance evaluation of the PCFB gasifier to study the effect of feed material, superficial velocity, and operating pressure on bed voidage, suspension density, solid circulation rate, and temperature distribution.
- Gasification study of the PCFB unit with coal and biomass as feed material.
- Performance evaluation of the gasifier in terms of gas composition, LHV, gas yield, cold gas, and carbon conversion efficiency, etc.
- Performance evaluation of co-gasification with blends of low-grade coal and sawdust in various proportions with and without the in-situ catalyst.

2.8 Summary

In the end, the review of the earlier work has clearly suggested that gasification is a novel and cleaner technology for sustainable power production. To improve the efficiency of the gasifier pressurized bed comes into picture and had a great effort on the efficiency of the plant. The future generation of ACFB will be through the gasification route under pressurized conditions. Finally, the need for improvement of ACFB gasifier under the pressurized condition and various feed materials such as low-grade coal and biomass such as sawdust, rice husk and sugarcane bagasse is the objectives of the present study.

Chapter – 3

Numerical Simulations on PCFB Riser

3.1 Introduction

Pressurized circulating fluidized bed (PCFB) is highly preferred among its other variants due to its compactness and high bed-to-wall heat transfer capability. Bed hydrodynamics, being closely associated with the heat transfer phenomenon, plays an essential role in designing the PCFB unit. Prior to actual experiments, it is always desirable to have a numerical estimate of the parameters related to bed hydrodynamics, as it will help the inefficient operation of the unit. Various experimental studies have been carried out to investigate the effect of operating parameters on bed hydrodynamics. Yates (1996, 1997) has performed experiments using Geldart A and B particles to study the effect of pressure and temperature on gas-solid fluidization. Kalita et al. (2013) and Gupta and Nag (2000) has conducted similar studies on PCFB which reported an increase in axial bed voidage at the bottom of the bed and a decrease of the same at the top zone with an increase in operating pressure. Monazam et al. (2016) observed T shaped voidage profile at the riser exit, which is linearly related to the solid flux and density of the gas and solids. Khurram et al. (2016) investigated the relationship between solid circulation rate and pressure drop of PCFB riser, where they found that the pressure drop increases as the solid circulation rate or the particle size increases.

Due to associated experimental uncertainties and complexities, it is always not possible to investigate the effect of operating parameters on bed hydrodynamics. Therefore, numerical studies for the PCFB unit is desirable. However, numerical analysis has been only limited to investigate different aspects of bed hydrodynamics and heat transfer for the ACFB unit. Benyha et al. (2000) have simulated the riser section of an ACFB through k-ε turbulence modeling. Neri and Gidaspow (2000) and Shah et al. (2012) have simulated the riser section to obtain the time-averaged data for particle concentrations and fluxes, which confirms the existence of core annulus flow regime. However, the literature on numerical simulation of a PCFB riser in investigating hydrodynamics is found to be limited.

In line with the above limitation, the present investigation has been focused to investigate the 2D bed hydrodynamics in a PCFB riser by using ANSYS FLUENT 14. The riser of height 2 m and diameter 0.054 m is considered for the present investigation. Air is considered as primary

fluid, whereas coal with a mean particle diameter of 307 μm is considered as secondary fluid. The present simulation has been carried out for an operating pressure range of 1 to 10 bar with 500^0 C input air temperature. A Eulerian-Eulerian model is considered for the multi-phase flow simulation. Results found in the present simulation are compared with the published data of Mahapatro et al. (2014) to demonstrate the effect of the type of inventory on bed hydrodynamics.

3.2 Governing Equations

For obtaining numerical results, mass, momentum, and energy conservation equations for each phase are solved simultaneously. The conservative form of the above-mentioned equations was solved by using the finite volume approach with the help of ANSYS FLUENT 14. The dispersed turbulence (k - ε) multiphase model has been incorporated for accurate modeling.

The mass conservation equation for the gas phase is Shah et al. (2012)

$$\frac{\partial(\varepsilon_g \rho_g)}{\partial t} + \nabla.(\varepsilon_g \rho_g \mu_g) = 0 \tag{3.1}$$

The mass conservation equation for the solid phase is given by

$$\frac{\partial(\varepsilon_s \rho_s)}{\partial t} + \nabla.(\varepsilon_s \rho_s \mu_s) = 0 \tag{3.2}$$

The volume fractions of solid and gas give

$$\varepsilon_s + \varepsilon_g = 1 \tag{3.3}$$

The conservation of momentum equations for the gas and solid phase are given in Eqs. (3.4) and (3.5), respectively.

where ε_g and ε_s are the volume fraction of the gas and solid phase respectively. ρ_g and ρ_s are densities of the gas and solid respectively. μ_g and μ_s are viscosity of gas and solid respectively.

The momentum equation for gas and solid phase are represented in Eqs. 3.4 and 3.5 respectively.

For gas

$$\frac{\partial}{\partial t}\left(\varepsilon_g \rho_g \vec{v}_g\right) + \nabla.\left(\varepsilon_g \rho_g \vec{v}_g \vec{v}_g\right) = -\varepsilon_g \nabla P_g + \nabla.\bar{\bar{\tau}}_g + \varepsilon_g \rho_g \vec{g} + \vec{F}_{d.g} + \vec{F}_{\mathrm{l}.g} + \vec{F}_{\mathrm{vm}.g} \tag{3.4}$$

For solid

$$\frac{\partial}{\partial t}\left(\varepsilon_s \rho_s \vec{v}_s\right) + \nabla.\left(\varepsilon_s \rho_s \vec{v}_s \vec{v}_s\right) = -\varepsilon_s \nabla P_g - \nabla P_s + \nabla.\bar{\bar{\tau}}_s + \varepsilon_s \rho_s \vec{g} + \vec{F}_{d.\mathrm{s}} + \vec{F}_{\mathrm{l}.\mathrm{s}} + \vec{F}_{\mathrm{vm}.\mathrm{s}} + \bar{S}_s \tag{3.5}$$

where $\overrightarrow{v_g}$ and $\overrightarrow{v_s}$ are the velocity vector for gas and solid, phase respectively. ∇P_g and ∇P_s are the pressure drop associated with gas and solid phase. $\overline{\overline{\tau_g}}$ and $\overline{\overline{\tau_s}}$ are the gas and solid phase stress tensor respectively. $\overrightarrow{F_{dg}}$ and $\overrightarrow{F_{ds}}$ are drag forces associated with the gas and solid phase respectively. $\overrightarrow{F_l}$ is the lift force and $\overrightarrow{F_{vm}}$ is the virtual masses, where the subscript g and s denotes for gas and solid phase, respectively. $\overline{S_s}$ is the solid-phase source term.

The constitutive equations are given in Eqs. (3.6-3.8).

$$\vec{F}_{d.g} = \beta_{gs}(\vec{v}_s - \vec{v}_g),\ \vec{F}_{d.s} = -\vec{F}_{d.g} \tag{3.6}$$

$$\vec{F}_{l.g} = 0.5\rho_g\varepsilon_s\left(\vec{v}_s - \vec{v}_g\right).\left(\nabla\times\vec{v}_g\right),\quad \vec{F}_{l.s} = -\vec{F}_{l.g} \tag{3.7}$$

$$\vec{F}_{vm.s} = -\vec{F}_{vm.g} \tag{3.8}$$

where the drag coefficient between the gas and solid phase is denoted by β_{gs}.

The drag model proposed by Syamlal- O'Brien is given in Eqs. (3.9-3.13)

$$\vec{F}_{vm.g} = 0.5\rho_g\varepsilon_s\left(\frac{D\vec{v}_s}{Dt} - \frac{D\vec{v}_g}{Dt}\right), \tag{3.9}$$

$$\beta_{gs} = \frac{3}{4}\frac{\varepsilon_g\varepsilon_s\rho_g}{v_{r,s}^2 d_s}C_D\left(\frac{\mathrm{Re}_s}{v_{r,s}}\right)\left|\vec{v}_s - \vec{v}_g\right| \tag{3.10}$$

$$C_D = \left(0.63 + \frac{4.8}{\sqrt{\mathrm{Re}_s / v_{r,s}}}\right)^2 \tag{3.11}$$

$$v_{r,s} = 0.5\left[A - 0.06\,\mathrm{Re}_s + \sqrt{(0.06\,\mathrm{Re}_s)^2 + 0.12\,\mathrm{Re}_s(2B - A) + A^2}\right] \tag{3.12}$$

$$A = \varepsilon_g^{4.14} \text{ and } B = 0.8\,\varepsilon_g^{1.28} \text{ for } \varepsilon_g \le 0.85 \text{ and } B = \varepsilon_g^{2.65} \text{ for } \varepsilon_g > 0.85 \tag{3.13}$$

where $\frac{D\vec{v}}{Dt}$ is the substantial time derivative for gas velocity where the subscript g and s denotes for gas and solid phase, respectively. $v_{r,s}$ is the relative velocity of solid particles, d_s is the diameter of the solid phase, C_D is the drag coefficient, Re_s is the solid Reynold number.

The granular temperature of solids is the one-third of the mean square velocity of particles i.e.,

$$\Theta_s = \frac{1}{3} v_s'^2 \tag{3.14}$$

where Θ_s granular temperature, $v_s'^2$ is the mean square velocity of particles

The kinetic fluctuation energy equation is given in Eq. (3.15-3.16)

$$\frac{3}{2}\left[\frac{\partial}{\partial t}\left(\rho_s \varepsilon_s \Theta_s\right) + \nabla.\left(\rho_s \varepsilon_s \vec{v}_s \Theta_s\right)\right] = \left(P_s \bar{I} + \bar{\tau}_s\right) : \nabla \vec{v}_s + \nabla.\left(k\Theta_s \nabla \Theta_s\right) - \gamma \Theta_s + \phi_{gs} \tag{3.15}$$

where $(-p_s \bar{I} + \bar{\tau}_s): \nabla \overrightarrow{v_s}$ is the generation of energy by the solid stress tensor, γ_{Θ_s} is the dissipation of energy due to collision

$$\phi_{gs} = -3k_{gs}\Theta_s \tag{3.16}$$

The collisional dissipation of energy is given in Eq. 3.17.

$$\gamma \Theta_s = \frac{12\left(1-e_{ss}^2\right) g_{o,ss}}{d_s \sqrt{\pi}} \rho_s \varepsilon_s^2 \Theta_s^{3/2} \tag{3.17}$$

The diffusion coefficient of energy is given in Eq. 3.18.

$$k\Theta_s = \frac{150\rho_s d_s \sqrt{\Theta_s \pi}}{384(1+e_{ss}) g_{o,ss}}\left[1 + \frac{6}{5} g_{o,ss} \varepsilon_s (1+e_{ss})\right]^2 + 2\rho_s \varepsilon_s^2 d_s (1+e_{ss}) g_{o,ss} \sqrt{\frac{\Theta_s}{\pi}} \tag{3.18}$$

The solid pressure is given in Eq. 3.19.

$$P_s = \rho_s \varepsilon_s \Theta_s + 2\rho_s \left(1+e_{ss}\right) \varepsilon_s^2 g_{o,ss} \Theta_s \tag{3.19}$$

The radial distribution function is given in Eq. 3.20.

$$g_{o,ss} = \frac{1 + 2.5\varepsilon_s + 4.59\varepsilon_s^2 + 4.52\varepsilon_s^3}{\left[1 - \left(\frac{\varepsilon_s}{\varepsilon_{s,\max}}\right)^3\right]^{0.678}} \tag{3.20}$$

The collision viscosity is given in Eq. 3.21.

$$\mu_{s.col} = \frac{4}{5} \varepsilon_s d_s \rho_s \left(1+e_{ss}\right) g_{o,ss} \sqrt{\frac{\Theta_s}{\pi}} \tag{3.21}$$

The solids bulk viscosity is given in Eq. 3.22.

$$k_s = \frac{4}{3} \varepsilon_s d_s \rho_s \left(1+e_{ss}\right) g_{o,ss} \sqrt{\frac{\Theta_s}{\pi}} \tag{3.22}$$

where k_s is the thermal conductivity of solids, $g_{o,ss}$ is the solid radial distribution function, e_{ss} is the particle–particle restitution coefficient.

3.3 Simulation Conditions

Figure 3.1 shows the riser section of a PCFB used developed by Kalita et al. (2013a) in numerical simulation of the multiphase flow. The geometry of the riser is 0.054 m in diameter (D) and 2 m in height (H).

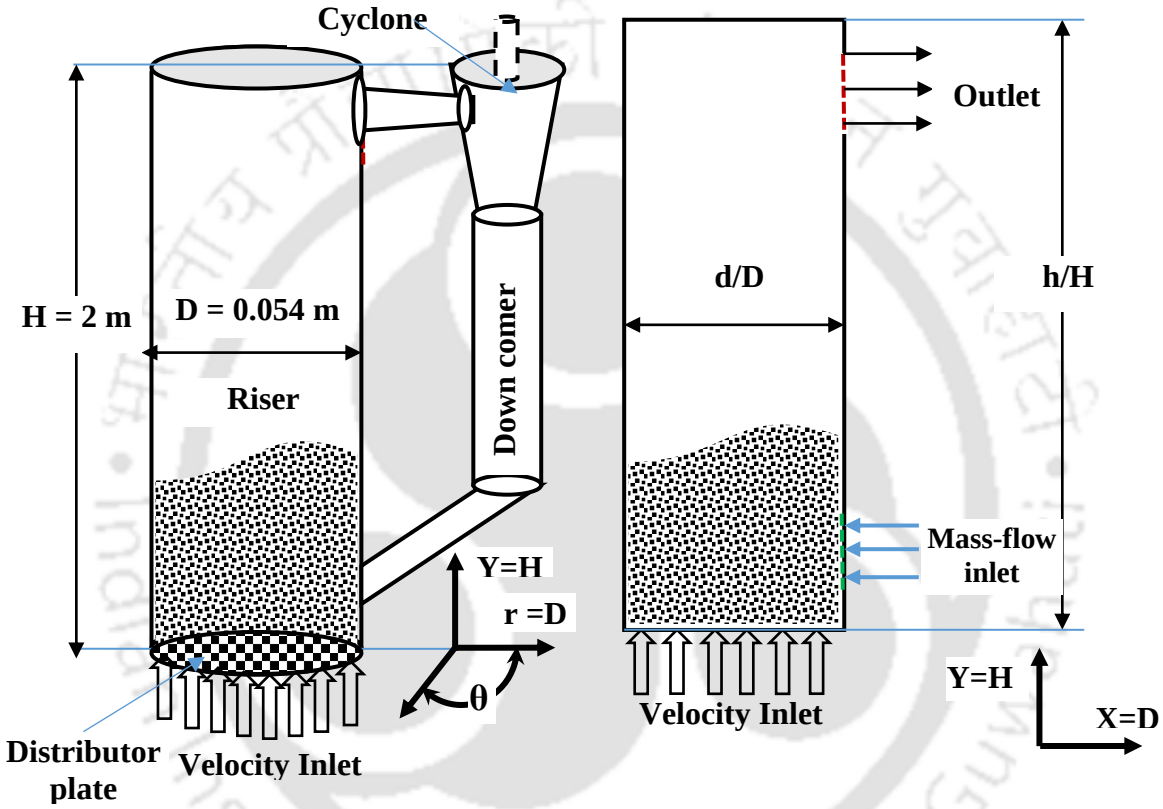

Riser set-up (Kalita et al., 2013a) Riser 2D computational domain

Fig. 3.1: Schematic diagram of simulated riser

The velocity inlet boundary condition for gas-phase entry, mass flow inlet for solid-phase entry, and pressure outlet boundary conditions for the exhaust of the solid-gas mixture has been considered. The multiphase simulation was performed for both the fluids viz. air and solid phases. The solid particles used in the simulation consist of sand with an average diameter of 307 μm and a density of 2300 kg/m^3. Simulations were performed with a constant superficial velocity of 6 m/s by varying the operating pressures from 1 bar to 15 bar. The geometric parameter of the riser and the properties of solid and gas considered in the present investigation are presented in Table 3.1.

Table 3.1: Basic Geometry and properties

Geometry and properties	Value	
	Sand	Coal
Riser diameter, *(m)*	0.054	0.054
Riser height, *(m)*	2	2
Particle size, (μm)	307	307
Gas density, $\left(kg\,m^{-3}\right)$	1.225	1.225
Solid density, $\left(kg\,m^{-3}\right)$	2300	1350
Gas viscosity, (Pas)	1.000000	1.000000

3.4 Numerical Solution Methodology

The geometry for the simulation work is created in the design modeler, and meshing has been done in ANSYS workbench mesh editor. The 2-D computational domain consists of 14 grids radially and 230 grids axially. As a result, 3228 numbers of cells are created during grid generation for the present domain. All the governing equations are solved by the finite volume approach. Phase coupled SIMPLE scheme is used for pressure-velocity coupling of gas-solid flow. The second-order upwind scheme is incorporated for momentum discretization; however, for calculating volume fraction QUICK scheme is used. To simulate the PCFB condition inside the flow domain, the operating pressure is initialized with the intended pressure. The simulation is carried out for a real-time of 40 s having a time step of 0.0001s with 20 iterations per time step. All the computational parameters are presented in Table 3.2.

Table 3.2: Simulation parameters

Simulation parameters	Value
Viscous model	Turbulent
Under-relaxation parameter	
Pressure	0.5
Momentum	0.4
Granular temperature and Volume fraction	0.2
Discretization	
Momentum and Granular temperature	Second-order upwind
Maximum particle volume fraction	0.63

3.5 Boundary Conditions

At the inlet section of the flow domain, superficial velocity is assumed as constant whereas, at the outlet, atmospheric exit condition for the gas-solid mixture is imposed. For the return leg, solid mass flux was taken to be constant. Johnson-Johnson wall boundary conditions consisting of no-slip condition for the gas phase and specified shear condition for the solid phase are considered. The quantitative data for all the boundary conditions are given in Table 3.3.

Table 3.3: Boundary conditions

Type	Conditions	Value
Inlet	Gas superficial velocity *(m/s)*	6
	Solid volume fraction	0.54
	Granular temperature	0.01
	Mass flux (kg/m^2s)	28.325
Outlet	Pressure outlet gauge pressure *(Pa)*	0
	Backflow granular temperature (m^2s^{-2})	0.01
	Backflow volume fraction	0.01
Wall	Specularity coefficient, φ	0.0005
	Particle-particle restitution coefficient, e_s	0.95

3.6 Grid Independence Test

To confirm the CFD results to be independent of mesh size, simulations were performed at three different mesh sizes viz. 1614 cells, 3228 cells, and 6456 cells. The computed local bed voidage along the height of the riser for different cell sizes are plotted in Fig. 3.2. It can be observed that for the cells sizes of 3228 and 6456, the bed voidage variation seems to be unaltered. However, the computational time required for 6456 cell sizes is 1.5 times more than that of 3228 cells. Henceforth, the cells sizes of 3228 are found suitable for providing a reasonably mesh independent result at the expense of less computational time. Hence, this mesh size is considered for further investigations.

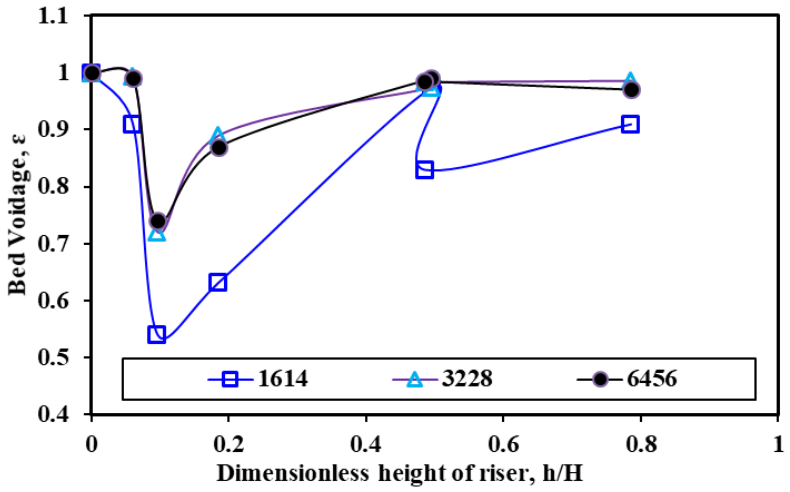

Fig. 3.2 Grid independency test

3.7 Results and Discussion

The axial and radial variations of bed voidage are compared with the experimental data of Kalita et al. (2013a) to validate the adopted numerical approach. The bed voidage, suspension density, voidage at the radial direction, axial velocity, and temperature profile for different simulations conditions for sand and coal is presented below.

3.7.1 Effect of pressure on bed voidage

Figures 3.3 and 3.4 show the comparison of bed voidage along with the height of the PCFB riser at operating pressures of 1 to 10 bar considering sand as the bed inventory. The bed voidage profile is obtained using the Gidaspow drag model, air velocity of 6 m/s, a particle size of 307 μm. It is observed that, particularly in the bottom portion viz. 0.2 (h/H) from the inlet zone, the voidage is lesser, and it increases along with the bed height. It is also observed that bed voidage decreases with an increase in operating pressure.

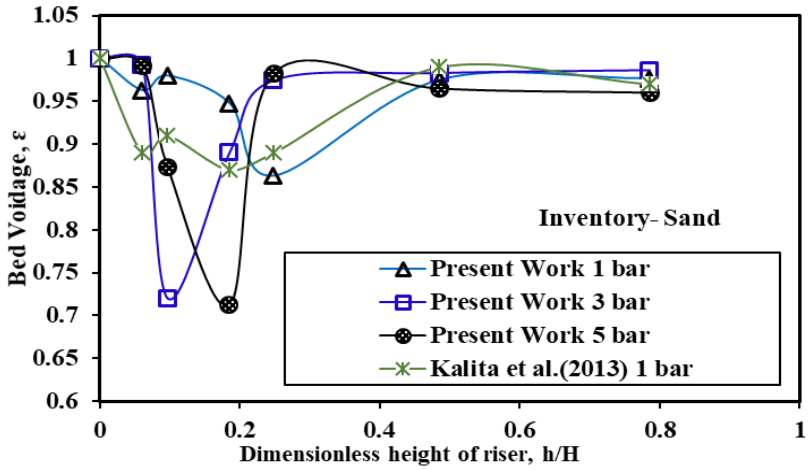

Fig. 3.3. Variation of bed voidage with different pressure

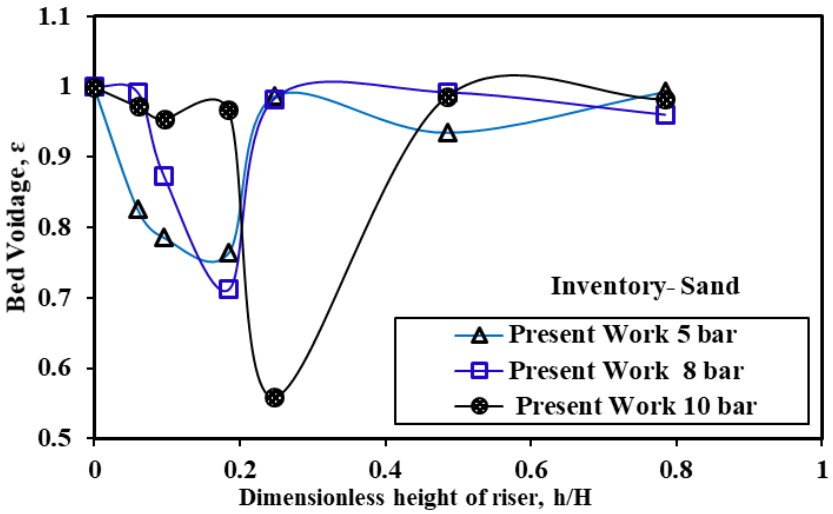

Fig. 3.4. Variation of bed voidage with different pressure

As observed in Fig. 3.3, the numerical results are found to be in good agreement with the experimental data in terms of peak magnitude, whereas there seems to be a minor deviation in trend as in the case of numerical simulation, there is a phase shift as compared to the experimental result. It is also observed that there is a phase shift for minimum voidage with an increase in bed pressure. This is due to the dominance of pressure drag over the frictional drag.

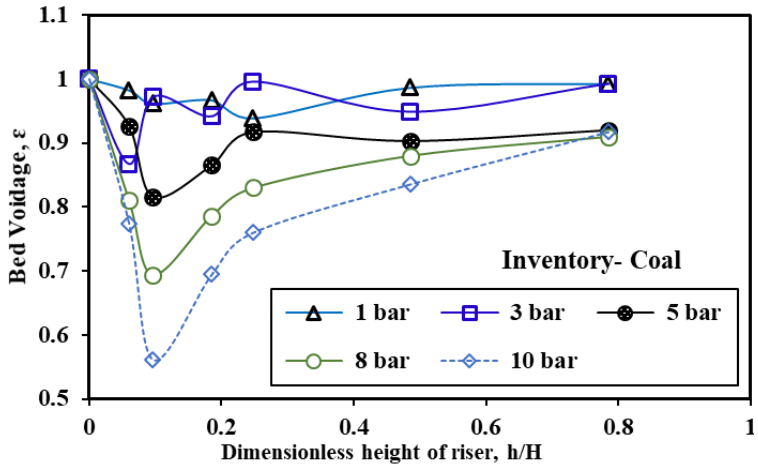

Fig. 3.5 Variation of bed voidage with different pressure

Similarly, the comparison of bed voidage along the height of the PCFB riser at operating pressures of 1 to 10 bar for coal as the bed material has been shown in Fig. 3.5. Here the bed voidage profile is also obtained using the Gidaspow drag model with a velocity of air as 6 m/s, and with the particle size of 307μm.

It is observed from the figure that the voidage increases along with the height of the bed. However, voidage is observed to be less at the bottom of the bed. It is also found that bed voidage decreases with an increase in operating pressure. A phase shift is prominent for minimum voidage with an increase in bed pressure. This indicates the dominance of pressure drag over the frictional drag. Bed voidage profile is flatter at high pressure (8 and 10 bar) same exhibits the typical S profile at relatively low operating pressure (1 to 5 bar).

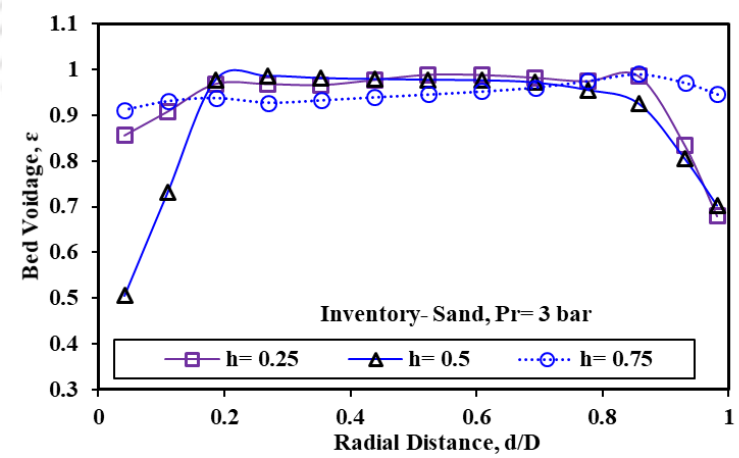

Fig. 3.6. Radial voidage distribution at different height of the riser for sand as inventory.

Further, the bed voidage profile across the radial direction is also investigated at different locations viz. 0.25, 0.5, and 0.75 (h/H) above the inlet for both sand and coal as the bed inventory at an operating pressure of 3 bar. From Fig.3.6, it has been observed that, with the

increase in height, the voidage profile becomes flattered in the radial direction for sand as the bed material. This is because the solid concentration decreases with the height of the riser. Similarly, Fig. 3.7 demonstrates the voidage profile for coal as bed inventory, which is observed to be flat in the core. However, voidage decreases near the riser wall. This is because of the increase in solid concentration near the wall.

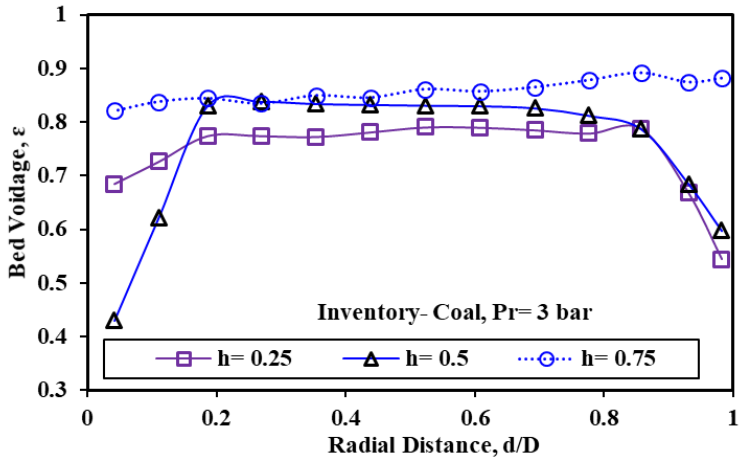

Fig. 3.7 Radial voidage distribution at different height of the riser for coal as bed inventory.

3.7.2 Effect of pressure on suspension density

Effect of pressure on suspension density along the height of the riser at an operating pressure of 1-10 bar for sand as inventory is given in Fig. 3.8, whereas for coal inventory it has been given in Fig. 3.9. The suspension density of the bed (ρ_{sus}) is defined by Kunii and Levenspiel (1991) as $\rho_{sus} = \rho_s(1-\varepsilon)+\varepsilon\rho_g$. The suspension density is made as custom field function in ANSYS FLUENT 14, and after the convergence of code, the profile is obtained for different pressure.

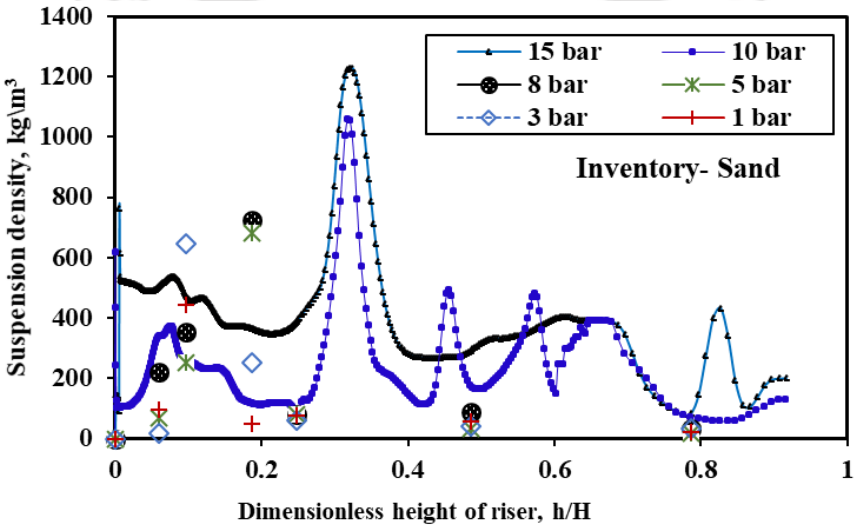

Fig. 3.8. Variation of suspension density at different pressure

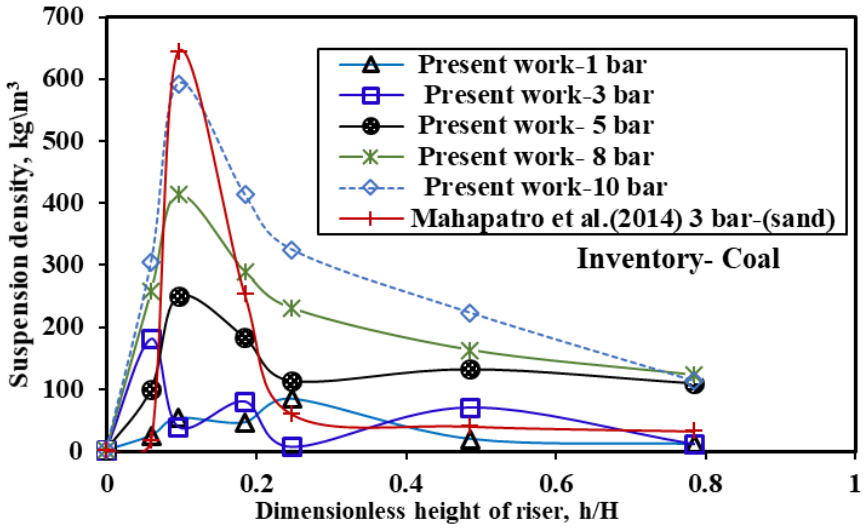

Fig. 3.9 Variation of suspension density at different pressure for present simulation

It is observed that for both the inventory, at higher pressure, the suspension density is more at the middle and top part of the riser, which delivers better heat transfer coefficient at these locations at higher pressure. It is noticed that suspension density increases as pressure increases along with the height of the PCFB riser in case of sand inventory for all the operating conditions.

The present simulation data of suspension density for operating pressure of 3 bar with coal particles as inventory is compared with Mahapatro et al. (2014) where the sand was used as inventory. The trend of suspension density (Fig. 3.9) is comparable to the data of Mahapatro et al. (2014), but the difference in value is due to the type of inventory used in both the simulations.

3.7.3 Variation of axial solid velocity

Figure 3.10 shows the contour of mean sand velocity throughout the riser. It is observed that, near the wall, there is a backward flow of solid particles as seen from negative velocity in contour. The maximum velocity of the solid particle is obtained at the central region of the riser and decreases gradually towards the wall.

Figure 3.11 shows that radial solid volume fraction at three axial positions (h/H) = 0.25, 0.5 and 0.75. The figure indicated that the solid volume increases near the wall of the riser. However, at the core, the volume fraction decreases which indicates that the core-annular structure of the riser has prevailed. The reason is due to the increase in solid velocity at the core of the riser and decrease in the solid velocity near the wall of the riser, which can be explained by Figure 3.12 radial solid velocity graph. Figure 3.12 shows the radial solid velocity

graph at three different axial positions. It was observed that the solid moves with a higher velocity at the core of the riser, whereas solid velocity near the wall decreases.

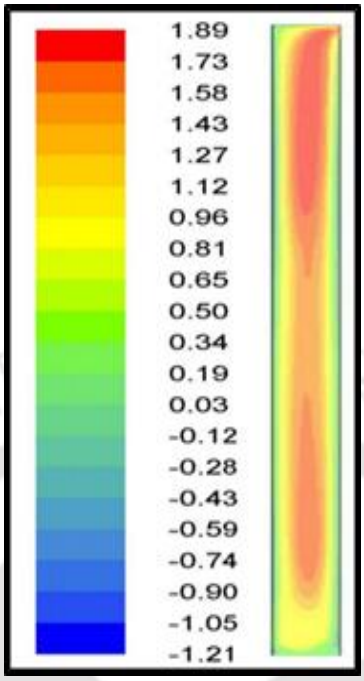

Fig. 3.10. Contours of mean sand velocity in m/s

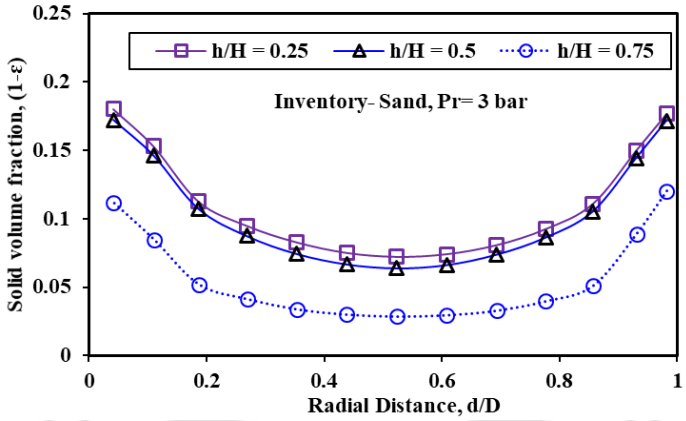

Fig. 3.11 Variation of solid volume fraction with sand as an inventory

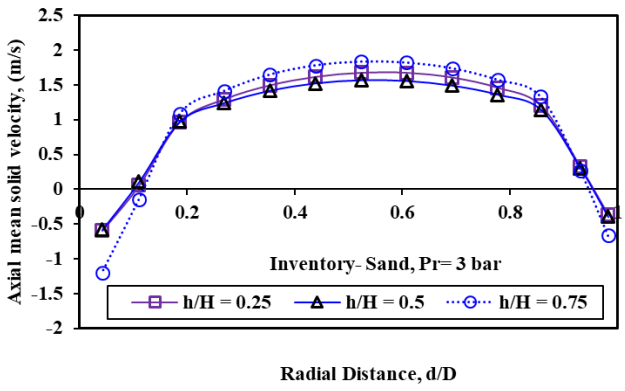

Fig. 3.12 Variation of axial mean solid velocity with sand as an inventory

3.7.4 Effect of pressure on temperature profile

The temperature variations along the bed height at a superficial velocity of 6 m/s and at an operating pressure of 1 bar to 10 bar for 600 g bed inventory as coal with the input air temperature at 500^0 C is shown in Fig. 3.13. It has been found that the bed is not isothermal. The maximum temperature is recorded at 0.35 (h/H) above the distributor. Then it tapers off along the height of the riser. It has been observed the bed temperature increases with higher inlet pressure. Due to the proper mixing of solid particles at higher pressure a uniform variation of temperature has been observed.

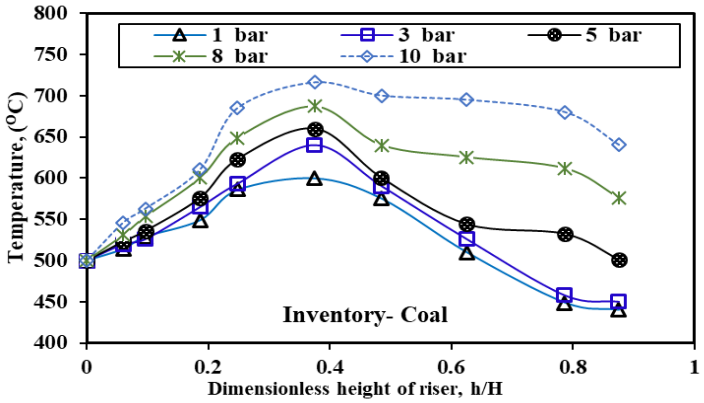

Fig. 3.13 Variation of bed temperature at different pressure for present simulation

3.8 Summary

From the present simulation, it can be concluded that the numerical results for bed voidage and suspension density along the height of the riser at an operating pressure of 1 bar are comparable with the earlier published results. Flatten S-Shaped bed voidage profile along the height of the riser has been observed. An increase of suspension density has been found with an increase in operating pressure. The bed temperature also seems to have an increasing trend with an increase in operating pressure. Results obtained during the study will be helpful for the scale-up and design of a PCFB riser. Bed voidage decreases with an increase in operating pressure.

- ✓ Suspension density is a strong function of pressure, and it increases with an increase in operating pressure as well as density of the inventory.
- ✓ The temperature inside the riser is also increased with an increase in operating pressure due to proper mixing and higher interaction between gas and solid particles.

Finally it is observed from numerical studies that suspension density and temperature are strong function of operating pressure. Based on the same, a PCFB gasifier with a riser diameter D = 0.1 m and a height H = 3 m is fabricated and installed subsequently.The detail description of experimental set-up and experimental procedure are described in the next chapter.

Chapter – 4

Experimental Set-Up and Procedure

4.1 Introduction

This chapter deals with the experimental setup and operating procedure for the developed Pressurized Circulating Fluidized Bed (PCFB), which is intended for investigating the bed hydrodynamics, gasification, and co-gasification studies. Typically, the different components of the PCFB units include riser, cyclone separator, downcomer, and distributor plate. These components are designed based on the theory of fluidization and numerical simulations done in the previous chapter.

4.2 Experimental Setup

The schematic and the pictorial view of the PCFB gasifier are shown in Figs. 4.1 and 4.2, respectively. The PCFB unit is comprising of a riser, downcomer, and cyclone separator. The riser is made of stainless-steel having ID 100 mm, the height of 3000 mm and thickness of 5 mm, which is further connected to cyclone separator through a horizontally connecting pipe of the inner diameter of 50 mm. The cyclone separator is also fabricated using stainless steel having dimensions of 660 mm in length and having a barrel ID of 160 mm. The detailed design of the same is presented in Appendix- I. The top of the cyclone separator remains open to the atmosphere, whereas the bottom end is connected to the downcomer of ID 50 mm. It can be also observed that half part of the return leg section is made of a transparent tube to facilitate the measurement of solid circulation rate. Afterward a return leg viz. downcomer is attached to the bottom of the riser column, at a distance of 150 mm above the distributor plate. A gateway valve is also installed in the downcomer section to avoid any backflow from the riser.

Initially, the PCFB unit is supplied with air through the bottom of the riser, i.e. distributor plate by using a centrifugal blower (15 hp electric motor). Simultaneously, a reciprocating compressor (Make: Ingersoll Rand (IR), capacity: 220 litters, run by 3 hp motor, model: S-01480) is incorporated to increase the system pressure inside the bed in case of pressurized bed experiments. The airflow rate from the blower has been measured using an orifice meter (BS 1042) and is regulated through a valve arrangement before sending it to the riser. This air is

further routed through a straight-hole based distributor plate which is having a 16.4% opening area. The geometrical details of the distributor plate is presented in Appendix- II. Pressure probes at ten discrete locations (above the distributor plate) have been mounted to measure the axial variation in static pressure magnitude. Calibration of these sensors are testified in Appendix- III. To avoid any entrainment of coal and sawdust particles into the pressure probes, a wire mesh size of 220 µm and cigarette filters are provided in front of the sensing surface. After obtaining a reduction in static pressure, the bed voidage and suspension densities have been estimated between these locations. Static pressures are measured along with the riser height at 10 (ten) different locations such as 175 mm, 355 mm, 540 mm, 720 mm, 895 mm, 1330 mm, 1580 mm, 1830 mm, 2420 mm and 2750 mm, respectively above the distributor plate. To avoid entrainment of coal particles into the pressure probes, fine wire mesh (Mesh size of 200 µm) and cigarette filters are used at the pressure tapping ends connected to the riser. After getting the static pressure drop, bed voidage and suspension densities have been estimated between these locations. Similarly, 18 (eighteen) K- type thermocouples are mounted at distance of 160 mm, 311 mm, 464 mm, 613 mm, 765 mm, 915 mm, 1235 mm, 1380 mm, 1520 mm, 1652 mm, 1797 mm, 1935 mm, 2245 mm, 2380 mm, 2518 mm, 2658 mm, 2797 mm, 2935 mm, respectively along the height of the riser from distributor plate to monitor the bed temperature. Also, 10 (ten) more thermocouples have been installed on the outer surface of the riser wall to measure the rise in wall temperature during experiments, which is also verified through the usage of temperature gun. Detailed Calibration of these thermocouples are described in Appendix- IV.

During the experiments with a hot PCFB unit, all the components remain unaltered with respect to the cold unit except the replacement of the transparent downcomer section by a stainless-steel section. Also, the inlet air from the blower is preheated using an electric heater box to the desired temperature before feeding it to the riser. Simultaneously, during the experiments at higher system pressure than the atmosphere, the pressurized exhaust air from the compressor is also passed through a tubular heater section to increase its temperature. Further, as both the air coming from the compressor and blower is fed to the riser, therefore a thermocouple has been installed before the distributor plate to monitor the inlet temperature of the air. The pressure sensor taps have been closed during these experiments, as the same can't be employed for high-temperature applications. The schematic of the hot PCFB unit is illustrated in Fig. 4.1.

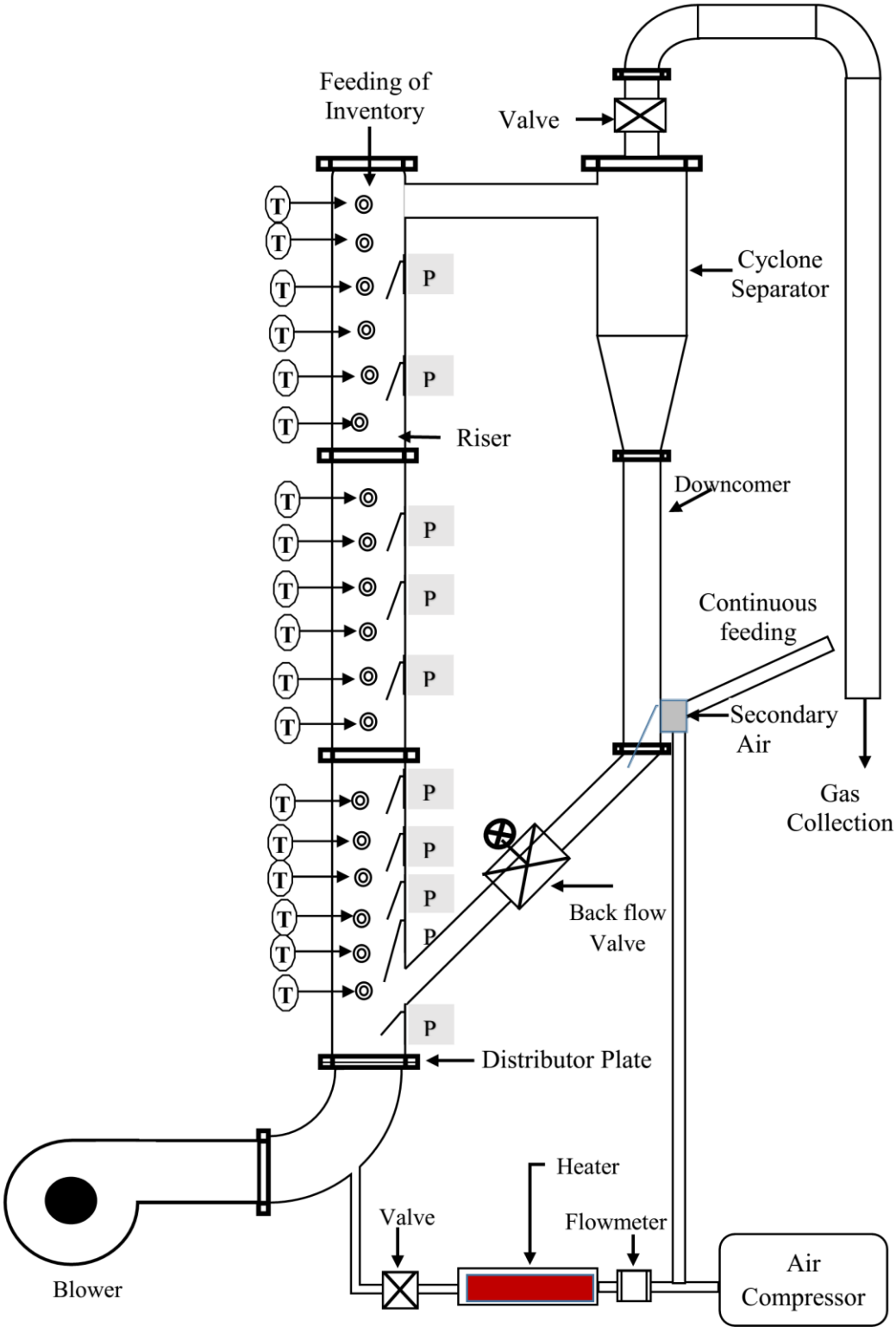

Component	ID (m)	OD (m)	Height (m)
Riser	0.1	0.11	3
Cyclone separator	0.16	0.17	0.66
Downcomer	0.05	0.06	--
Gas collection unit	0.04	0.05	2.5

Fig. 4.1 Schematic diagram of the PCFB experimental setup

Fig. 4.2 Photograph of the PCFB experimental setup

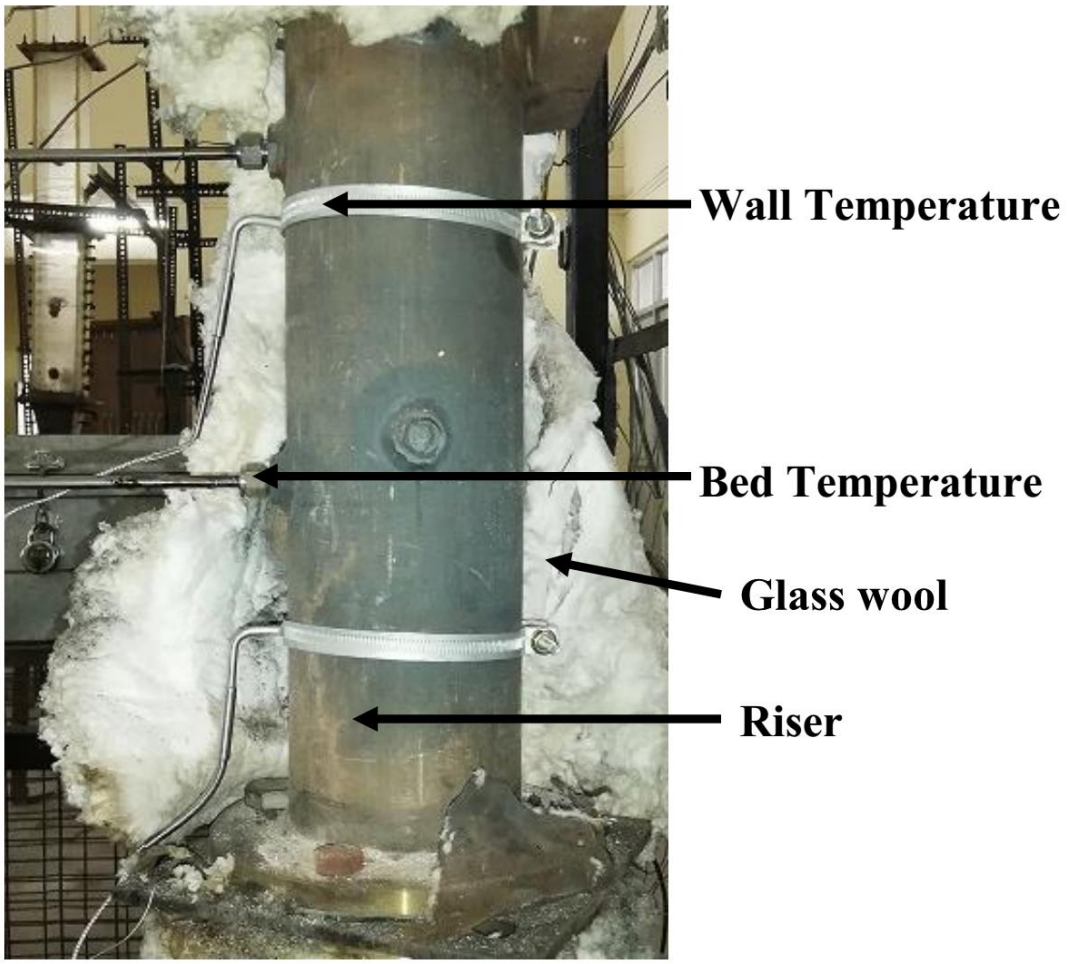

Fig. 4.3 Thermocouple arrangements

Before collecting the syngas in a telder bag it needs to be cooled for analysys in gas cromotogphy. For cooling the gas, a heat exchanger is developed where water is considered as the cold medium which absorbs heat from the hot syngas, thereby reducing its temperature to ambient condition.The heat exchanger comprises of a stainless steel tube of 40 mm outer diameter, 5 mm thickness and having a length of 2500 mm. A closely packed helical copper coil is having an outer and inner diameter of 6.8 mm and 5.04 mm, respectively is placed interior to the tube section. Through this coil water is passed in the counter-flow direction,while, the hot gas passes through the core of the heat exchanger downwards. to monitor the inlet and outlet temperature, thermocouples were installed at the inlet and outlet of of the gas flowing section for measuring the tempearute of the product gas.

The mounting of thermocouples are presented in Fig. 4.3. The accessories and sensors used for the experiments are presented in Fig. 4.4 and their specifications are given in Appendix V.

Blower

Compressor

Pipeline connection with blower

Electric Heater

Pressure Sensor

Thermocouple

Data Accucation System

Dc power supply

Roll Crusher

Sieves

Fig. 4.4 Instrumentation and sensors used in experiments

4.3 Experimental Procedure

The experimental procedure for cold-bed hydrodynamic study and hot-bed gasification study is described below.

4.3.1 Hydrodynamic study

A desirable quantity of coal and sawdust blends are provided into the PCFB unit through upstream of the riser. Sawdust was chosen as inventory due to its availability, moderate calorific value with ready to use form. Air is fed from the blower into the PCFB unit through the distributor plate placed at the bottom section of the riser. To regulate the airflow rate from the blower, a gate valve has been installed. Further to measure the inlet air flow rate, an orifice meter is incorporated at 1,000 mm ahead of the gate valve. Also, a U-tube manometer whose ends are connected to D and D/2 tappings of the orifice meter is used to measure the differential pressure across the flow. This estimate is used to calculate the superficial velocity corresponding to the particular experimental condition. During the cold bed studies, experiments have been conducted both at atmospheric as well as pressurized system conditions. For pressurized bed experiments, a reciprocating compressor is used simultaneously to increase the operating pressure. The compressor delivery pressure is measured using a high precision pressure gauge (**make**: Swagelok). The air from the blower and compressor are mixed in the plenum chamber before feeding it to the riser section. As already mentioned, the pressure sensors are mounted at the locations above to measure the absolute pressure along with the riser height, and thereby, the pressure difference along the length of the riser is used for evaluating the bed voidage and suspension density at the desired locations. Further, the mixture of coal and sawdust particles and the air is directed towards the cyclone separator where the air moves out of the PCFB unit to the atmosphere, whereas the blends of coal and sawdust particles due to high density move through the separator to the downcomer. During the cold bed studies, one half of the downcomer section has been made transparent to measure the solid circulation rate. To get an estimate of the same, for a certain time scale, a ball valve is installed at the end of the transparent section, so that the height of the solid particles accumulated during that time can be measured through a vertical scale. Further, this measured height can be used to calculate the solid circulation rate. The employed pressure sensors are calibrated beforehand. These pressure sensors have been connected to a data acquisition system for the measurement of local pressure variation. All the readings are recorded with the help of the data acquisition system

once the steady-state is achieved. It takes normally 20-25 min for achieving steady flow in the riser during cold bed studies.

4.3.2 Gasification and co-gasification studies

During gasification studies, hot air at the range of 500 to 700^{0}C is produced and compressor is used for the fluidization of feed materials. The operating procedure Later to cold bed studies, hot-bed related investigations have also been carried out. During the experiments, the operating procedure for the set-up is the same regardless of the nature of the experiments viz. cold bed or hotbed. However, during hot bed studies, the inlet air to the riser from the compressor and blower is heated to a specific temperature through providing heater coils for both the unit separately. The input power to the heater coils are controlled through auto transfer assembly, and also both the heater boxes are sealed properly using glass wools and aluminum foil to restrict any heat loss to the atmosphere. Further, the input heat flux is calculated using the values of the power supplied to the heater coils. To monitor the inlet temperature of the air, also a thermocouple has been installed before the distributor plate. As mentioned earlier, the temperature variation along the height of the riser is measured using 18 thermocouples installed in the axial direction. From these estimations of the rise in temperature and the input heat flux, bed to wall heat transfer coefficient is evaluated.

For proper utilization of the heat content available in the flue gases that are being exhausted through the top of the cyclone separator, it is further connected to the inlet of a shell and tube heat exchanger. During the operation of the heat exchanger, water is considered as the working medium. The inlet and outlet temperatures of both water and flue gas are measured using thermocouples. Afterward, the exhaust air from the heat exchanger is collected in telder bags, which is analyzed using gas chromatography to get an estimate of the percentage composition.

4.4 Working Formula

The bed hydrodynamics investigations are carried out through measurements of parameters like bed voidage, suspension density, and solid circulation rate. Similarly, for the heat transfer studies, temperature profile along the height of the riser is measured. Lower heating value (LHV), dry gas yield (Y), carbon conversion efficiency (CCE) and cold gas efficiency (CGE) have been calculated from experimental data. The working formula to evaluate all the pertaining parameters are given in following sub-sections.

4.4.1 Superficial velocity

The superficial velocity $\left(U_{sup}\right)$, defined as the volume flow rate of air per unit cross-section of the bed (Kalita et al. 2013a), can be expressed as

$$U_{sup} = \frac{\dot{m}_a}{\rho_g \times A_B} \tag{4.1}$$

Once a U-tube water manometer measures the pressure drop through the orifice, the superficial velocity (m/s) may be calculated (Kalita et al. 2013a) by using the following relation

$$U_{sup} = \frac{\dot{m}_a}{\rho_g \times A_B} = 4.844 \times \sqrt{\Delta P} \tag{4.2}$$

where $\dot{m}_a$ is the mass flow rate of the air, A_B is the crossectional area of the pipe through which air is flowing, ρ_g is the density of the air, and ΔP is the difference in the height of manometric fluid (water) in cm of water measured across the orifice plate.

4.4.2 Bed voidage

The bed voidage (ε) is defined as the volume fraction of the bed occupied by air bubbles. In this case, the static pressures are measured using piezoresistive type pressure transmitters, and the difference between two consecutive pressure tapping is calculated. Then bed voidage may be calculated (Kalita et al. 2013a) by using the Eq.4.3

$$\varepsilon = 1 - \frac{10 \times \Delta h}{\rho_s \times L_m} \tag{4.3}$$

$$\varepsilon = 1 - \frac{10 \times \Delta h}{\rho_s \times L_m} \times 1019.72 \tag{4.4}$$

where Δh is the difference in water column between two consecutive water columns and L_m is the distance between them in m. ρ_s is the density of solid in kg/m^3.

A constant of 1019.72 is used as a conversion factor for converting one bar to a centimeter of the water column. Initially, the experiments are conducted using both pressure sensors and manometric boards. It is observed from experiments that in atmospheric bed both pressure sensors and manometric board give almost the same results, but at the elevated bed, the pressure

sensors give the accurate result. This is because it is very difficult to take readings by using a manometric board at high pressures. In our case, the bed voidage is calculated using Eq. 4.4.

4.4.3 Suspension density

The suspension density (ρ_{sus}) can be evaluated by the relation as proposed by Kunni and Levenspiel (1991)

$$\rho_{sus} = \varepsilon \rho_g + (1-\varepsilon)\rho_s \tag{4.5}$$

where ε is the voidage and ρ_g is the density of air in kg/m^3.

4.4.4 Solid circulation rate

The solid circulation rate or solid mass flux (G_s) is one of the critical parameters in the PCFB units. To increase the heat transfer coefficient while the plant is running, only one thing is possible, i.e., to increase the solid mass flux because other parameters are difficult to control. The solid mass flux is calculated by measuring the solid accumulation height in the transparent downcomer at a particular time. The solid mass flux is calculated by using the equation 4.6

$$G_s = \frac{\rho_s \times L_a \times A_D \times (1-\varepsilon_{mf})}{A_B t} \tag{4.6}$$

ε_{mf} : Bed voidage at minimum fluidization

L_a : Solid accumulation height in m

A_B : Cross-sectional area of the riser in m^2

A_D : Cross-sectional area of downcomer in m^2

t : Time required (in sec) to accumulate a particular height after the closure of ball valve

G_s : Solid circulation rate in kgm^{-2}s^{-1}

4.4.5 Lower heating value (LHV)

The lower heating value (LHV) of the syngas has been calculated using the Eq.4.7 (Pan et al. 2000, and Xiong et al. 2004).

$$\mathrm{LHV}_{Syngas} = 4.2 \times \left[\begin{matrix} (25.7 \times H_2) + (30 \times CO) + (85.4 \times CH_4) \\ +151.3 \times (C_2H_2 + C_2H_4 + C_2H_6) \end{matrix} \right] \tag{4.7}$$

where H_2, CO, and CH_4 are the volumetric percentage of the components of the syngas obtained from gas C. In the present case, higher-order terms of C_mH_n is neglected because these terms cannot be obtained from gas chromatography analysis (Mallick et al. 2019, and Duan et al. 2010).

4.4.6 Dry gas yield (Y)

The dry gas yield (Y) of the syngas is defined as the ratio of the mass flow rate of nitrogen into the gasifier to the product of mass flow rate of the feed material and volumetric percentage of nitrogen obtained from gas chromatography analysis. Xiao et al. (2006) and Ju et al. (2010) have calculated Y using the Eq. (4.8) where the ash content of the feed material was not considered. Other researches such as Mallick et al. (2019) have calculated Y considering the ash content of the feed material using Eq.4.9. Since in our experiments, low-grade coal with high ash content is used as the feed material, so Y is calculated by using Eq.4.9.

$$Y = \frac{Q_a \times 0.79}{M_b \times N_2\%} \tag{4.8}$$

$$Y = \frac{Q_a \times 0.79}{M_b (1 - X_{ash}) \times N_2\%} \tag{4.9}$$

where Q_a is the mass flow rate of air in Nm^3/hr, M_b is the mass flow rate of the feed material in kg/hr, N_2 is the volumetric percentage of nitrogen present in the syngas obtained from gas chromatography and X_{ash} is the percentage of ash present of the feed material from the proximate analysis.

4.4.7 Carbon conversion efficiency (CCE)

The carbon conversion efficiency (CCE) is the ratio of the volumetric percentage of carbonaceous gas species present in the syngas to the solid carbon present of the feed material. The solid carbon present of the feed material is calculated from the ultimate analysis. The CCE is calculated based on Y using Eq. 4.10 (Ju et al. 2010, Liu et al. 2012, and Sharma et al. 2015).

$$\eta_{CCE} = \frac{Y \times (CO\% + CH_4\% + CO_2\%)}{22.4 \times (C/12)} \tag{4.10}$$

4.4.8 Cold gas efficiency (CGE)

The cold gas efficiency (CGE) is the ratio of chemical energy of the syngas to the energy content of the feed material. The CCE is calculated based on Y using the Eq.4.11 (Xiao et al. 2006, Ju et al. 2010, Liu et al. 2012, and Niu et al. 2019).

$$\eta_{CGE} = \frac{LHV_{gas} \times Y}{LHV_{fuel}} \tag{4.11}$$

4.5 Summary

The experimental setup and procedure are described in this chapter. All the equations related to the hydrodynamics and gasification study are also presented with a brief description. Results and discussion on the hydrodynamic and heat transfer study of coal and blends of sawdust with coal is presented in Chapter 5.

Chapter – 5

Results and Discussion of Hydrodynamic and Heat Transfer Studies in PCFB Unit

5.1 Introduction

This chapter presents the results of the experiments carried out to investigate the bed hydrodynamics viz. variation of bed voidage, suspension density and solid circulation rate along with the height of the riser of a PCFB gasifier under different operating conditions. Further, the heat transfer study viz. bed and wall temperature profiles along the height of the riser are also presented. Superficial velocity, inventory, and operating pressure are identified as the operating parameters for the current analysis which is briefly described in the subsequent sections. Also, the effect of particle size on bed hydrodynamics has also been investigated as a part of the current study.

5.2 Hydrodynamic studies

This section deals with investigating the performance analysis of the PCFB unit due to the variation in operating parameters such as superficial velocity, Geldert B particle size, amount of solid inventory, and operational pressure. The low- grade Indian coal and sawdust are used as solid fuel in the present experiments. The coal is collected from Mahanadi coalfield, Odisha, India, and sawdust from local woodshop Guwahati, Assam, India. Three different mean diameter viz. 300, 600, and 770 µm of coal as bed inventory have been chosen. Procedure for calculation of mean particle size is given in Appendix-.VI. Experiments have been accomplished at three different solid inventory such as, 600, 800, and 1,000 g as well as at three overall system pressure conditions of 1, 2, and 4 bars. All the aforementioned test cases have also been performed in conjunction with superficial velocity values of 3, 4 and 5 m/s, respectively. However, due to handling issues with the small-diameter particles and small quantity of inventory experiments were designed with trial and error basis. For example, experiments with coal particle size 300 µm could not be performed due to fast entrainment in the bed upto 800 gm inventory. Hence only one set of experiements of 300 micron is conducted

successfully with bed inventory of 1000 g. Experiments for other selected mean particles were xonducted for all the inventories, pressure and superficial velocities.

Experiments have also been conducted with different weight percentages viz. 5%, 10%, 15%, 20% of sawdust blends with low grade Indian coal having a mean particle diameter of 600 µm as bed inventory. Total inventory of blends of saw dust and coal was maintained at 1000 g and all the experiemnts with blends were conducted at a superficial velocity of 4 m/s. The velocity is chosen from the interpretations based on the experiments conducted with coal particles in sub-section 5.3.2. The mean particle size of the blended inventory was maintained at 600 micron. Table 5.1 gives the mixture of coal and saw dust in 1000 gm inventory for various experiments.

Table 5.1 Amount of sawdust and coal in a inventory of 1000 g

Percentage of Sawdust in blends Col-1 (wt/wt)	**Sawdust by weight, Col-2= (Col-1/100)×I**	**Coal by weight, Col-3 = (1000-Col-2)**	**Total inventory By weight, I=(Col-2+Col-3)**
5	50	950	1000
10	100	900	1000
15	150	850	1000
20	200	800	1000

The physical properties of coal and sawdust are shown in Table 5.2 Proximate analysis of coal is conducted at IIT Guwahati using proximate analyzer (ASTM E871-82). Both the ultimate and proximate analyses of coal and sawdust are shown in Table 5.3.

Table-5.2 Properties of coal and sawdust particles

Name of the properties	**Coal**	**Sawdust**
Mean diameter (µm)	300-770	300-770
True density (kg/m^3)	1350	210
Bulk density (kg/m^3)	900	380
Spherocity, ϕ_s	0.7	0.71

Table-5.3 Properties of Coal and Sawdust

Sample	**Ultimate analysis (wt %, dry basis)**				**Proximate Analysis (wt %, dry basis)**				**LHV (kJ/kg)**
	C	**H**	**N**	**S**	**MC**	**VM**	**FC**	**Ash**	
Coal	39.33	3.29	1.632	1.802	8.54	23.3	28.19	39.9	15480
Sawdust	52.30	5.17	0.40	0	9.43	73.84	15.63	1.10	17420

5.3 Results and Discussion on Bed Hydrodynamics

The detailed experimental matrix for the present study is shown in Table 5.4.

Table-5.4 Experimental matrix for hydrodynamic study

Feed Material	Blending	I (gm)	d_p (µm)	U_{sup} (m/s)	Pr (bar)
Coal	100%	600	300	3	1
		800	600	4	2
		1000	770	5	4
Coal + sawdust blends	5%, 10% 15%, 20%	1000	600	4	1 2 4

As a part of the bed hydrodynamics study, preliminary experiments have been conducted for measuring the static pressures along with the riser height at 10 (ten) discrete locations above the distributor plate. Further, the bed voidage is calculated at the above-stated locations by the usage of the static pressure and density of solid inventory using Eq. 4.4 After that, the corresponding suspension densities are estimated using Eq. 4.5. The effect of particle size, superficial velocity, solid and biomass inventory, and operating pressure, on various bed hydrodynamics parameters, have been studied and discussed. The corresponding experimental uncertainty is presented in Appendix- VII.

5.3.1 Effect of pressure, inventory and particle size on bed voidage

The variation of bed voidage profile along the riser height of the PCFB at different operating pressures and weight of solid inventories are presented in Figs. 5.1 through 5.3. For all the cases, the coal having a mean particle diameter of 600 µm as bed inventory and superficial velocity of air as 4 m/s has been considered. Figure 5.1 represents the bed voidage along with the height of the riser for 600 g of coal as a bed inventory. It is observed that with an increase in operating pressure, the bed voidage decreases along with the height of the riser. The bed voidage also decreases with an increase in the inventory, which is shown through Fig, 5.2, and 5.3. In all the operating pressures, due to the diffusion of solid particles along the axial direction, a typical S-shaped profile for the bed voidage has been noticed. However, a reduction of gas velocity in the near the wall region as compared to the core flow also seems to be a matter of concern for the variation in bed voidage along the riser length.

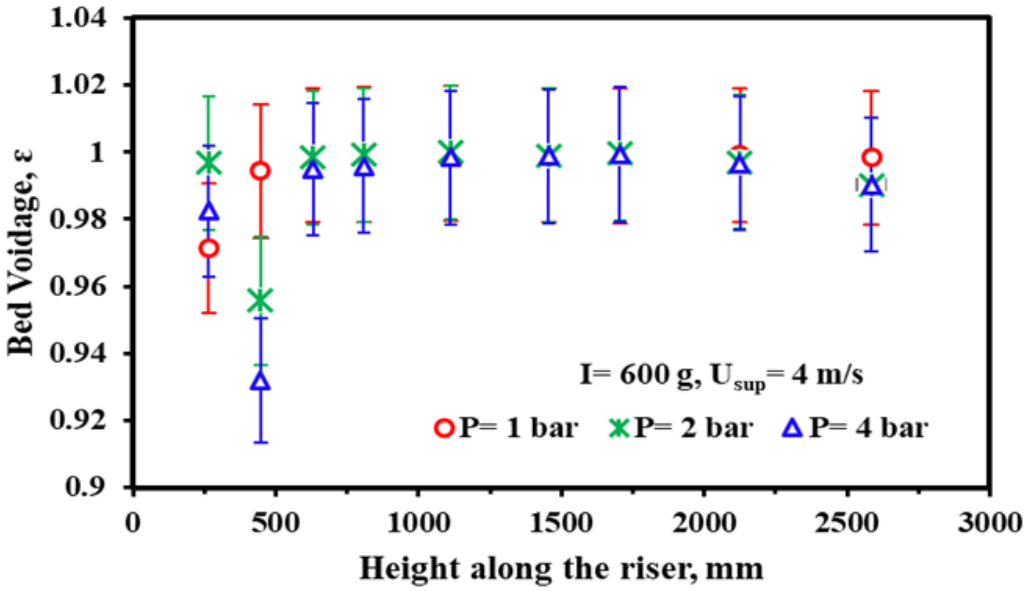

Fig. 5.1 Variation of bed voidage with operating pressure at I = 600 g

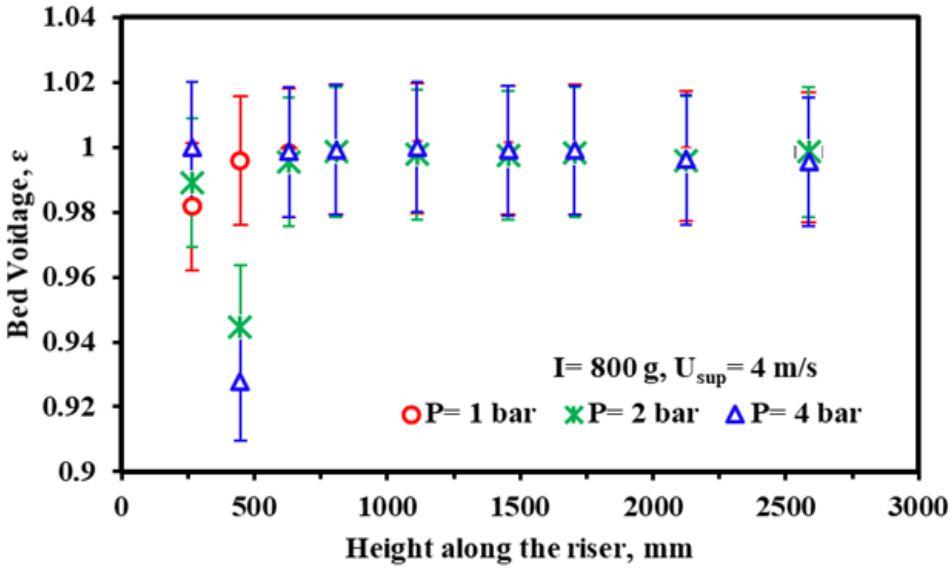

Fig. 5.2 Variation of bed voidage with operating pressure at I = 800 g

Moreover, it is also noticed that the increase in the effective operational pressure and weight of inventory results in a decrease in bed voidage for all the locations. In the bottom portion (0.447 m from the distributor plate), the magnitude of voidage seems to be decreased significantly, and it increases along with the bed height for all the inventories and operating pressure. Further, there is a phase shift for minimum voidage with the increase in bed pressure due to the dominance of pressure drag over the frictional drag. The bed voidage is found to be the least for the higher solid inventory and operating pressure condition. As the effective bed pressure increases, it resulted in higher drag force on the coal particles along the riser length due to which the coal particles accumulate in the upper section of the riser. Thereby, a more

bed voidage reduction is perceived at the riser exit with an increase in operating pressure. The overall error of ± 2% is found for the bed voidage along with the riser height, which is illustrated in Fig. 5.1 through 5.3.

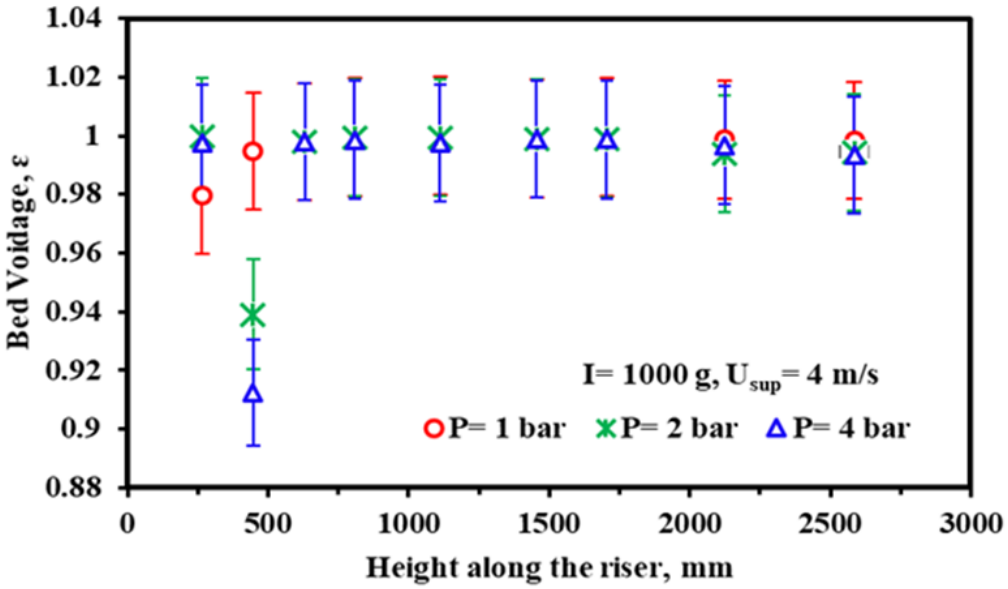

Fig. 5.3 Variation of bed voidage with operating pressure at I = 1000 g

A comparative assessment of three different coal particle sizes viz. 300, 600 and 770 µm, on variation in bed voidage with respect to different operating pressures are illustrated in Figs 5.4 through 5.6 respectively.

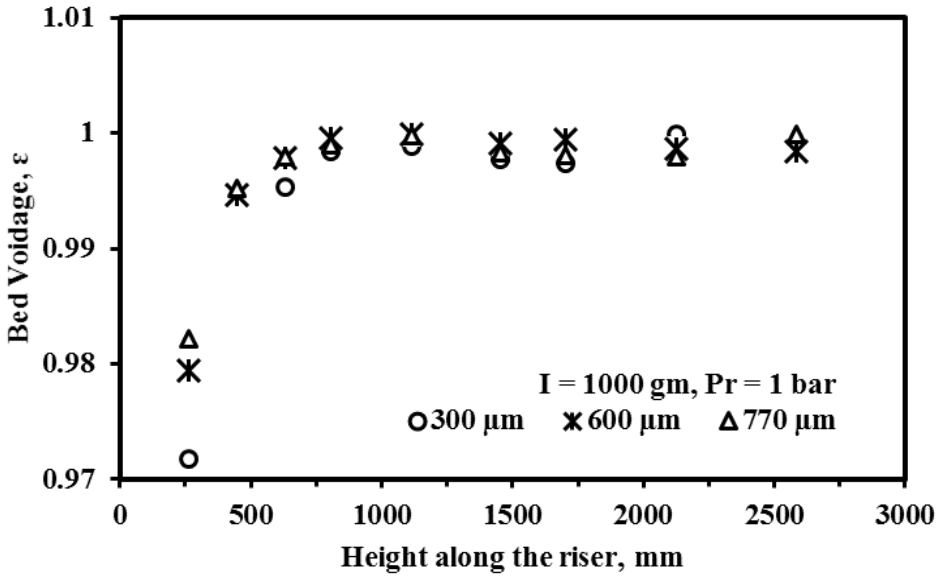

Fig. 5.4 Variation of bed voidage with particle size at P = 1 bar and I = 1000 g

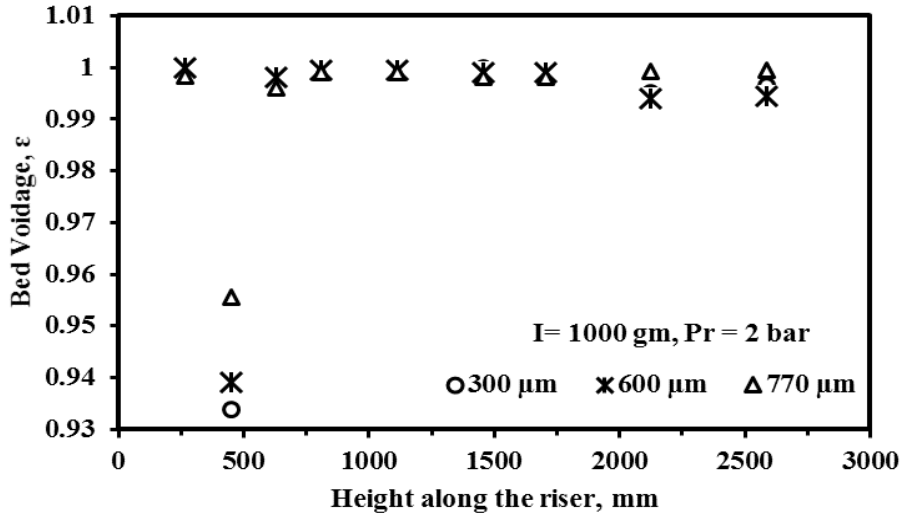

Fig. 5.5 Variation of bed voidage with particle size at P = 2 bar and I = 1000 g

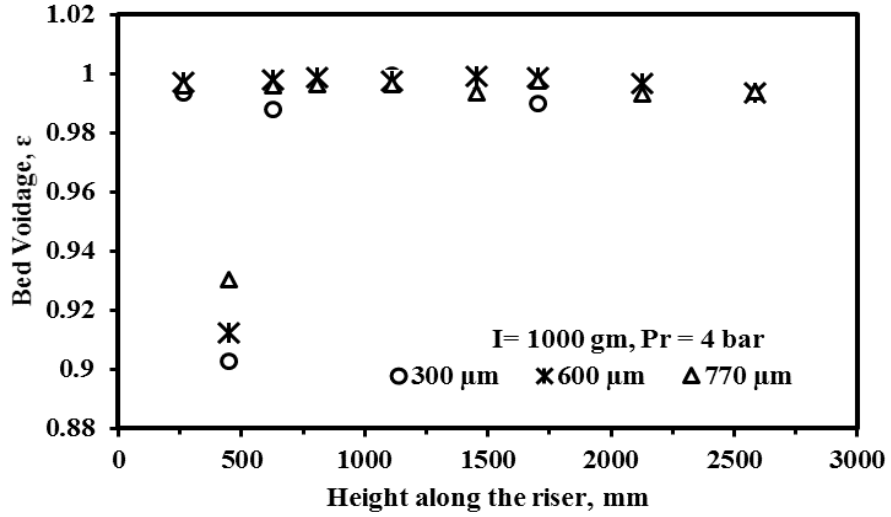

Fig. 5.6 Variation of bed voidage with particle size at P = 4 bar and I= 1000 g

The particle bed voidage is found to decrease as the mean particle diameter of the solid inventory decreases. This may be attributed to the fact of enhancement of particle accumulation at the riser exit, as the pressure increases. However, a significant reduction is observed at a higher operating pressure of 4 bar rather than at atmospheric and at 2 bar. A maximum decrement in bed voidage at 447 mm from the bottom of the riser is noticed for all the cases of variation in the particle diameter.

5.3.2 Effect of operating parameters on suspension density

The significance of bed inventory and operating pressure on suspension density variation has been analyzed along the length of the riser where the superficial velocity and the solid particle diameter has been kept constant. With the increase in pressure, the suspension density is found to rise considerably for all the cases of bed inventories, as shown in Fig. 5.7 through Fig. 5.9.

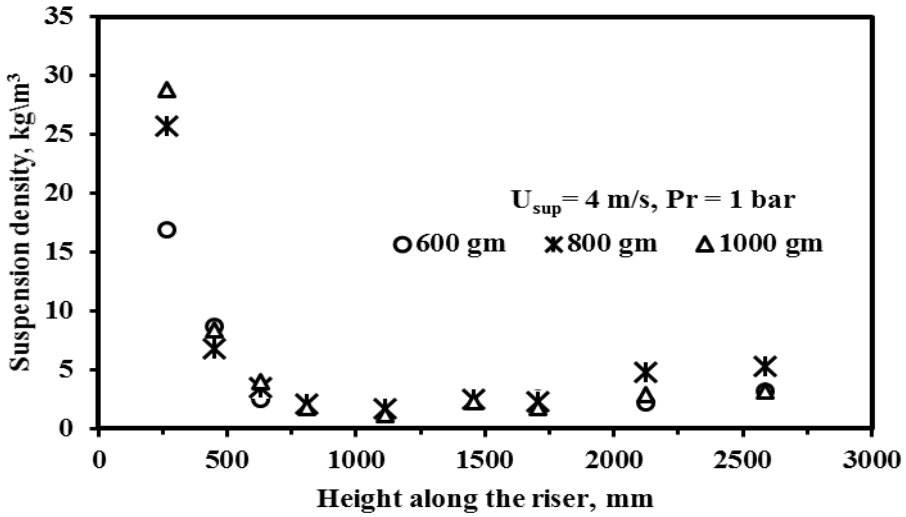

Fig. 5.7 Variation of suspension density with bed inventory at P = 1 bar

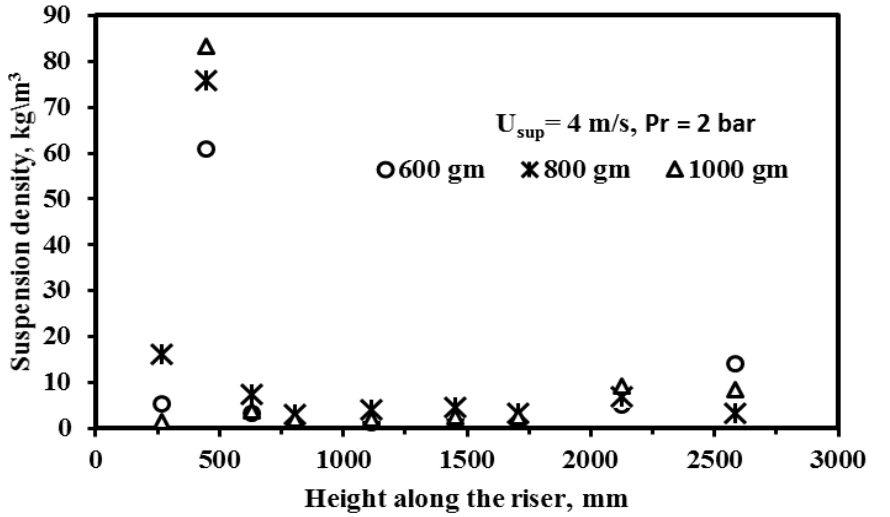

Fig. 5.8 Variation of suspension density with bed inventory at P = 2 bar

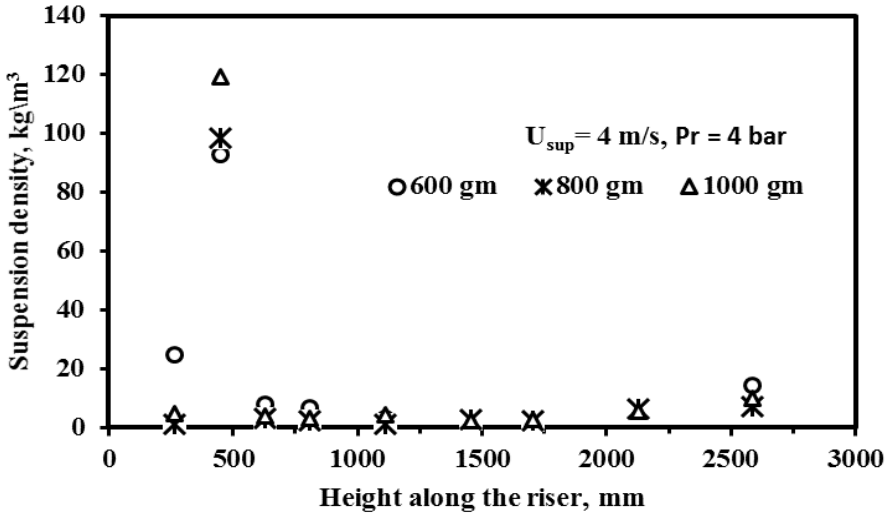

Fig. 5.9 Variation of suspension density with bed inventory at P = 4 bar

At a specific operating pressure, as the bed inventory increases, a notable enhancement on suspension density is observed. The maximum suspension density location is the same as the position for minimum bed voidage for all the cases. The location of maximum suspension density is found to be independent of variation in inventory and operating pressure.

Subsequently, the effect of superficial velocity on suspension density at different operating pressures and keeping other parameters constant, are illustrated in Fig. 5.10 through 5.12.

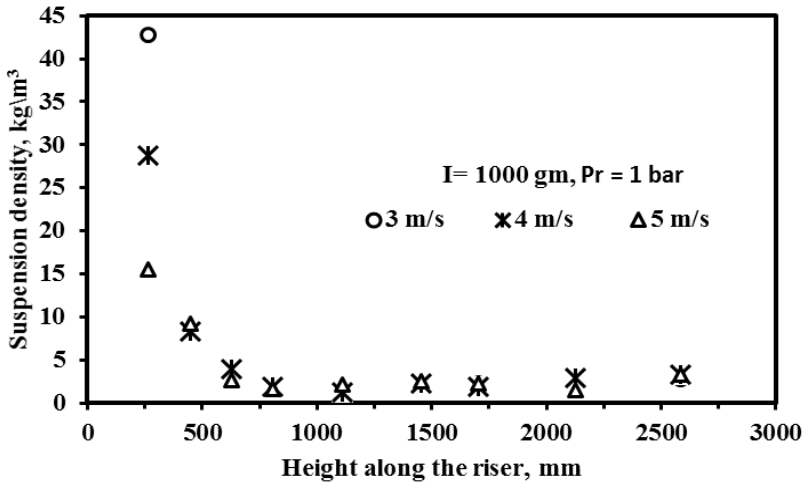

Fig. 5.10 Variation of suspension density with superficial velocity at P = 1 bar

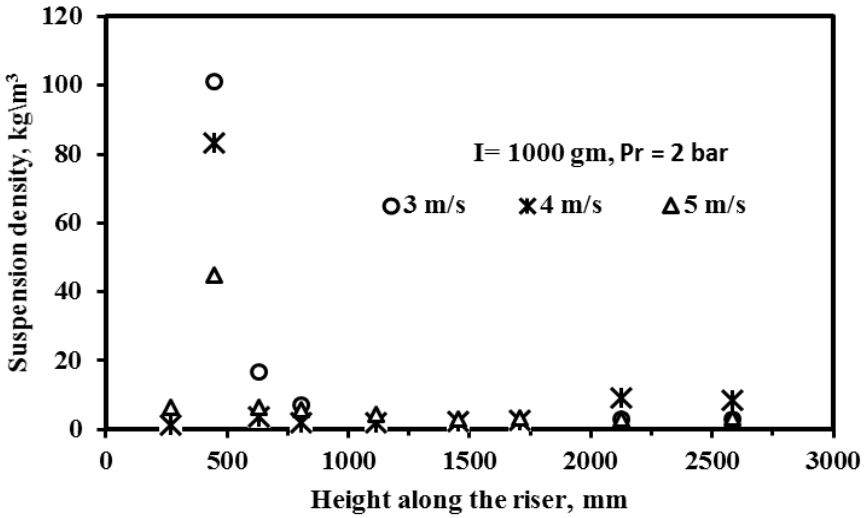

Fig. 5.11 Variation of suspension density with superficial velocity at P = 2 bar

For the comparative assessment, the particle diameter of 600 µm and a bed inventory of 1000 gm is selected. As seen, a significant decrease in suspension density is noted as the superficial velocity increases. Further, it has been noticed that irrespective of the operating pressure, the percentage decrement in suspension density with respect to superficial velocity remains unaltered.

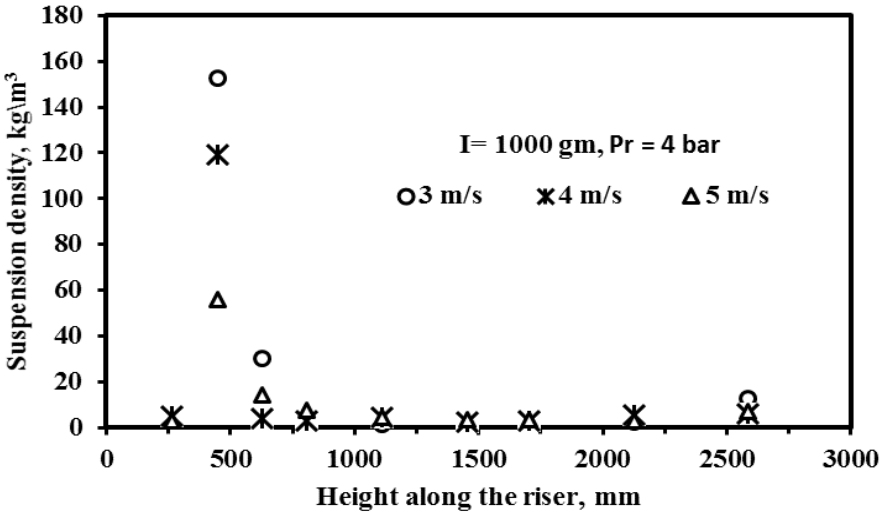

Fig. 5.12 Variation of suspension density with superficial velocity at P = 4 bar

However, the suspension density is seem to have an increasing trend with respect to rising in pressure for a particular case of the superficial velocity. The maximum suspension density for all the variations is located at the same distance as observed earlier. Nevertheless, a higher magnitude of suspension density is found at the riser inlet for the operating pressure of 1 bar. However, this peak magnitude has been shifted away from the inlet in case of pressurized conditions. Hence it is inferred that for a fixed inventory and mean particle size, superficial velocity of 4 m/s gives better suspension density under pressurized condition which is desirable.

5.3.3 Bed voidage variation for coal-sawdust blends as bed inventory

To determine the effectiveness of incorporating biomass as inventory material along with coal, the bed voidage profiles during cold bed analysis have been assessed. In this regard, the different weight percentages of biomass and coal have been considered as the bed inventory. For this analysis, the coal having a particle diameter of 600 µm, a net inventory of 1000 gm, and a superficial velocity of 4 m/s have been considered. However, experiments at different operating pressure and different weight percentage of biomass have been carried out to estimate the effective change in voidage, as shown in Figs. 5.13 through 5.15. It is observed that for all the pressurized bed experiments, the bed voidage is having an S-shaped profile having the least value near to the bottom of the bed viz. 0.447 m from the riser inlet. However, for atmospheric pressure condition, a minimum value is observed at 0.265 m from the bottom. Further, irrespective of the weight percentage of biomass blending with coal, as the operating pressure is increased, a significant decrement in bed voidage and homogeneous mixture of biomass and coal is observed throughout the height of the riser.

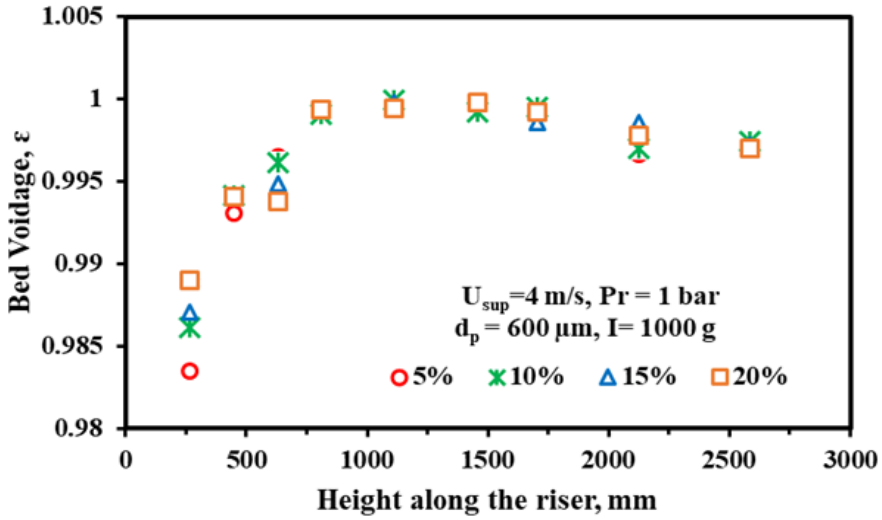

Fig. 5.13 Bed voidage with different weight percentage of sawdust blending at 1 bar

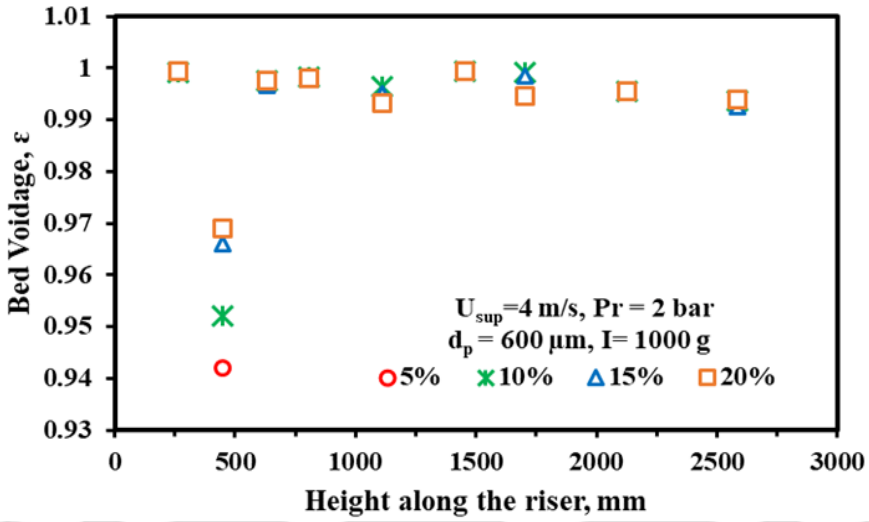

Fig. 5.14 Bed voidage with different weight percentage of sawdust blending at 2 bar

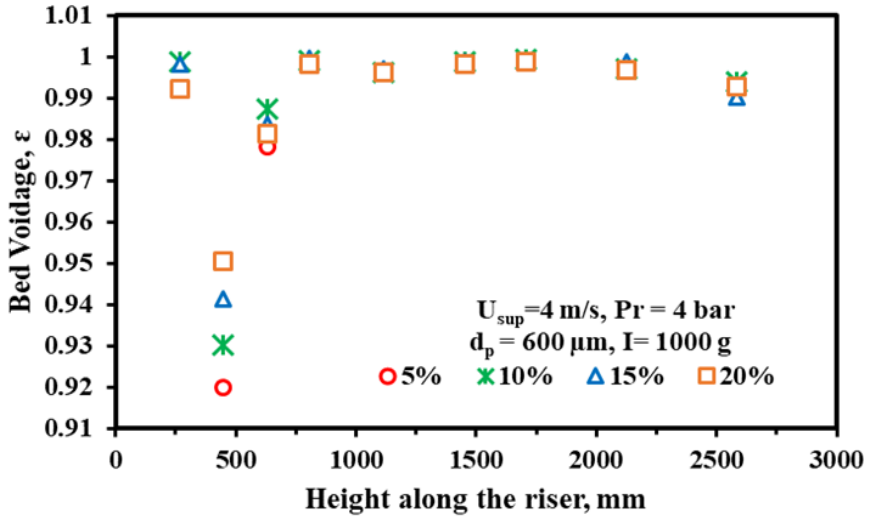

Fig.5.15 Bed voidage with different weight percentage of sawdust blending at 4 bar

Moreover, for a specific operating pressure, as the percentage of biomass blending with coal is increased, the bed voidage shows an increasing trend, and this seems to be more prominent in case of pressurized bed conditions viz. at 2 and 4 bars.

5.3.4 Suspension density variation for coal-sawdust blends as bed inventory

During the cold bed experiments, the variation of suspension density is analyzed to estimate the effect of the percentage of biomass blending with coal as bed material at different operating pressure. Biomass having 5%, 10%, 15% and 20% weight composition with respect to the total mass of the inventory are considered for this study and its effect on suspension density with respect to the operating pressure of 1, 2 and 4 bars are illustrated in Figs. 5.16 through 5.19.

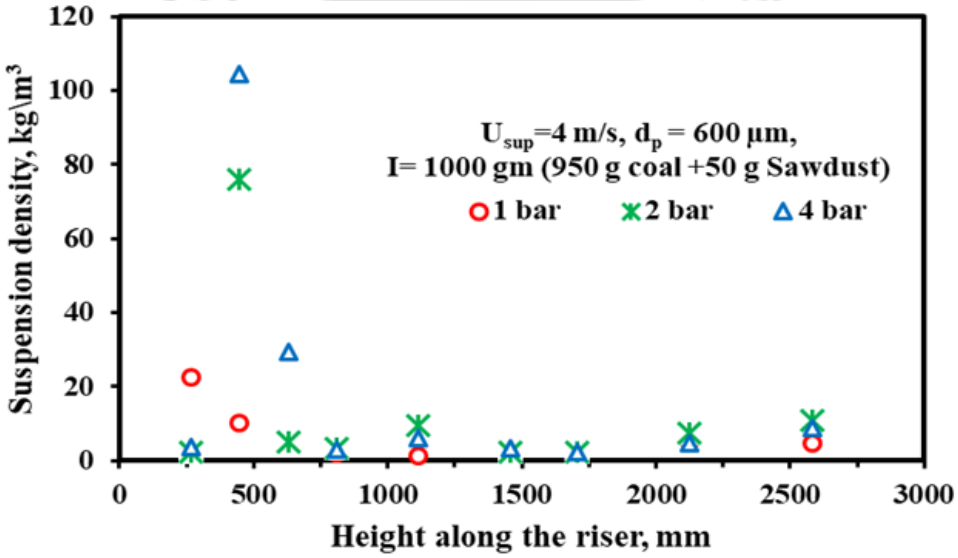

Fig. 5.16 Suspension density with different operating pressure at 5% of sawdust blending

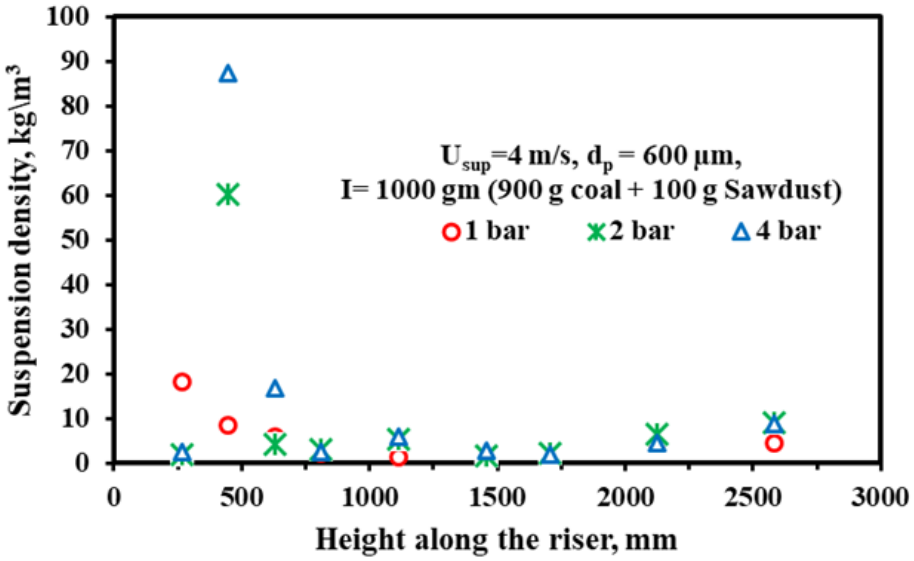

Fig. 5.17 Suspension density with different operating pressure at 10% of sawdust blending

For this analysis, the total inventory weight of 1000 gm consisting of coal particles having a size of 600 µm is chosen. It has been noticed that irrespective of the percentage of biomass blending, suspension density magnitude is increasing with operating pressure due to a significant increase in mass entrainment of solid particles. Further, as the percentage of blending increases, a noticeable decrement in suspension density is found due to variation in density between coal and biomass. At 4 bar operating pressure, the peak magnitude of suspension density for 5% blending is observed to be 104.58, whereas it reduces to a value of 56.72 at 20% blending.

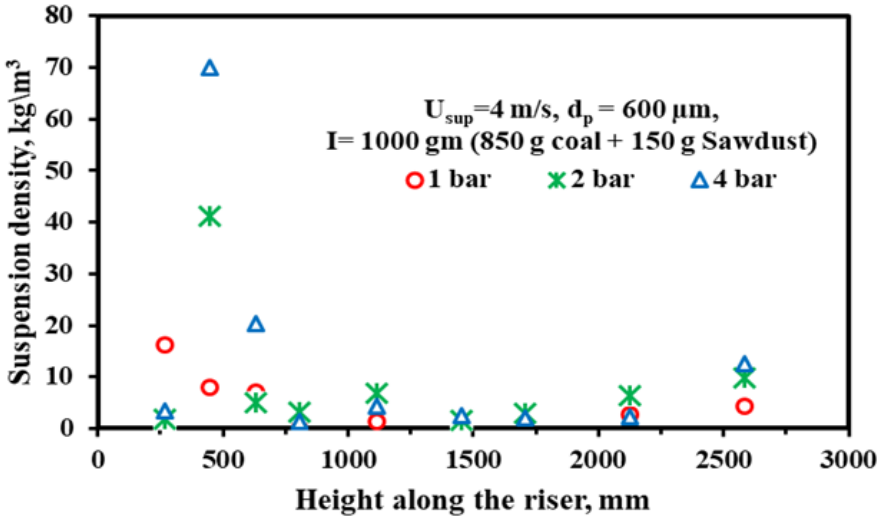

Fig. 5.18 Suspension density with different operating pressure at 15% of sawdust blending

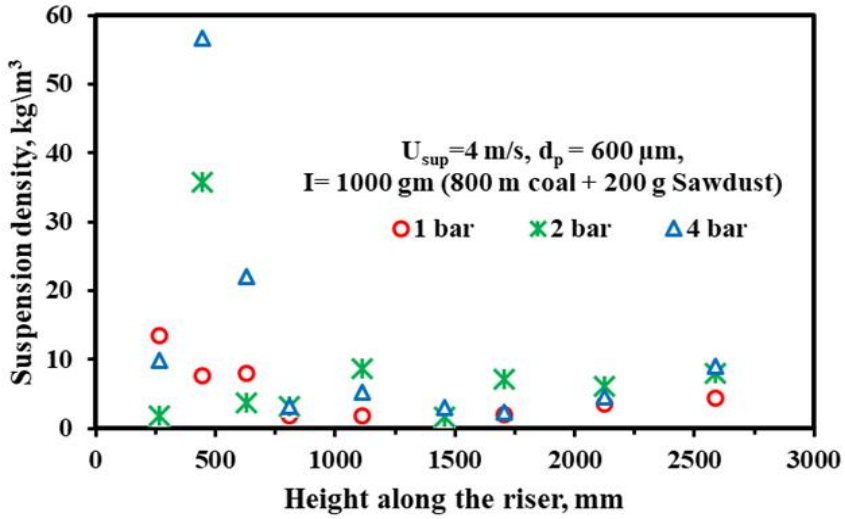

Fig. 5.19 Suspension density with different operating pressure at 20% of sawdust blending

The suspension density directly plays an essential role in enhancing the heat transfer of a fluidized bed. Many researchers have found suspension density for their operating conditions. The suspension density obtained from the present work is compared with the reported data as

shown in Table-5.5, and it is observed that it lies within the range. The suspension density is a direct function of density of the particle and increases with an increase in particle density. It is revealed, now comparing with Das et al. (2008) suspension density was obtained comparable within the range.

Table-5.5 Comparison of suspension density with other operating conditions

Investigators	Riser dimension		U_{sup} (m/s)	Pressure (bar)	I	(d_p)	ρ_s	ρ_{Sus}
	D (m)	H (m)						
Basu and Nag (1987)	0.102	5.5	3-5	ACFB	Sand	87 227	2650	21.5-96.79
Basu et al. (1996)	0.0525	2.02	3.6-4.8	1- 7	Sand	232, 507	2818	600
Kolar and Sundaresan (2002)	0.1×0.1	5.5	4.5-7.3	1	Sand	363	2740	330
Gupta and Nag (2002)	0.0375	1.94	0.25-1.25	2-6	Sand	264	--	160
Das et al. (2008)	0.1016	5.62	2.01	1	Coal	215	1150	5-138
Patil et al. (2011)	0.15×0.15 0.20×0.20 0.25×0.25	2.85	2.5-4	1	Sand	460	2600	7.2-288
Kalita et al.(2013a)	0.054	2	5-7	1,3, and 5	Sand and sawdust	278, 307, 469	2300	11-800
Present Work	0.10	3	3-5	1, 2, and 4	Coal and sawdust	300, 600, 770	1350	10-152

U_{sup} = Superficial Velocity; I= Inventory; d_p = Particle size;
ρ_s = Particle density in (kg/m^3); ρ_{Sus} = Suspension density in (kg/m^3)

5.3.5 Parametric variation effect on solid circulation rate

The alteration in solid circulation rate due to variation in operational pressure at different superficial velocities and weight of inventories are shown in Table 5.6. The solid circulation rate is having an increasing trend with respect to both solid inventory and operating pressure. This inference seems to be independent of the type of inventory viz. coal or blends of coal with sawdust. The solid circulation rate decreases with an increase in particle size, i.e. at pressure 4 bar and velocity 4 m/s the solid circulation rate decreases from 37.20 to 31.86 kg/m^{2}s while

increasing the particle size from 300 to 770 µm. The solid circulation rate increases with an increase in superficial velocity, pressure as well as bed inventory.

Table 5.6 Variation of Solid circulation rate

Bed Material	Pressure (bar)	Velocity (m/s)	d_p (µm)	Inventory (g)	Solid Circulation Rate (kg/m^{2}s)
Coal	1	3	600	1,000	13.06
		4	600	600	14.26
		4	600	800	15.68
		4	600	1,000	17.2
		4	300	1,000	19.3
		4	770	1,000	16.28
		5	600	1,000	22.32
	2	3	600	1,000	20.96
		4	600	600	22.38
		4	600	800	24.66
		4	600	1,000	26.08
		4	300	1,000	30.24
		4	770	1,000	24.62
		5	600	1,000	28.16
	4	3	600	1,000	29.64
		4	600	600	29.48
		4	600	800	31.39
		4	600	1,000	34.42
		4	300	1,000	37.24
		4	770	1,000	31.86
		5	600	1,000	36.78
5% Saw dust blending	1	4	600	1,000	17.96
	2				27.32
	4				35.38
10% Saw dust blending	1	4	600	1,000	18.32
	2				27.96
	4				36.32
15% Saw dust blending	1	4	600	1,000	19.24
	2				28.65
	4				37.14
20% Saw dust blending	1	4	600	1,000	19.84
	2				29.47
	4				38.09

5.4 Heat Transfer Studies

Apart from the hydrodynamic study, a heat transfer study is also conducted in the same PCFB unit. The local temperature at the bed and wall also recorded during gasification and co-gasification studies. The variation of temperature along the height of the riser is presented

below. The temperatures are recorded at a time interval of 5 minutes, and the steady-state temperature is also recorded once the system becomes steady.

5.4.1 Effect of pressure on temperature

The temperature profile for a certain operating condition is obtained after achieving the steady-state values for the corresponding thermocouples. The temperature profile along the height of the riser for coal as a feed material is shown in Fig. 5.20. The variation in temperature profile is more significant up to 1 m height from the distributor plate due to the dominance of gasification reactions in this zone. In this section, a higher temperature gradient is also evident. From Fig. 5.20, it is perceived that with an increase in operating pressure, the temperature increases in all the sections. For gasification of coal at 1 bar operating pressure, the bulk mean temperature in the gasification section is calculated to be 484°C, whereas it increases to 490°C, 593°C, and 640°C at 2, 3 and 4 bar, respectively. A similar trend with marginal variation in temperature is also observed for other inventories such as rice husk and sawdust.

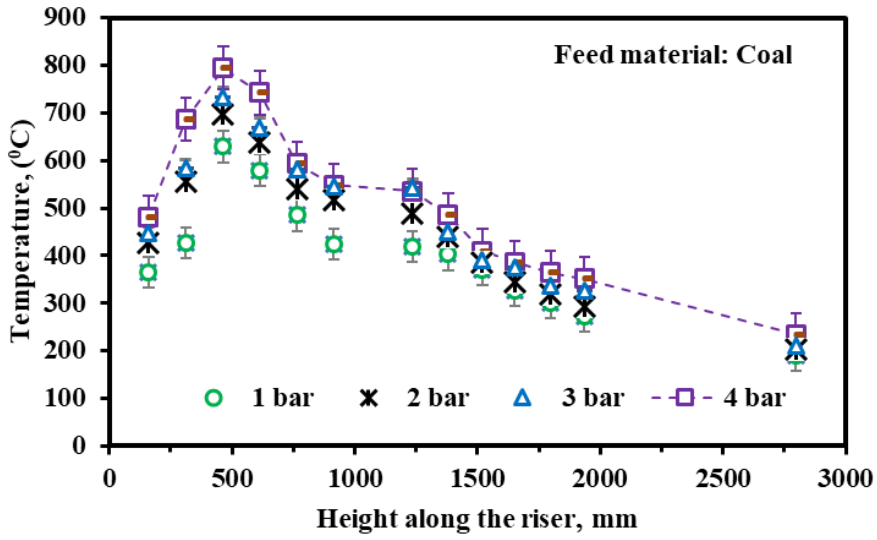

Fig. 5.20 Variation of temperature with pressure along height of the riser

Moreover, the time required for achieving the steady temperature inside the gasifier varies with respect to the type of inventory used. The gasification commences as the bulk mean temperature inside the gasifier (up to 1 m height) reaches a temperature in the range of 500-550°C for sawdust and rice husk, while for coal, the temperature is found to be around 600°C. For the initial production of syngas, it takes normally 15-20 minutes for coal, whereas it takes about 10-15 minutes for sawdust and rice husk. This can clearly be seen in Fig. 5.21 when sawdust is used as an inventory. The trend of temperature variation also seems to be similar to

the earlier obtained results. Once the syngas production is initiated, it is being produced continuously as long as the mass flow rate of the feed material is maintained inside the gasifier.

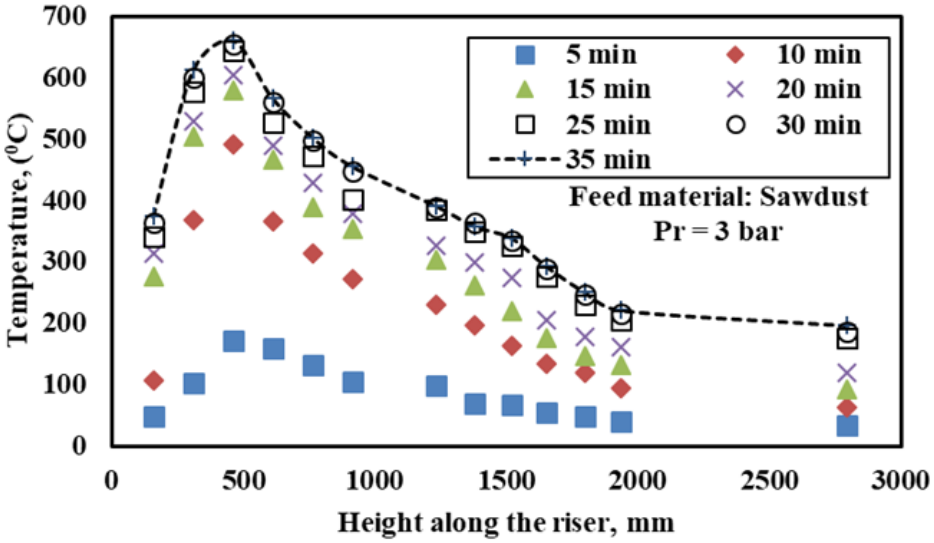

Fig. 5.21 Variation of temperature with time along height of the riser

For 5%, 10%, 15% and 20% coal-sawdust blend the suspension density and the steady-state temperature are presented in Figs. 5.22 and 5.23. From the figures, it is observed that suspension density has a strong function with temperature inside the riser, and the peak for both suspension density and bed temperature is obtained from 500 mm from the distributor plate. Since suspension density is found to be decreased with an increase with the percentage of blending, but the steady-state temperature profile is almost the same for both the blendings. The input supply in terms of heating time is less with an increase in percentage of blending.

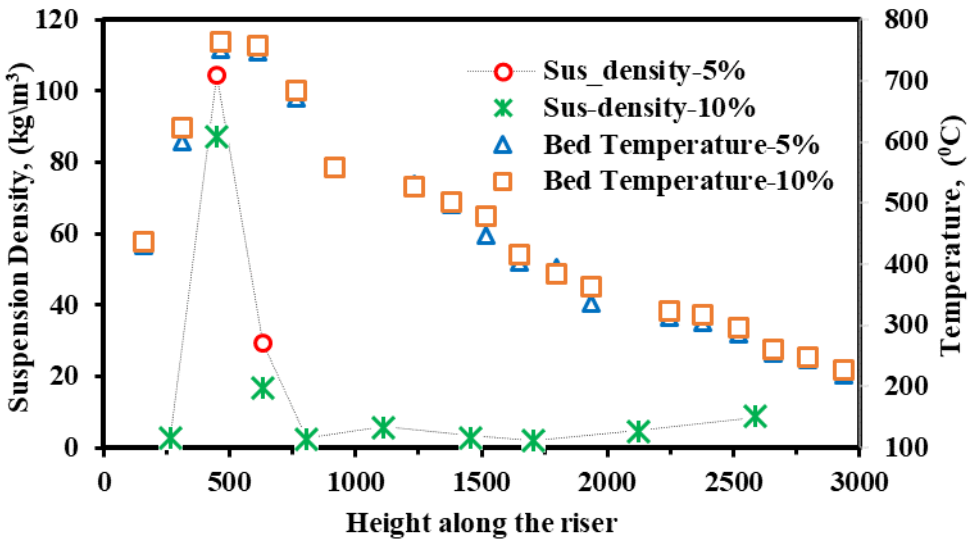

Fig. 5.22 Variation of suspension density and temperature along height of the riser

This is may be due to the self-ignition temperature of sawdust is less than coal and that helps to reduce the input heating with an increase in the percentage of blending.

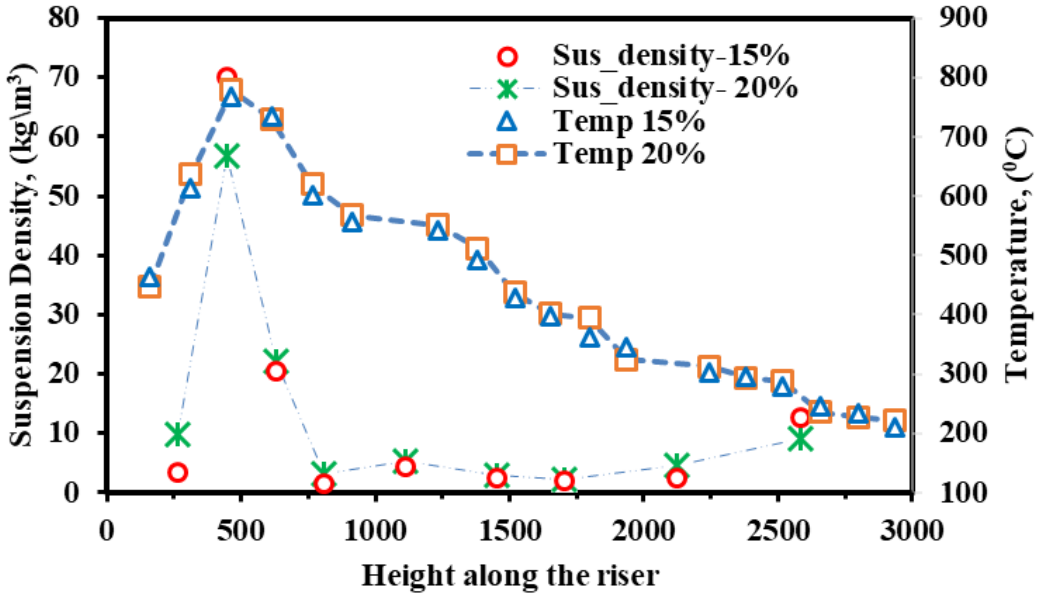

Fig. 5.23 Variation of suspension density and temperature along height of the riser

The steady-state local bed temperature and the local temperature at the wall is presented in Fig. 5.24. The wall temperature is measured by using a particular type of thermocouples (Fig.4. 3). The difference in temperature is less in the combustion zone, i.e. up to one-meter height and after that, the difference in bed and temperature increases.

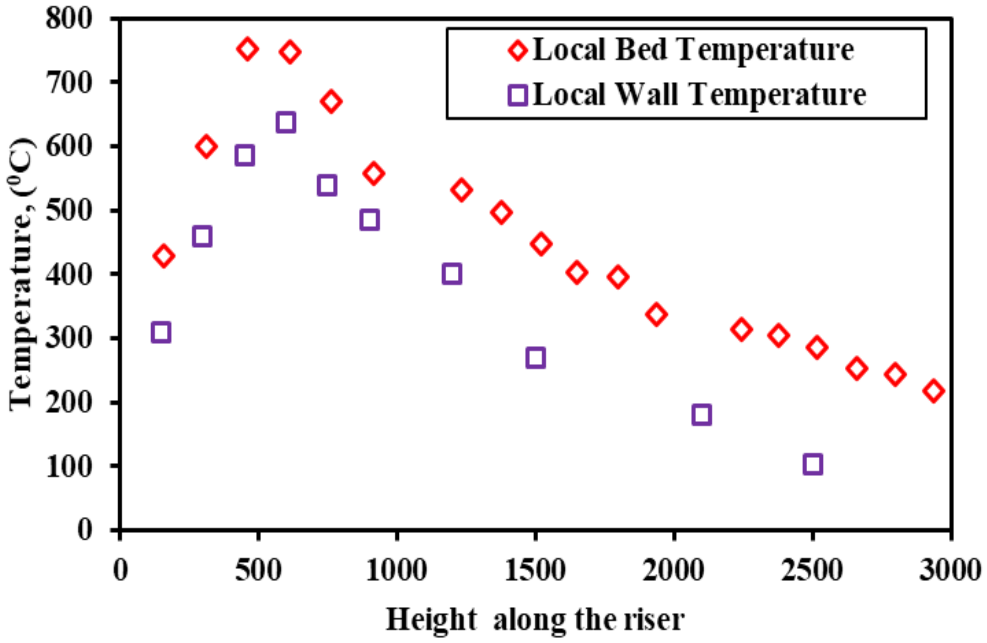

Fig. 5.24 Variation of temperature along height of the riser

The bed to wall heat transfer coefficient cannot be calculated in the present case due to continuous burning of feed material and generation of heat inside the riser.

5.5 Summary

In a conventional pulverized coal-based power plant, the utilization of low-grade coal is difficult due to low calorific value and high ash content, though the availability of this type of coal is significant in India. The PCFB is a promising option for utilizing this low-grade Indian coal. The detailed hydrodynamic study is required for the design of a PCFB boiler/gasifier. This hydrodynamic study will help in combustion and gasification study in the future. In the present investigation, the effect of superficial velocity and operating pressure on bed hydrodynamics of a PCFB unit is studied. A strong functional relationship between the suspension density and bed temperature is observed. There is a phase shift for minimum voidage with the increase in bed pressure due to the dominance of pressure drag over the frictional drag. Overall error in voidage calculation is founf to be $\pm 2\%$. The variation of suspension density of coal is found in the range of 10-152 kg/m^3 which is comparable to Das et al. (2008). The suspension density is found to be decreasing with increase in percentage of sawdust blends. Chocking of the system is observed above the sawdust blends of 15% and inventory above 1000 gm in the present set-up. The favoriable temperature for gasification is observed upto 1250 mm above distributor palte. However, the upper splash region indicates relatively low temperature retarding the process of gasification. Operating paramenters and results obtained from this chapter are utilized in the subsequent chapters.

The gasification studies in the same PCFB gasifier considering low-grade coal and biomass like sawdust, rice husk and sugarcane bagasse as feed material is described in Chapter 6.

Chapter – 6

Results and Discussion of Gasification Studies

6.1 Introduction

This chapter deals with the experimental investigation on gasification of various feed materials in a PCFB gasifier. Effect of operating pressure on asyngas gas composition, lower heating value (LHV), dry gas yield (Y), carbon conversion efficiency (CCE), cold gas efficiency (CGE) are found out. Low- grade Indian coal, sawdust, rice husk, and sugar cane bagasse are considered as feed material for individual gasification study.

6.2 Gasification Studies Considering Sawdust as a Feed Material

For the preliminary experiments, similar to earlier hydrodynamics study, batch type experiments with one of the inventory viz. sawdust is carried out to assess the feasibility of the same towards hot mode working of PCFB. It is planned herein to investigate the effect of pressure on temperature and gas composition. Further, an attempt has been made to check the viability of the batch mode method towards longer duration operation of the PCFB unit. The gasification occurs inside the gasifier due to the following reactions. The composition of syngas is an active function of the temperature, and the temperature inside a gasifier mostly depends on gasification reactions (Eqs. 6.1- 6.10). The composition of syngas obtaining from gasification at particular operating conditions is a concern of numerous concurrent reactions (Eqs. 6.1- 6.10) happening inside the gasifier, which are listed below.

$$\text{Oxidation}: H_2 + \frac{1}{2}O_2 \rightarrow H_2O \quad (6.1)$$

$$\text{Oxidation}: CO + \frac{1}{2}O_2 \rightarrow CO_2 \quad (6.2)$$

$$\text{Boudard reaction}: C + CO_2 \leftrightarrow 2CO \quad (6.3)$$

$$\text{Steam reforming}: CH_4 + H_2O \leftrightarrow CO + 3H_2 \quad (6.4)$$

$$\text{Dry reforming}: CH_4 + CO_2 \leftrightarrow 2CO + 2H_2 \quad (6.5)$$

$$\text{Water gas reaction}: C + O_2 \leftrightarrow CO + H_2 \quad (6.6)$$

$$\text{Tar Cracking}: C_nH_m + n\,CO_2 \leftrightarrow \frac{m}{2H_2} + 2n\,CO \quad (6.7)$$

$$\text{Methanation reaction: } C + 2H_2 = CH_4 \quad (6.8)$$

$$\text{Methanation reaction: } CO + 3H_2 = CH_4 + H_2O \quad (6.9)$$

$$\text{Char reaction: } \text{Char} + O_2 \rightarrow CO_2 + CO \quad (6.10)$$

6.2.1 Effect of pressure conditions on gas composition

The variation in gas composition with a change in operating pressure from 1 to 4 bar is shown in Fig. 6.1. The effect of pressure on gas composition is very less significant for hydrogen formation. The percentage of CO increases from pressure 1 to 2 bar and decreases gradually from 2 to 4 bar. However, enhancement in CO_2 from 11.2 to 15.2 % with an increase in pressure from 1 to 4 bar, is evident. The concentration of methane also increases slowly as pressure increases. The syngas composition is different as suggested by various researchers, but most of them indicated an increase in CO_2 with an increase in pressure, which is also evident in Fig. 6.1.

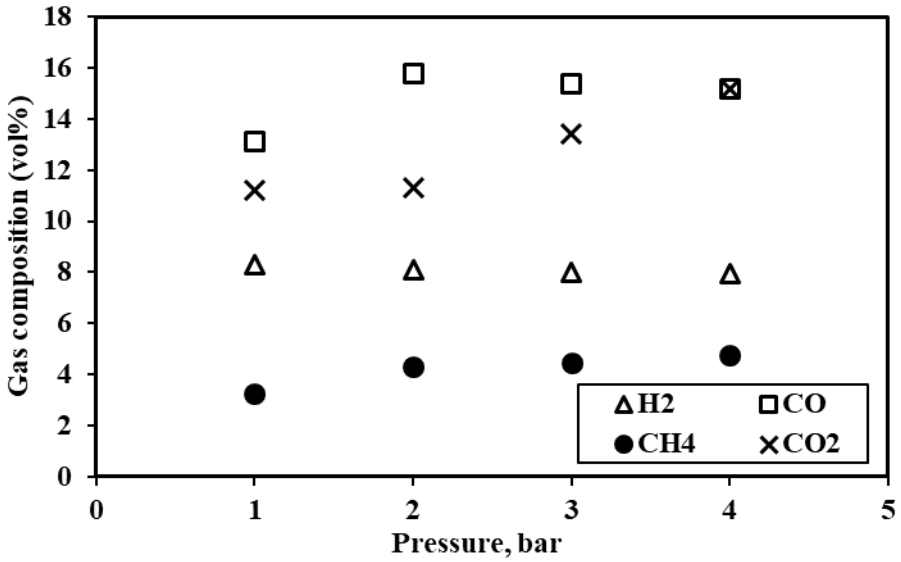

Fig. 6.1. Variation of gas composition with operating pressure

From the above study, it can be figured out that the trend of the gas composition in terms of CO_2 emission is in line with batch type studies. Nevertheless, the time period for which the syngas is being produced during these experiments is very small and it mostly depends upon the temperature developed during this time frame. Also, this temperature requirement for the production of syngas is different for various feeding material. Keeping in view of this temperature requirement, electrical energy is added through the usage of electrical heaters. However, the loss in electrical energy is usually more towards the end of the experiments. Further, as the experiment progresses, the weight of the inventory keeps on reducing whereas the airflow rate remains the same, which results in the combustion of the particles thereby leads to less production of syngas. Therefore, to effectively utilize most of the electrical energy input as well as to increase the time duration of syngas production, continuous feeding of inventory is necessary.

6.3 Gasification Studies in Continuous Feeding Mode

In view of the aforementioned remedy for the batch type study, the following experiments have been performed with a continuous supply of inventory into the riser section, through a passage present over the (Fig. 4.2). For these experiments, the effect of inventory viz. coal, as well as different biomass viz. sawdust, rice husk, and sugar cane bagasse, on gasification parameters, are assessed under the pressurized condition for the range of pressure 1 to 4 bar. The effect of pressure on gasification studies, i.e., variation in temperature, gas composition, LHV, gas yield, CCE, and CGE, are described in subsequent sections for the continuous feeding mode in a PCFB gasifier. The experimental matrix for the continuous mode gasification study is presented in Table. 6.1.

Table 6.1 Experimental Matrix for gasification study

Feed Material	Feeding type-continuous Initial feeding (gm)	d_p (µm)	Pr (bar)
Coal	1000	600	1-4
Sawdust		600	1-4
Rice husk		600	1-4
Sugarcane bagasse		600	1-4

The proximate, ultimate analysis and the LHV of the feed materials are given below in Table 6.2

Table 6.2 Properties of the feed material

Sample	**Ultimate analysis (wt %, dry basis)**				**Proximate Analysis (wt %, dry basis)**				**LHV (kJ/kg)**
	C	**H**	**N**	**S**	**MC**	**VM**	**FC**	**Ash**	
Coal	39.33	3.29	1.632	1.802	8.54	23.3	28.19	39.9	15480
Sawdust	52.30	5.17	0.40	0	9.43	73.84	15.63	1.10	17420
Rice husk	38.5	4.89	1.13	0	9.82	58.6	11.83	19.7	14100
Sugarcane bagasse	44.7	5.8	0.25	0.1	3.98	72.4	20.8	2.67	16120

6.3.1 Effect of pressure on syngas composition

The effect of pressure on syngas composition viz. concentration of H_2, CO, CH_4 and CO_2 is presented in Fig. 6.2 through 6.5. These compositions have been inferred from the gas chromatography of the collected syngas. From figure 6.2, it is observed that the concentration of H_2 slightly decreases with an increase in operating pressure from 1 to 4 bar. However, this decrement is again substantial in low pressure operating range and seems to be diminishing as pressure increases. The H_2 concentration is found to be highest for sawdust as inventory

whereas it is minimum for coal irrespective of the pressure conditions. Similarly, for rice husk and sugarcane bagasse, the concentration of H_2 decreases from 6.54 to 5.81 and 7.62 to 6.75 respectively, with an increase in pressure from 1 to 4 bar. Lesser significance of pressure on hydrogen composition can be attributed to further oxidation reaction which is induced as it reacts with oxygen, which can be represented by $H_2 + \frac{1}{2}O_2 \rightarrow H_2O$.

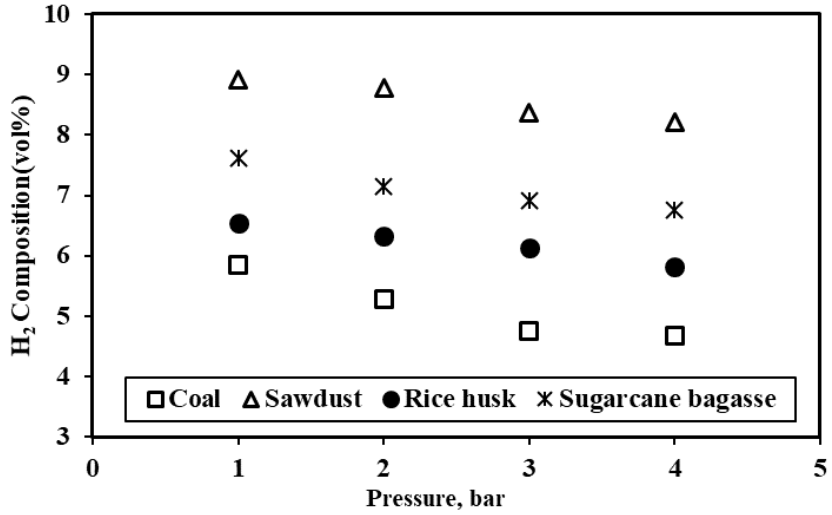

Fig. 6.2. Variation of H_2 gas composition with operating pressure

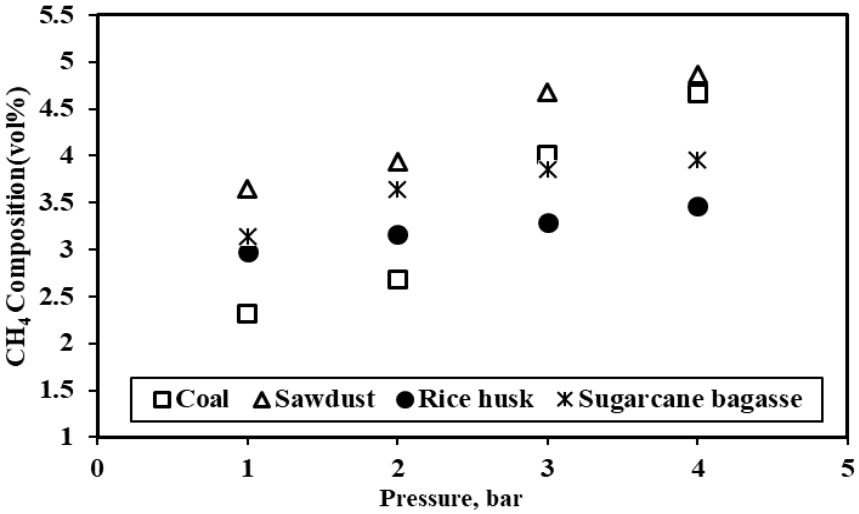

Fig. 6.3. Variation of CH_4 gas composition with operating pressure

Figure 6.3 represents the concentration of CH_4 with operating pressure. Unlike H_2 concentration, the composition of CH_4 shows an increasing trend with the rise in pressure for all types of feeding material. Most of the earlier studies reported an increase in CH_4 content in correspondence with an increase in gasifying pressure, which is also evident in Fig. 6.4.

Moreover, for lower pressure range operating conditions, coal has a minimum methane concentration in syngas whereas, for higher pressure magnitudes, the use of rice husk leads to the same condition. In contrary, irrespective of pressure conditions, sawdust provides highest CH_4 composition in syngas. The decrement of H_2 and increment in CH_4 concentration are due to enhancement of methanation reaction which can be represented by $C + 2H_2 = CH_4$ and $CO + 3H_2 = CH_4 + H_2O$.

The effect of pressure on the concentration of CO is shown in Fig. 6.4. The concentration of CO increases from 1 to 2 bar, and it decreases gradually with a further increase in operating pressure. It is observed that for coal, the volumetric concentration of CO is highest among all inventories.

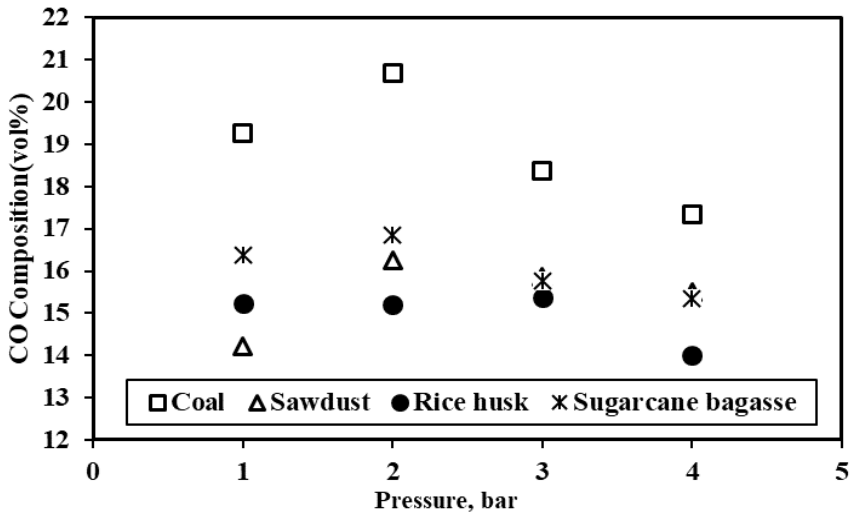

Fig. 6.4. Variation of CO gas composition with operating pressure

It increases from 19.26 at atmospheric pressure condition to 20.69 for 2 bar operating case and subsequently decreases to 17.34 percentage (by vol). A similar observation is also reported for sawdust, rice husk, and sugarcane bagasse. The water-gas shift reaction and partial combustion of CO at higher pressure can be attributed for the reason towards decrement in the composition of CO. The reaction can be symbolized by $CO + H_2O = CO_2 + H_2$ and $CO + 0.5O_2 = CO_2$.

Figure 6.5 illustrates the concentration of CO_2 variation with operating pressure. An increase in CO_2 concentration in the syngas is evident, as pressure increases from 1 to 4 bar. In the case of coal as feed material, the reaction $Char + O_2 = CO_2 + CO$ plays a vital role in enhancing the CO_2 concentration. However, in case of remaining inventory particles, water-gas shift reaction $(CO + H_2O = CO_2 + H_2)$ and oxidation reaction $(C + O_2 = CO_2)$ leads to increment in the

concentration of CO_2 with operating pressure. Moreover, the CO_2 concentration for coal and sawdust is found to be minimum and the same for most of the operating conditions. A similar trend has also been observed for the case of sugarcane bagasse and rice husk but the magnitude seems to be higher than earlier.

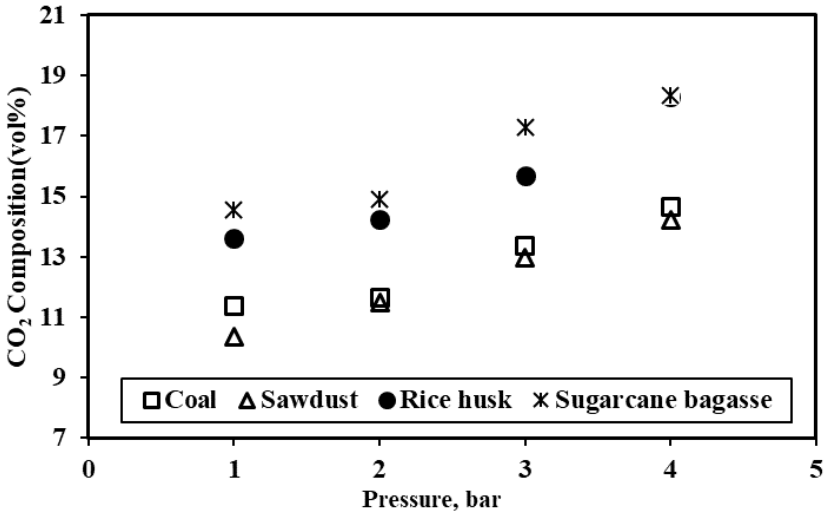

Fig. 6.5. Variation of CO_2 gas composition with operating pressure

6.3.2 Effect of pressure on LHV

The quantity of heat released during the complete combustion of a specific amount of substance is termed as the heating value of the corresponding substance. In a reaction, when the product is in the form of water H_2O (liquid), it is designated as a higher heating value (HHV). However, if the final product contains water vapor, the net available heat is called as LHV. This decrement in HHV which leads to LHV can be attributed to the utilization of heat towards converting the H_2O (liquid) to H_2O (vapor). Lower heating value can be estimated as the net calorific value of the syngas on a volumetric basis. During the calculation of LHV of the syngas, the concentration of different gases obtained during gas chromatography is usually incorporated. It can be represented by using Eq. 4.7.

From the aforementioned equation, it can be perceived that a slight increase in the percentage of methane can significantly alter the magnitude of LHV. Further, for calculation of LHV, the higher-order terms of C_mH_n is neglected, as, during gas composition analysis, these values can not be measured using gas chromatography. The LHV of the syngas with different operating pressure and inventory is displayed in Fig. 6.6. The LHV of syngas gas increases with an increase in operating pressure from 1 to 3 bar for all cases except sugarcane bagasse as feed material. At higher pressure operating conditions with sugarcane bagasse and rice husk as

inventory, the rate of decrement in hydrogen and carbon monoxide concentration in the syngas is more in comparison to rising in concentration for methane. Therefore, this results in a decrement in LHV for those cases at an operating pressure of 4 bar whereas for coal and sawdust, still LHV increases.

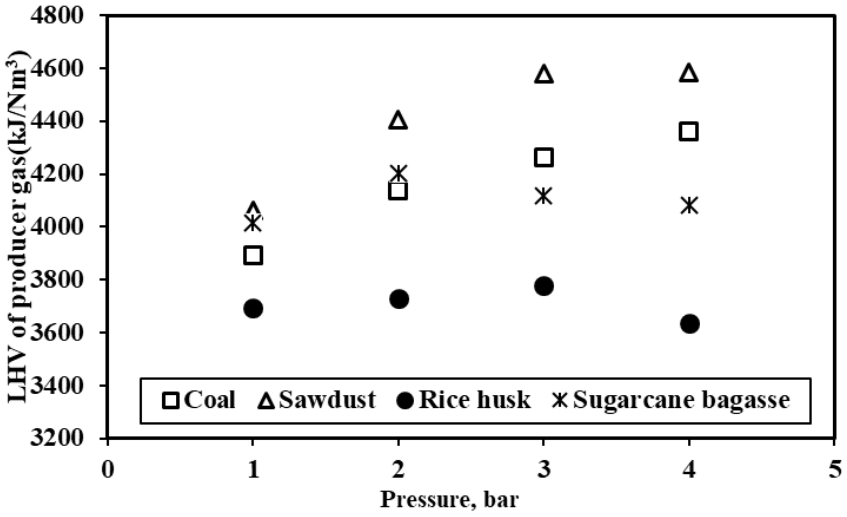

Fig.6.6. Variation of LHV with operating pressure

6.3.3 Effect of pressure on dry gas yield

The dry gas yield (Y) of the syngas relates the mass flow rate of nitrogen in the gasifier to the mass flow rate of the feed material and volumetric percentage of nitrogen obtained from gas chromatography analysis. However, in the present study, 'Y' is calculated based on the outgoing dry gas flow rate per kg input of feed material along with the concentration of nitrogen in the syngas. The value of 'Y' can be calculated using Eq. 4.9. The variation in 'Y' of the syngas with pressure for coal and biomasses is shown in Fig. 6.7.

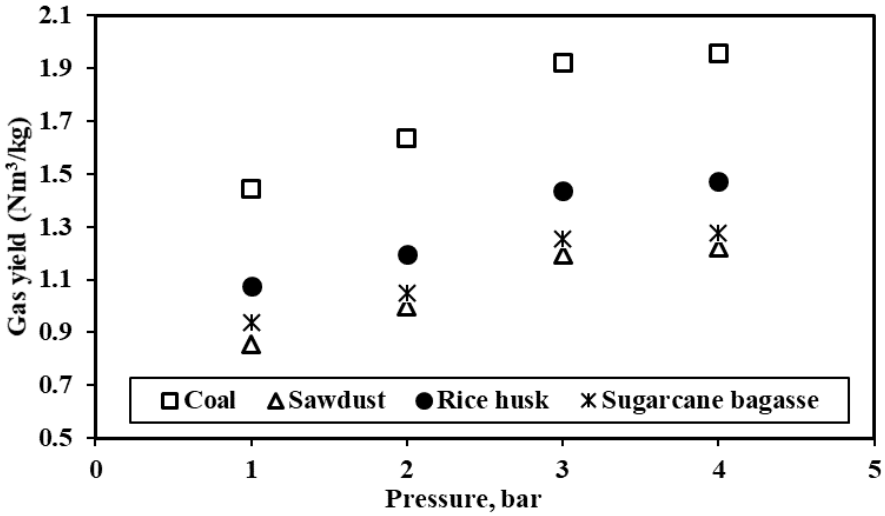

Fig. 6.7. Variation of dry gas yield with operating pressure

The magnitude of 'Y' is found to be increasing as operating pressure increases with sawdust having minimum yield and coal as maximum. As the concentration of N_2 decreases with increasing pressure, so the same can attribute to the enhancement of Y of the producer gas. Further, Y is also a strong function of the ash content of the feed material. For the present study, coal is found to have 39.9% of ash content while this value for sawdust, rice husk, and sugarcane bagasse is 1%, 19%, and 2.67%, respectively. Higher ash content in coal also leads to the maximum value of Y among all the inventories. Moreover, as bed temperature increases with pressure, this can enhance the gasification rate, pyrolysis, steam reforming and cracking of hydrocarbons which thereby can also add to the increase in the magnitude of Y.

6.3.4 Effect of pressure on CCE

Carbon conversion efficiency (CCE) is defined as the ratio of the volumetric percentage of carbonaceous gas species present in the syngas to the solid carbon present in the feed material. The variation of CCE of the syngas with pressure for all the inventory is shown in Fig. 6.8. The CCE can be defined as per the below using Eq. 4.10.

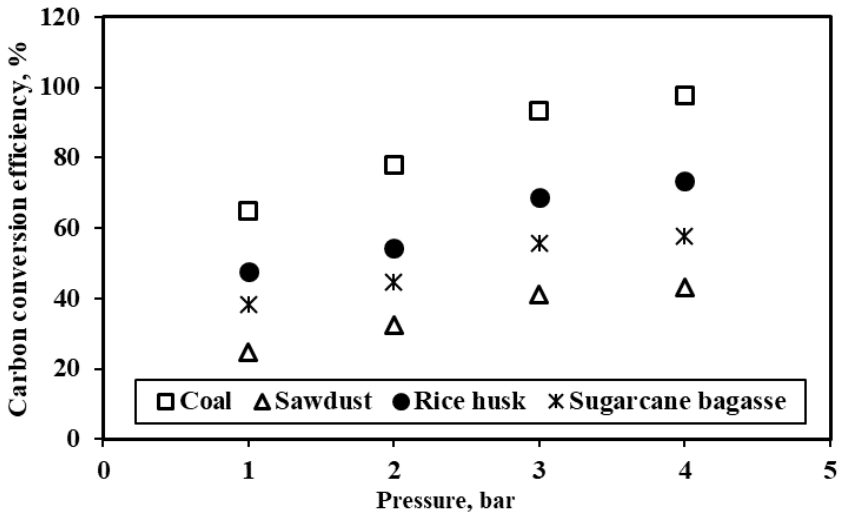

Fig. 6.8. Variation of carbon conversion efficiency with operating pressure

It is calculated based on the value of Y corresponding to the procedure gas, volume percentage of concentration of syngas (CO, CH_4, CO_2), and mass percentage of the carbon content in the feed material, which is obtained from the ultimate analysis. CCE increases with pressure with having lower magnitude for sawdust and highest for coal. From the figure, it can be perceived that for coal, CCE increases from 64% to 97% with an increase in pressure from 1 to 4 bar. Similarly, for sawdust, rice husk, and sugarcane bagasse, CCE increases in the range of 24-43%, 47-73% and 38-57%, respectively. As operating pressure increases, the mass flow rate

of air increases, thereby enhances the oxygen content. This results in a higher gasification rate. Also, due to temperature increase in association with pressure, more heat is supplied into the gasifier which also assists tar cracking reaction and steam gasification of carbon in the char increasing the CCE.

6.3.5 Effect of pressure on CGE

Cold gas efficiency (CGE) is defined as the ratio of the chemical energy produced by syngas to the energy content of the feed material. The variation of CGE of the syngas with respect to pressure is presented in Fig. 6.9. The CGE is calculated based on dry gas yield using the underlined Eq. 4.11.

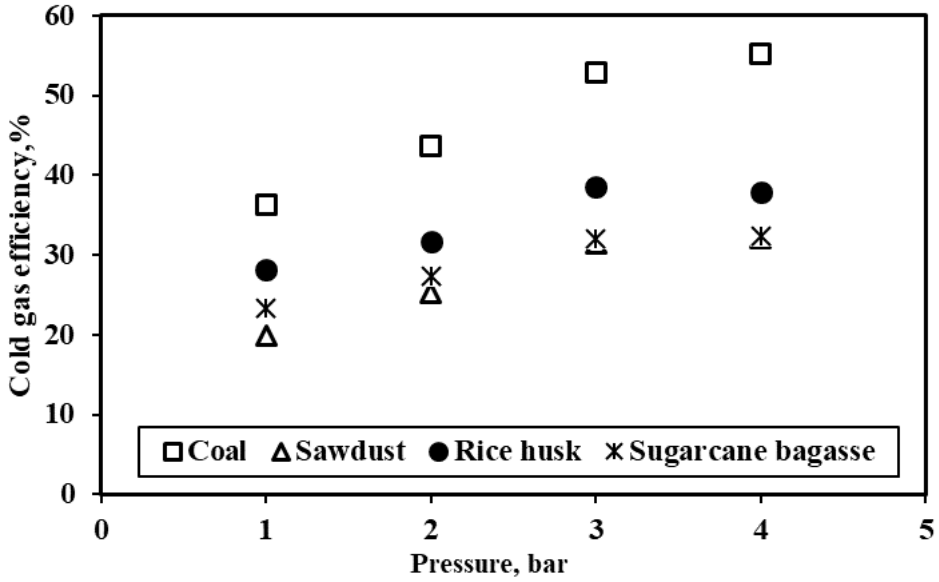

Fig. 6.9. Variation of cold gas efficiency with operating pressure

With an increase in pressure, both the value of Y and LHV of syngas increases for all the inventories. This results in an increase in CGE with respect to operating pressure which can be also deduced from Fig. 6.12. The maximum CGE is obtained with coal as feed material, and it is found to be increasing from 36 to 55% with an increase in pressure from 1 to 4 bar.

6.4. Summary

In the present investigation, the effect of operating pressure on the gasification of a PCFB gasifier is studied. The temperature increases rapidly due to the minimum heat loss to the atmosphere at the pressurized condition. All the feed materials are successfully fired under different parametric conditions. Sawdust is found to be having higher LHV in comparision to rice husk and sugarcane bagasse. The co-gasification study considering various blends of coal with sawdust is presented in Chapter 7.

Chapter – 7

Results and Discussion of Co-gasification Studies

7.1 Introduction

This chapter deals with the experimental results carried out to investigate the co-gasification of coal and sawdust blends in a PCFB gasifier. Gas composition, lower heating value (LHV), dry gas yield (Y), carbon conversion efficiency (CCE), cold gas efficiency (CGE), and tar content for various blends of low-grade coal and sawdust were estimated. Moreover, the effect of different parameters such as operating pressure, particle size and feed material on the same were evaluated. Results with and without the addition of in-situ catalyst were compared.

7.2 Co-gasification Studies Considering Coal-sawdust Blends as a Feed Material

In the previous chapter, out of the three-biomass used as feed material, sawdust has the highest LHV. So, for co-gasification studies, sawdust is preferred as feed material over rice husk and sugarcane bagasse, although rice husk and sugarcane bagasse also successfully proved as feed material for gasification studies. In the present co-gasification studies, blends of coal and sawdust (wt/wt) is used as feed material where, the percentage of saw dust is varied from 5% to 25% (5%, 10%, 15%, 20%, and 25%) by mass of the mixture. The reason behind choosing up to 25% is that with an increase in the percentage of the blending of sawdust, the suspension density of the feed material decreases, which results in choking inside the lower and upper part of the riser. The low density of sawdust tends to lower retention time, thus from the practical operation point of view chocking becomes frequent, and the bed becomes non-operative.

Apart from this, other researchers Mallick et al. (2019) used sand as a bed material for gasifying biomass in their experimental unit. In the modern CFB power plants, the bed ash formed acts as a bed material that replaces sand as bed material. The disadvantage of sand also is that it causes chocking in the nozzle area near the distributor plate. Mixing of sawdust with coal helps in creating a synergistic effect, which enhances the rate of gasification. The ash formed from sawdust and low-grade coal also act as a bed material inside the bed.

7.3 Effect of Pressure on Syngas Composition

To ensure the production of syngas and in order to appreciate the quality, the lighting of the gas is tested by using a kindler, and the same is reported in Fig. 7.1. The composition of syngas

is different for all experiments; however, the syngas upon lighting for all test cases shows a blue flame. Subsequently, the gas is collected in telder bags for gas chromatography.

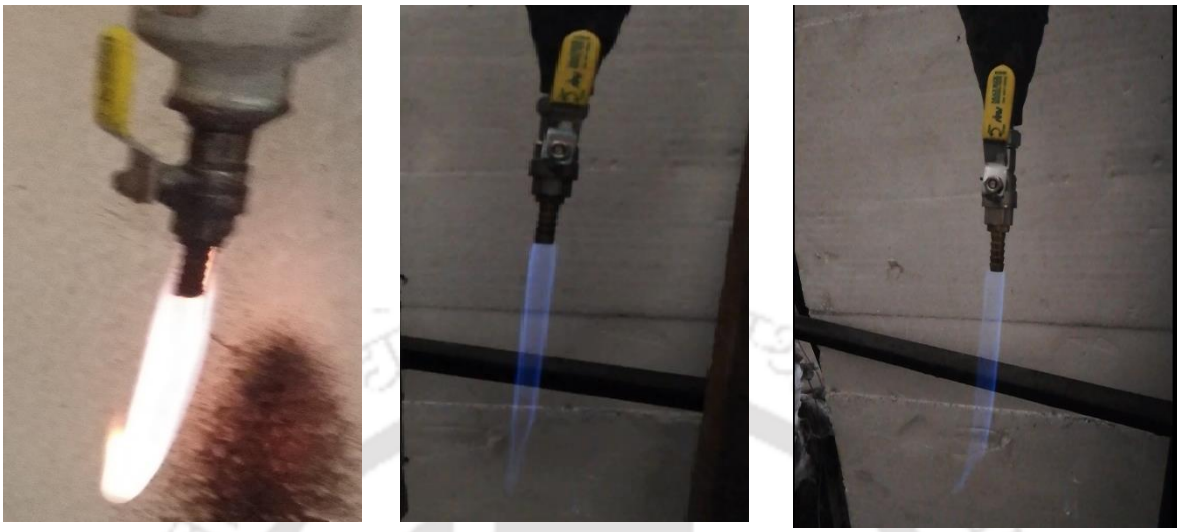

Fig. 7.1. Flames during experiments

The effect of pressure on syngas composition viz. concentration of H_2, CO, CH_4 and CO_2 is presented in Fig. 7.2 through 7.5. These compositions have been inferred from the gas chromatography of the collected syngas from co-gasification studies for each blend. From Fig. 7.2, it is observed that the concentration of H_2 is found to be decreasing with an increase in operating pressure for most of the coal-sawdust blends, however with the increase in the percentage of blending, the concentration of H_2 seems to be increased for any particular operating pressure. For 5% blends the concentration of H_2 is found to be decreasing from 6.25 to 5.84 vol% with an increase in pressure 1 to 4 bar.

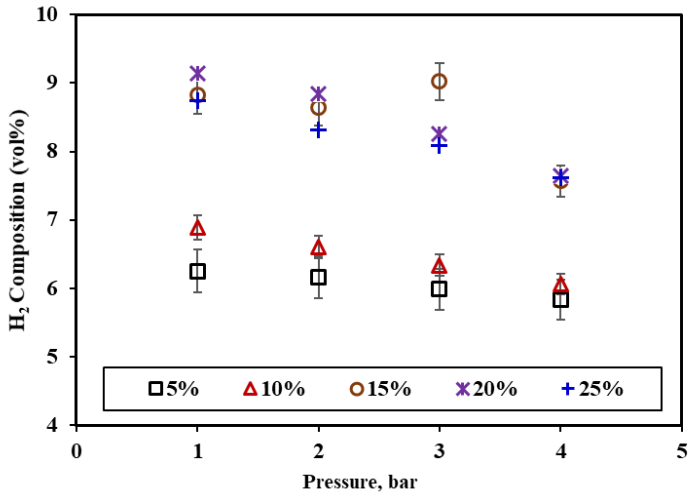

Fig. 7.2. Variation of H_2 gas composition with operating pressure

In a similar manner, significant reduction is observed for other blending ratios. As the blending ratio is increased, the percentage of reduction in H_2 concentration also increases due to an increase in pressure except for the 25% blending case. With an increase in pressure, methanation reaction takes place due to which reduction in the concentration of H_2 is evident. The concentration of H_2 is found to be increased up to 20% blends for most of the cases except 3 bar operating pressure and a decreasing trend in concentration of H_2 is perceived as blending percentage is increased from 20 to 25%. Furthermore, at the operating pressure of 4 bar, no significant variation in concentration of H_2 is observed at higher blending ratios. Similarly, the concentration of CO is measured, and as can be seen from Fig. 7.3, it is having an increasing trend from 1 to 3 bar for all the coal-sawdust blends except 10% and 25%. For operating pressure of 4 bar, all the blending ratios except 10% seems to have lower CO emission as compared to the 3 bar case.

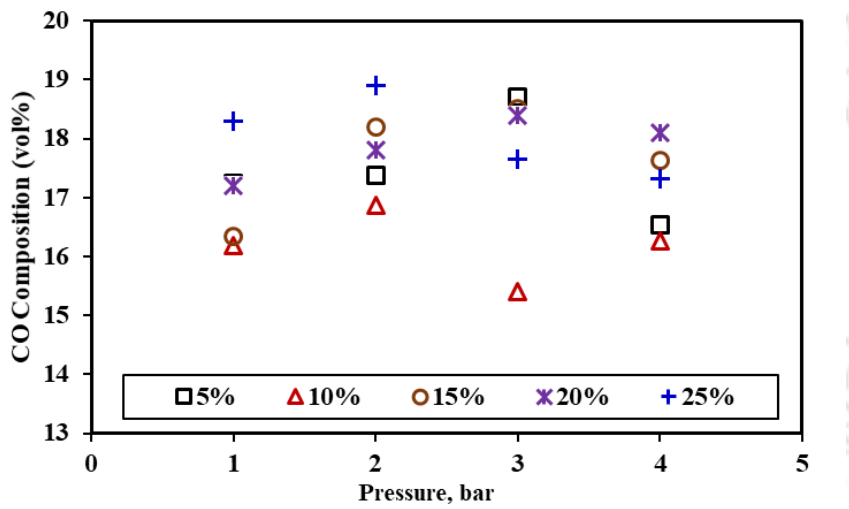

Fig. 7.3. Variation of CO gas composition with operating pressure

The concentration of CH_4 in syngas has also been analyzed and presented in Fig. 7.4 which justifies the increasing trend of CH_4 content for all the coal-sawdust blends with increment in operating pressure. Nevertheless, minor decrement in the concentration of CH_4 is evident for 25% sawdust blend with an increase in pressure from 3 to 4 bar. The increasing trend of CH_4 concentration can be attributed to the methanation reaction. Further, at higher pressure, the rate of reaction for carbon-hydrogen enhances thereby results in a further increase in the concentration of CH_4. As, pressure increase from atmospheric condition to 4 bar operating case, the concentration of CH_4 is found to increase by 28.9%, 15.3%, 15.8%, 14.5% and 7.5% for 5%, 10%, 15%, 20% and 25% blends, respectively. Therefore, it can be perceived that as the percentage of blending increases, the rate of increase in CH_4 content decreases.

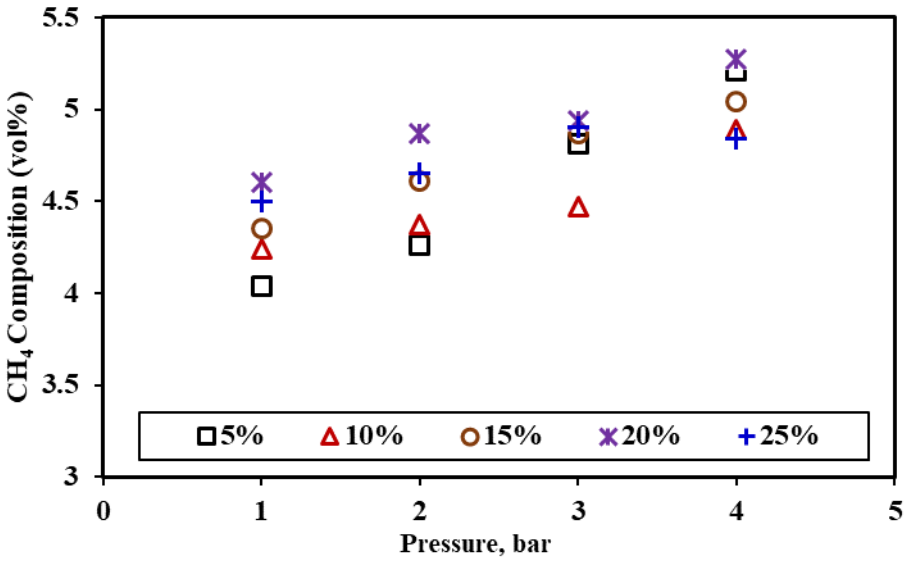

Fig. 7.4. Variation of CH_4 gas composition with operating pressure

The variation of CO_2 content in syngas due to the change in operating conditions and the blending ratio is illustrated in Fig. 7.5. The CO_2 concentration is found to be increased for all the coal-sawdust blends for an increase in pressure from 1 to 4 bar with the exception of 20% blending at 2 bar and 25% blending at 3 bar. The maximum content of CO_2 is found to be 12.89 vol% for the coal-sawdust blend of 15% at operating pressure 4 bar. The increase in the concentration of CO_2 is mostly due to the oxidation reaction in which carbon reacts with oxygen molecules resulting in further enhancement in the concentration of CO_2. Moreover, with an increase in pressure, airflow into the riser increases which decreases the residence time of the burning of feedstock.

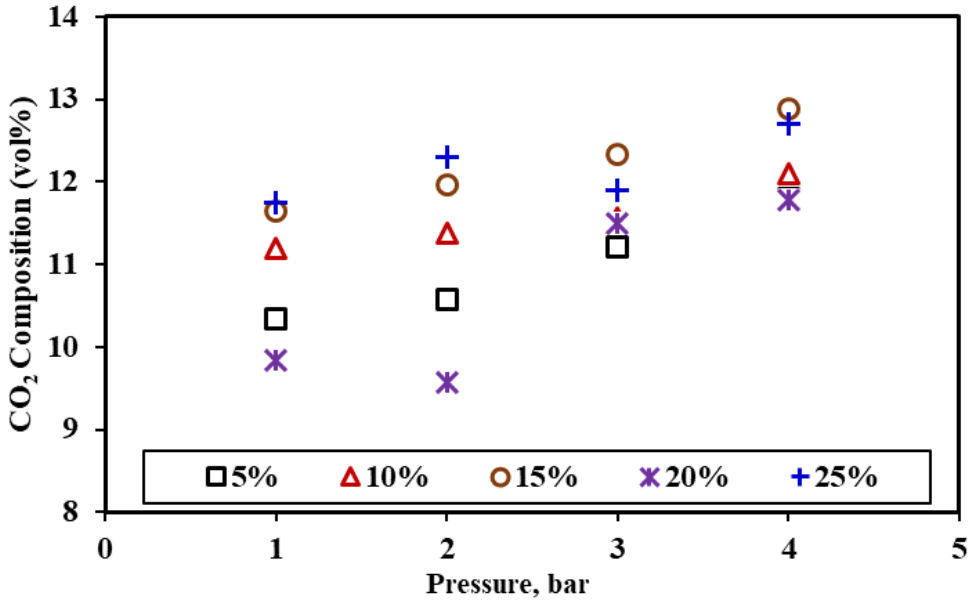

Fig. 7.5. Variation of CO_2 gas composition with operating pressure

7.4 Effect of Pressure on LHV

The lower heating value of the syngas with different operating pressure at various coal-sawdust blends is presented in Fig. 7.6. The LHV of syngas gas increases with an increase in operating pressure from 1 to 3 bar for all cases except 10% and 25% coal-sawdust blends. As discussed in the earlier chapters, LHV mostly depends on the concentration of CH_4, CO, and H_2 (Figs. 7.2-7.4). Furthermore, it has been observed from Fig. 7.3 that there is a significant decrement in CO content with 10% and 25% blending at 3 bar. This decrement leads to lowering of the magnitude of LHV at those conditions. At 4 bar operating pressure, LHV of the producer gas for all the blending conditions decreases except the 10% case. The maximum LHV of 5051.3 kJ/Nm^3 is found for 15% coal-sawdust blend operating at a pressure of 3 bar.

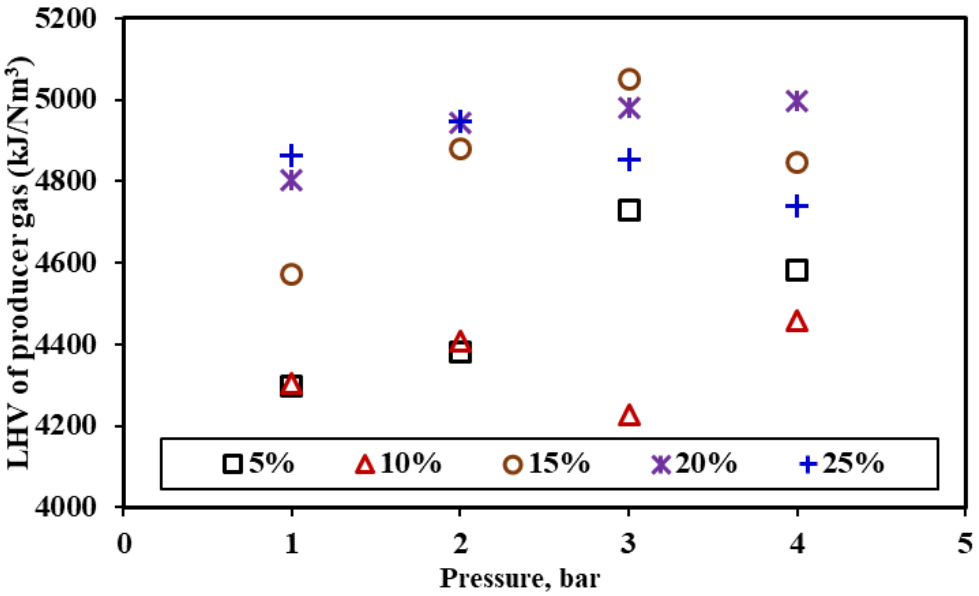

Fig. 7.6. Variation of LHV with operating pressure

7.5 Effect of Pressure on Dry Gas Yield (Y)

The variation in 'Y' of the syngas with pressure for coal-sawdust blends is shown in Fig. 7.7. The dry gas yield associated with syngas is found to have an increasing trend with an increase in operating pressure from 1 to 3 bar. However, with increase in pressure from 3 to 4 bar, significant variation in the magnitude of Y is observed only for 10% and 15% blending. The maximum dry gas yield of 1.88 is calculated for 15% coal-sawdust blends at the operating pressure of 3 bar. The gas yield is thereby observed to be a strong function of operating pressure along with temperature due to the dominance of pyrolysis, char gasification, and deformation of hydrocarbons inside the gasifier.

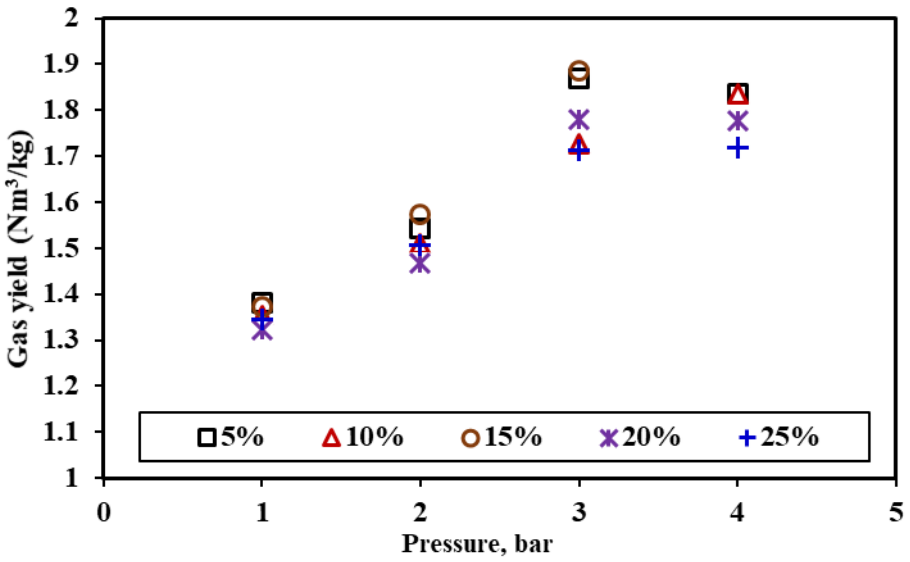

Fig. 7.7. Variation of dry gas yield with operating pressure

7.6 Effect of Pressure on Carbon Conversion and Cold Gas efficiency

The effect of pressure on CGE and CCE is shown in Fig. 7.8 and 7.9, respectively. The CGE is found to be increased upto 3 bar for all the blending composition. This can be attributed to the increment in the value of Y and LHV of the syngas with increase in pressure. However, a further increase in operating pressure seems to be invariant in terms of the effect on CGE for 20%, and 25% sawdust blending. Nevertheless, notable variation is observed, also at a higher pressure for remaining blending cases. The maximum CGE is obtained with 15% coal-sawdust blend as feed material, and it is found to be 60.4% for operating pressure of 3 bar.

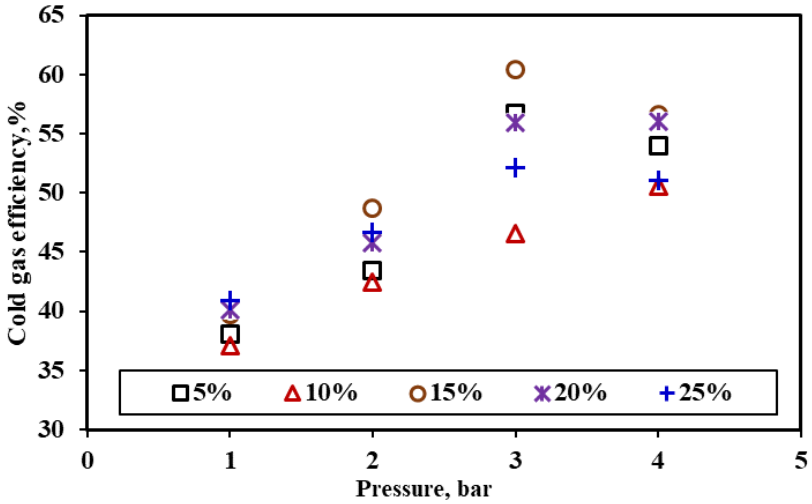

Fig. 7.8. Variation of CGE with operating pressure

Similar variation as that of CGE is also evident in the case of carbon conversion efficiency. CCE is found to be increasing from 1 to 3 bar irrespective of the coal and sawdust proportion.

However, at higher pressure, significant decrement in CCE is observed for 5% and 15% blending which can be correlated to the rapid reduction in the concentration of CO at 4 bar. The maximum CCE is found to be 79.78% for 15% coal-sawdust blending at the operating pressure of 3 bar.

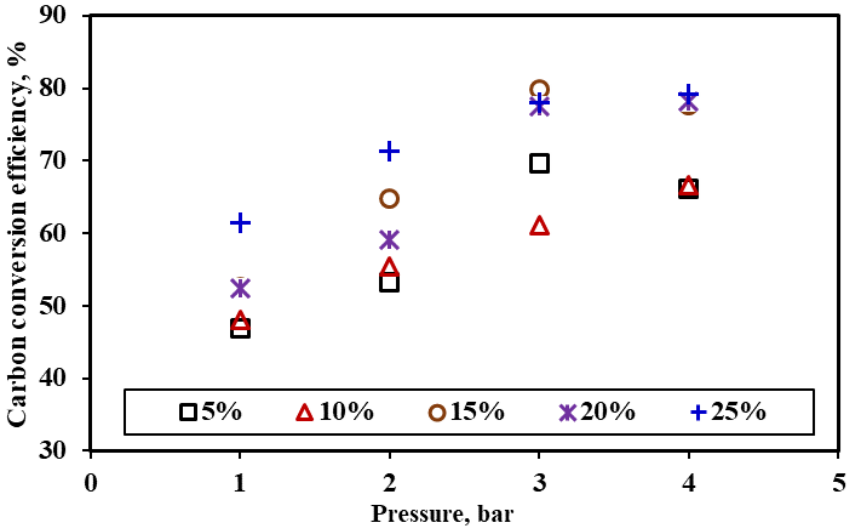

Fig. 7.9. Variation of CCE with operating pressure

7.7 Effect of Pressure on Tar Content

Tar usually comprises of aromatic compounds having a higher molecular weight that forms during the gasification process. These compounds condense in the form of highly viscous fluid after the reduction of syngas temperature to ambient conditions. High tar content syngas is unsuitable for many applications because as tar condenses, it gets deposited on the wall of the riser, heat exchanger, and gas engine that creates operational problems. This is one of the significant challenges that need to be monitored as a part of the gasification process and reducing the tar content is also an essential part of this investigation. The tar formed during each experiment is collected and measured. The tar content for different coal-sawdust blends with pressure is shown in Table 7.1.

Table 7.1: Tar content with different blending ratio

Blending Ratio, % (wt/wt)	Tar content (g/kg of dry fuel) Operating Pressure (bar)			
	1 bar	2 bar	3 bar	4 bar
5	3.65	3.84	2.09	1.91
10	4.7	3.97	2.16	1.97
15	4.85	4.14	2.24	2.04
20	5.25	4.48	3.24	2.61
25	5.97	5.09	3.63	3.25

From Table 7.1, it is observed that the tar content decreases with an increase in operating pressure; however, tar content is found to be increasing as the percentage of sawdust blending increases at a particular operating pressure. Maximum tar content (5.97 g/kg of dry fuel) is observed for 1 bar and 25% coal-sawdust blends while the minimum value of 1.91 g/kg of dry fuel is detected for 4 bar with 5% coal-sawdust blends.

7.8 Effect of LHV and Gas Yield with Coal-sawdust Blends

In order to obtain the optimum operating pressure magnitude that needs to be maintained for further co-gasification experiments, LHV and gas yield variation at different pressure is revisited and has been presented in Fig. 7.10 and 7.11, respectively.

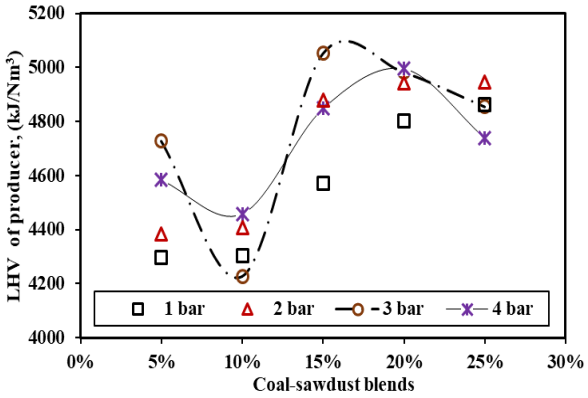

Fig. 7.10. Variation of LHV with blends

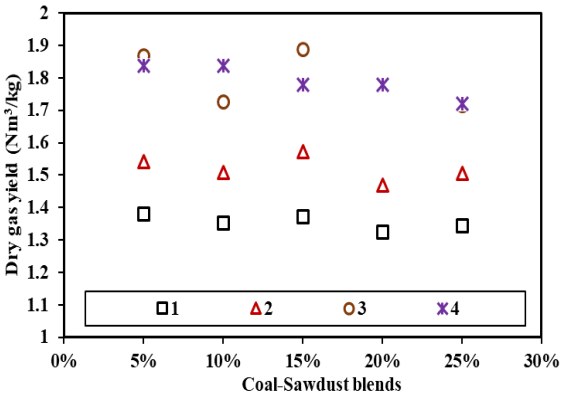

Fig. 7.11. Variation of gas yield with blends

From Fig. 7.10, as far as the effect of operating pressure is concerned, it can be perceived that no specific variation is evident. However, for most of the blending cases, 3 bar operating pressure yields in the maximum value of LHV. A similar observation can also be deduced from the gas yield variation subjected to different operating pressures as shown in Fig. 7. 11. Hence, based on these observations, afterward, all the experiments in PCFB gasifier have been conducted at an operating pressure of 3 bar only.

7.9 Effect of Dolomite as a Catalyst in Co-gasification Studies

The efficacy of dolomite as a catalyst towards enhancing the gasification rate is assessed herein for the coal-sawdust blends at the operating pressure of 3 bar. Coal-sawdust blends of 5% to 25% are used as feed material with a 10% addition of dolomite. The variation in gas composition, LHV, Y, CCE, and CGE is evaluated for better insight.

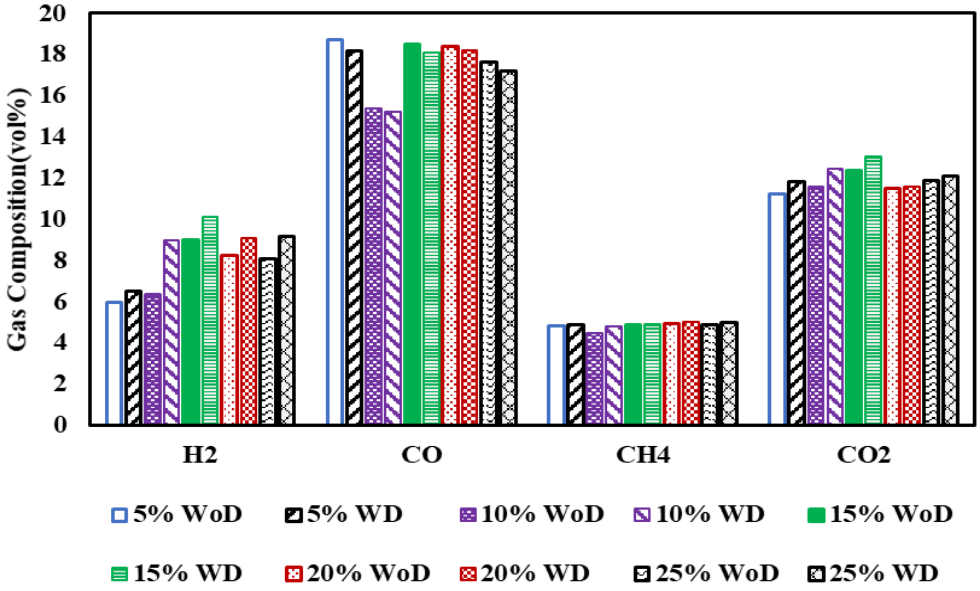

Fig. 7.12. Variation of gas composition with dolomite as a catalyst

The gas composition for coal-biomass blends (wt/wt) for 3 bar operating pressure is presented in Fig. 7.12. Results without dolomite (WoD) and with dolomite (WD) are presented in the figure. The concentration of hydrogen is found to be increasing with the incorporation of dolomite as a catalyst. Maximum enhancement of 41% is found for 10% blending whereas 8-12% increment is observed for other blending percentages. The increase in methane content is almost constant and seems to be invariant of the dolomite addition. However, a small increase in methane content can also lead to a significant rise in the LHV magnitude due to the associated higher heat-carrying coefficient. The concentration of CO is found to be decreasing while the concentration of CO_2 increases with the inclusion of dolomite. Nevertheless, CO and CO_2 variation for a higher percentage of blending cases seem to be nominal in terms of magnitude.

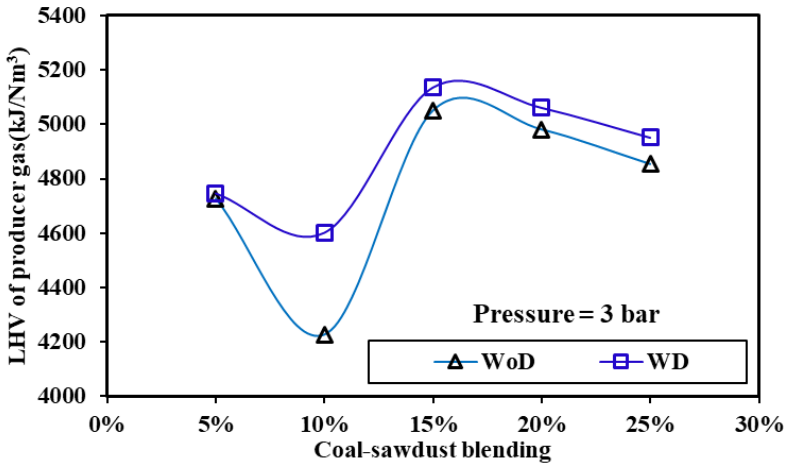

Fig. 7.13. Variation of LHV with dolomite as a catalyst

The enhanced magnitude of LHV is estimated for all the coal-sawdust blends with the addition of dolomite in the feed material (Fig. 7.13). The maximum increase is observed for 10% blending, where LHV increases from 4228 to 4600 kJ/Nm^3, while for other cases, an increase in LHV is found to be minimal. The increase in LHV is mostly due to the significant increase in hydrogen content in the syngas. Minor increment in methane concentration is also a potential factor towards increment of the LHV, as it has a higher heat-carrying coefficient (Eq. 4.7).

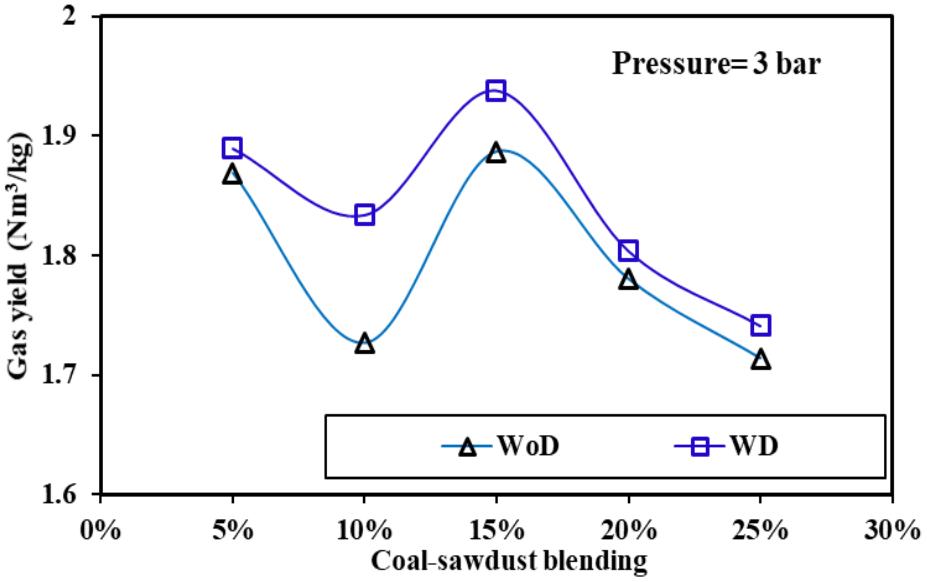

Fig. 7.14. Variation of gas yield with dolomite as a catalyst

The change in gas yield for the coal-sawdust blends is presented in Fig. 7.14, which seems to have a similar variation as that of LHV. With the addition of dolomite, the gas yield increases for all the blends. A maximum gas yield value of 1.93 is found for the 15% blend, whereas the maximum percentage of increment in gas yield is calculated to be for the 10% coal-sawdust blend, as can be seen from Fig. 7.14.

The alteration in values of CCE and CGE with the addition of dolomite as a catalyst are shown in Fig. 7.15 and 7.16, respectively. The CCE for 5%, 20%, and 25% coal-sawdust blending is found to be mostly invariant to the inclusion of catalyst; however 9.65% and 3.69% increase in CCE is observed for 10% and 15% blending, respectively. Furthermore, the profile of CGE is found to be similar to that of CCE, where at 5% blending has the least effect. The maximum increase (46.2 to 53.4) in CGE is observed for 10% blending, whereas maximum magnitude viz. 63% of CGE is obtained for the coal-sawdust blending of 15%, as seen from Fig. 7.16.

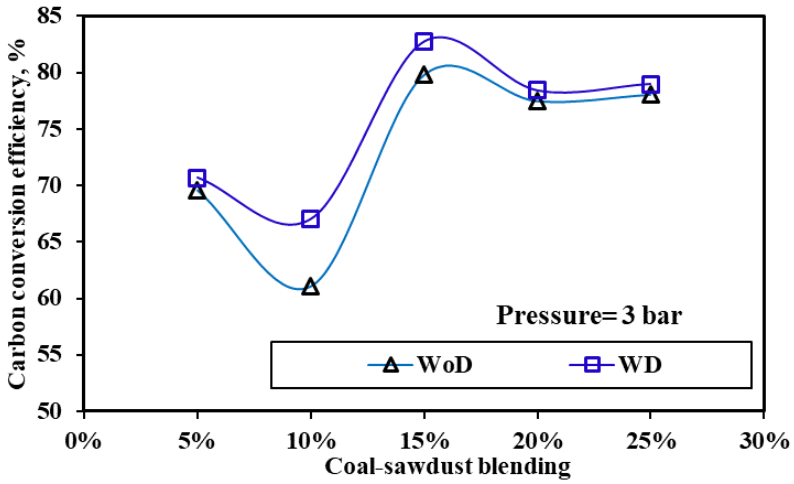

Fig. 7.15. Variation of CCE with dolomite as a catalyst

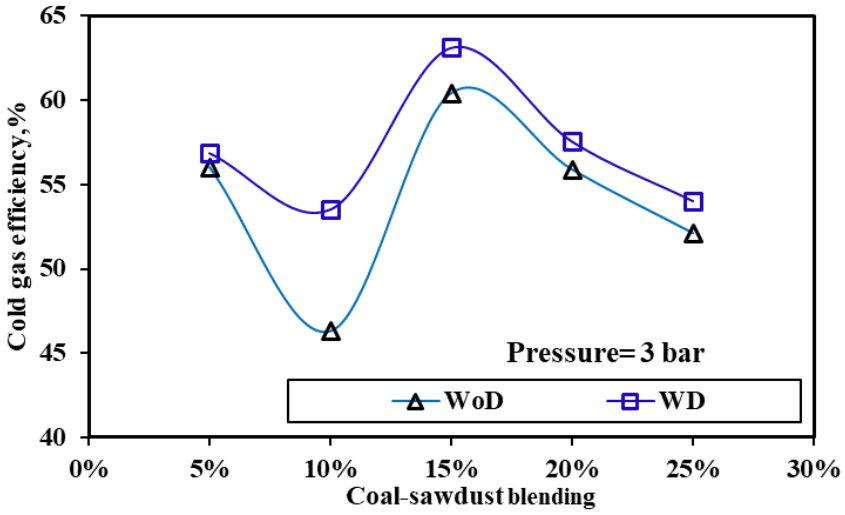

Fig. 7.16. Variation of CGE with dolomite as a catalyst

The tar content in the syngas with and without the presence of dolomite is presented in Table 7.2. The effect of using an in-situ catalyst is found to have a positive effect on the tar content. The tar content is found to be decreasing by using dolomite as a catalyst. The percentage of decrement in tar content seems to be increasing as the blending ratio increases. A maximum of 38% decrement in tar content is observed for 25% sawdust blending.

Table 7.2: Tar content with and without dolomite

Coal- sawdust blends, % (wt/wt)	Tar content (g/kg of dry fuel)	
	3 bar-WOD	3 bar-WD
5	2.09	1.81
10	2.16	1.91
15	2.24	1.94
20	3.24	2.37
25	3.63	2.89

7.10 Bottom Ash Analysis

Catalysts are used to enhance the quality of product gas and to reduce the formation of tar content. Commercial catalysts like nickel, dolomite, and olivine are extensively used in the gasification of biomass, but they have their limitations like a short active lifetime and costly. The bottom ash as the additional catalyst in gasification of biomass is discussed (Shahbaz et al. 2019, Herman et al. 2016, Shahbaz et al. 2017, and Xiong et al. 2010). The characteristics of the bottom ash are analyzed to obtain the surface morphology, pore size, chemical compound, pore-volume, bulk density and surface area of the bottom ash. The bottom ash contains the main elements such as silicon oxide (SiO_2), iron oxide (Fe_2O_3), aluminum oxide (Al_2O_3), calcium oxide (CaO), and magnesium oxide (MgO) which can be used as the catalyst in gasification of biomass. A large amount of SiO_2 present in the bottom ash can also be used as a bed material for the gasification process. However, Fe_2O_3 improves the reduction of tar content in produced syngas whereas the presence of CaO supports the enhancement of the produced syngas yield by reducing the concentration of CO_2.

Bottom ash also contains the element such as Fe, Al, Ca, Mg, K, and Na which are used as a catalyst in gasification. Xiong et al. (2010) used bottom ash in the gasification of coal as bed material and used air as a gasifying agent. They observed that for reduction of tar content, the minerals present in the bottom ash are responsible. With the use of bottom ash, the concentration of CO_2 is also reduced to some extent. They also found that bottom ash had not been investigated in the light of its use as a catalyst in biomass gasification.

Tian et al. (2019) used bottom ash as the bed material and compared the results with silica sand. They found that with the addition of the bottom ash as bed material, the concentration of H_2 is enhanced while the concentration of CO, CO_2, and CH_4 reduced. The increase in concentration of H_2 is due to steam reforming as well as water gas shift reaction. They also noticed the decrement of tar content is more in case of bottom ash when compared to silica sand as bed material.Bottom ash is one of the significant waste products for coal power plants. Toraldo et al. (2013) studied the characteristics of the bottom ash and observed bottom ash as the appropriate candidate for an alternative material to make road construction mainly in foundation and asphalt concretes. Arenas et al. (2013) reported that bottom ash could be used as the common noise barrier to reduce sound reflection towards noise-sensitive areas near the highway. They observed that the bottom ash has the admirable potential for noise absorption characteristics and it can be used commercially near the noise-sensitive area**.** Herman et al.

(2016) surveyed the thermal power plant waste of bottom ash. They observed that normally the bottom ash is used in the cement industry as well as in the construction industry.

Inspite of many usage of the bottom ash as indicated above, it is still disposed of rather than being recycled in a useful way. The traditional method for disposal of the solid waste is pond disposal and filling of land. However, bottom ash is considered as a hazardous material because it contains heavy metal and high chloride which can results in environmental pollution to the landfill as well as water bodies. Jiang and Roy (1992) and Zermeno et al. (2014) reported that the disposal of bottom ash in water bodies and landfilling method are not supportable as new land and pond needs to be acquired once the existing land and pond reaches its capacity.Bottom ash is one of the by-products that remain after the end of the combustion or gasification process. The majority of this type of ash is usually deposited at the lower part of the combustor, which needs to be taken care of and thereby requires proper treatment as the quantity of such ash is huge.

Figure 7.17 presents the XPS analysis of the bottom ash collected after co-gasification at 3 bar with 15% coal-sawdust blends (wt/wt). The XPS analysis of the same was conducted at CSIR Jorhat, Assam, India.

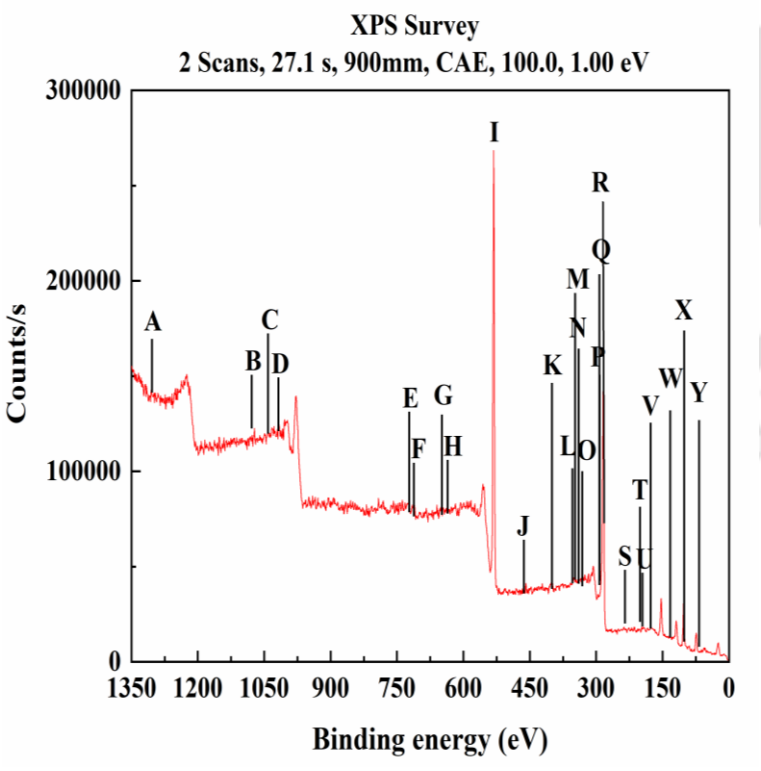

	Elements	Peak
A	Mg1s	1304.62
B	Na1s	1072.5
C	Zn2p1	1041.75
D	Zn2p3	1019.74
E	Fe2p1	723
F	Fe2p3	710.28
G	Mn2p1	651
H	Mn2p3	636
I	O1s	531.74
J	Ti2p1	463.09
K	N1s	400.71
L	Ca2p1	349.32
M	Ca2p3	349
N	Pd3d3	341.82
O	Pd3d5	335.15
P	K2p1	296
Q	K2p3	295.84
R	C1s	284.03
S	Mo3d5	232
T	Cl2p1	201.11
U	Cl2p3	197.31
V	Zr3d3	183.2
W	P2p	131
X	Si2p	102.23
Y	Al2p	74.07

Fig. 7.17. XPS survey for coal-sawdust blends

The counts/s with binding energy is shown for the coal-sawdust blend. The peak value for different elements has been obtained, and the corresponding atomic percentage are calculated, which is reported in Fig. 7.18.

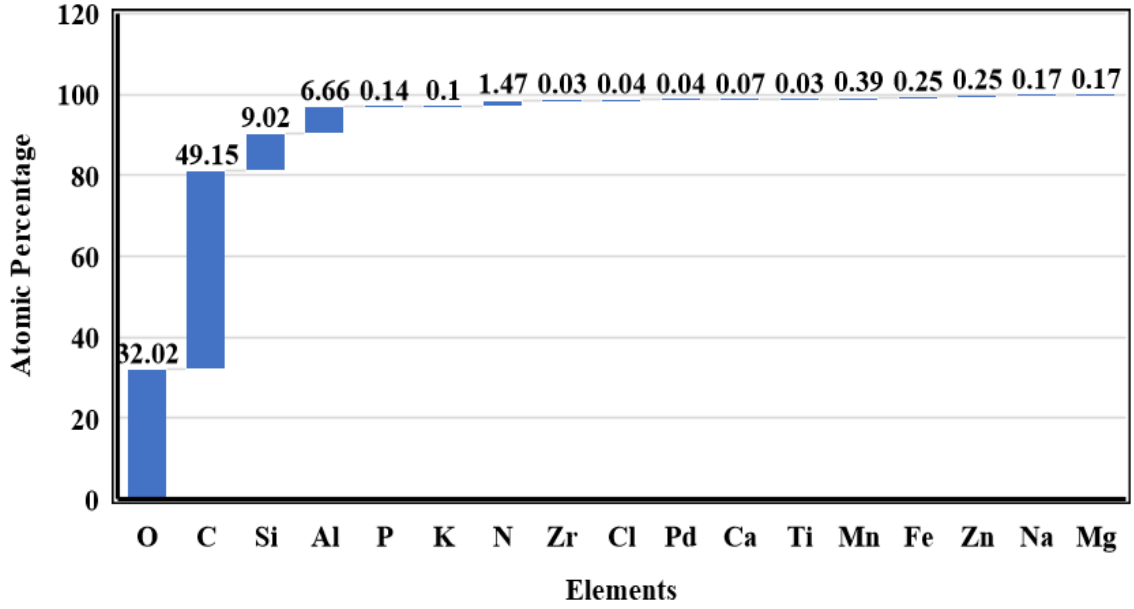

Fig. 7.18. Atomic percentage for different elements

From the analysis, different elements such as oxygen, carbon, silica, aluminum, phosphorus, potassium, nitrogen, zirconium, chlorine, palladium, calcium, titanium, manganese, iron, zinc, sodium, and magnesium are found with different electronic states and atomic percentage. The atomic percentage presented in Fig. 7.18 reveals that bottom ash is having a maximum percentage of carbon viz. 49.12%. However, it also comprises of 32.02% oxygen, 9.02% silica, 6.66% aluminum along with 1.47% nitrogen. These elements are mainly found in the form of oxides that can be further utilized for different applications.

Further, as reported in the literature (Shahbaz et al. 2017, Xiong et al. 2010, Tian et al. 2019), the bottom ash can also be used as a catalyst or as a bed material which is solely determined based on the composition of the same. In the current studies, as can be confirmed from Fig. 7.17, elements such as SiO, Fe_2O_3, CaO, Al_2O_3, MgO, and K_2O_3 are present in the bottom ash. Therefore, the bottom ash can be utilized as a catalyst for enhancing the gasification rate. Moreover, mixing sawdust with coal helps in creating a synergistic effect, which enhances the rate of gasification. Nevertheless, the ash formed from sawdust and coal also acts as a bed material inside the bed, which suppresses the disadvantage of using sand, which at a later stage can result in chocking in the nozzle area near the distributor plate.

7.11 Effect of Particle Size on Co-gasification

The effect of particle size on co-gasification studies has been described in the following section. Four Gildert particle size having a mean particle diameter of 300, 450, 600 and 770 μm is considered for the current studies. During the assessment of the effect of these particle diameters on co-gasification, operating parameters associated with experiments such as pressure has been kept constant. However, in line with the previous experiments, all the blending cases of sawdust with low-grade coal has been considered with dolomite as 10%. As a part of determining the effectiveness of the co-gasification study, as like previous instances, performance parameters like syngas composition, LHV, Gas yield, CGE, and CCE have been analyzed. During the experiments, it is observed that with the decrease in particle size, the input energy required for electrical heating is getting decreased. This can be due to the associated higher value of heat transfer with a decrement in particle size. The effects on gas composition, LHV, Y, CCE, and CGE are discussed below.

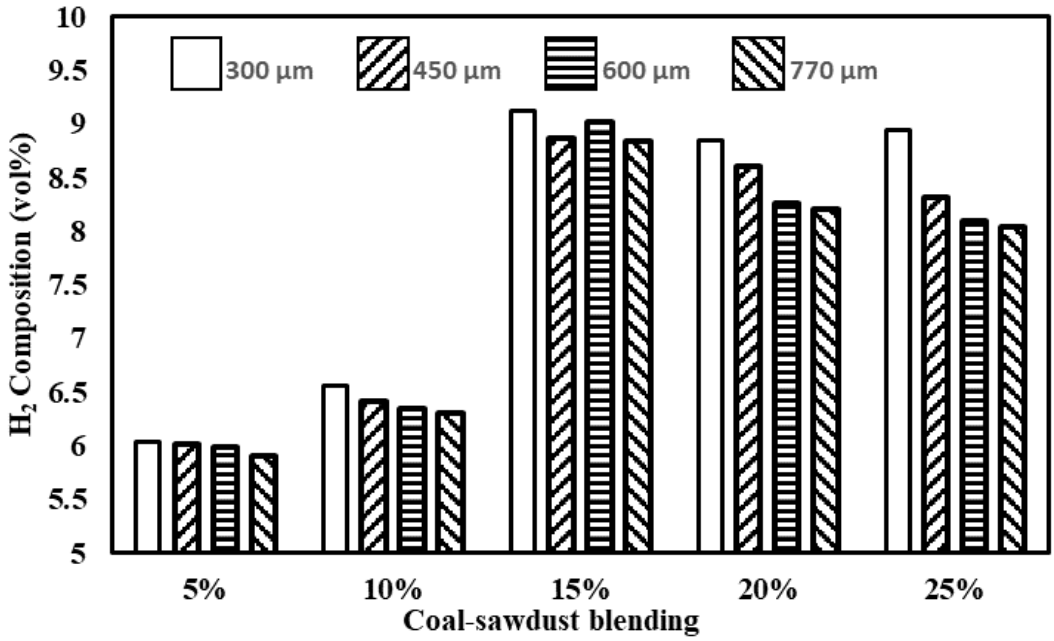

Fig. 7.19. Variation of H_2 gas composition with coal-sawdust blends

The variation of gas composition with coal-biomass blends for four mean particle size are presented in Fig. 7.19 through Fig. 7.22. From Fig. 7.19 it is observed that the effect of particle size is minimal for 5% to 15% coal-sawdust blends, whereas the effect is found to be significant for high blending ratios. At these higher blends, the concentration of hydrogen is found to be decreasing as the particle size is increased. The maximum value of hydrogen content is obtained as 9.12% for 300 μm particle size and 15% blending.

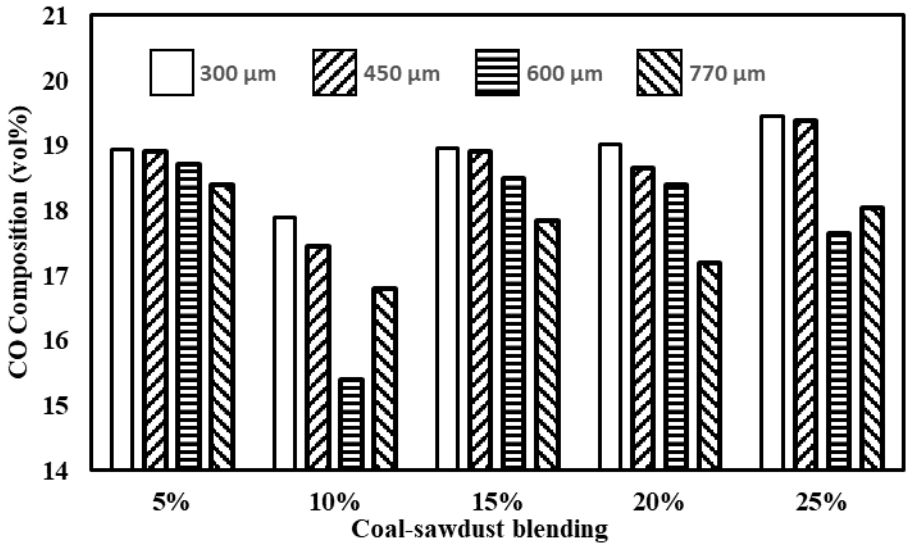

Fig. 7.20. Variation of CO gas composition with coal-sawdust blends

The concentration of CO for different coal-sawdust blends along with varying diameters of the particle is presented in Fig. 7.20. The trend of CO composition is similar to that of hydrogen, where, with an increase in particle size, CO concentration is found to be decreasing for most of the cases. However, some discrepancy has been perceived for the case of 770 µm particle diameter having a blending ratio of 10% and 25%.

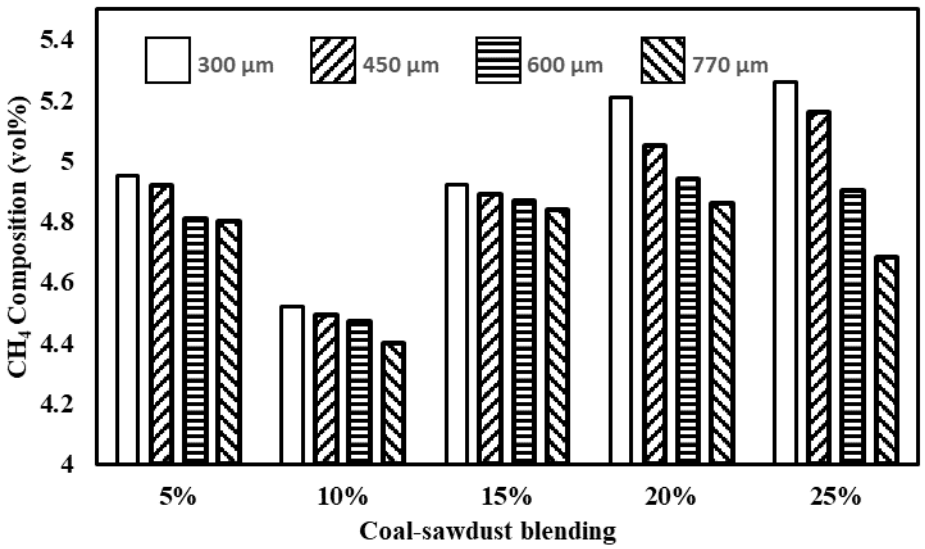

Fig. 7.21. Variation of CH_4 gas composition with coal-sawdust blends

The concentration of CH_4 in the syngas for different coal-sawdust blends and particle diameter is presented in Fig. 7.21. The CH_4 concentration is found to be decreasing with an increase in mean particle size; however, the decrement is notable for 20% and 25% blends whereas nominal for all other blends. The maximum CH_4 concentration is found to be 5.26 vol% for 300 µm particle size and 25% coal-sawdust blending.

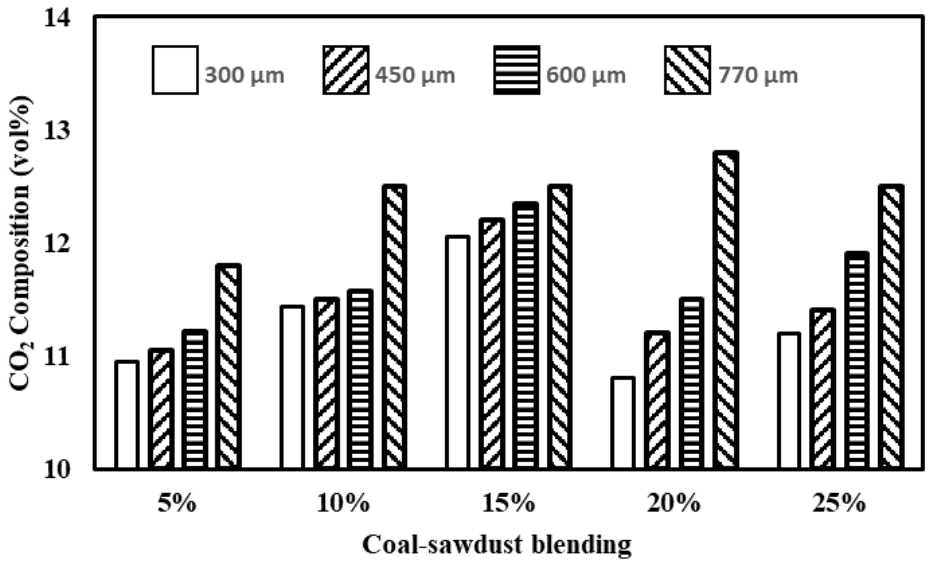

Fig. 7.22. Variation of CO_2 gas composition with coal-sawdust blends

Similarly, the variation in the concentration of CO_2 due to different coal-sawdust blends, as well as particle diameter, is shown in Fig. 7.22. Contrary to other components, the concentration of CO_2 is found to be increasing as the mean particle size is varied from 300 to 770 µm. Further, the variation in CO_2 composition is significant for all the cases with a maximum variation for 20% blending. The maximum concentration of CO_2 is observed to be 12.8 vol% for 770 µm particle size and 20% coal-sawdust blends.

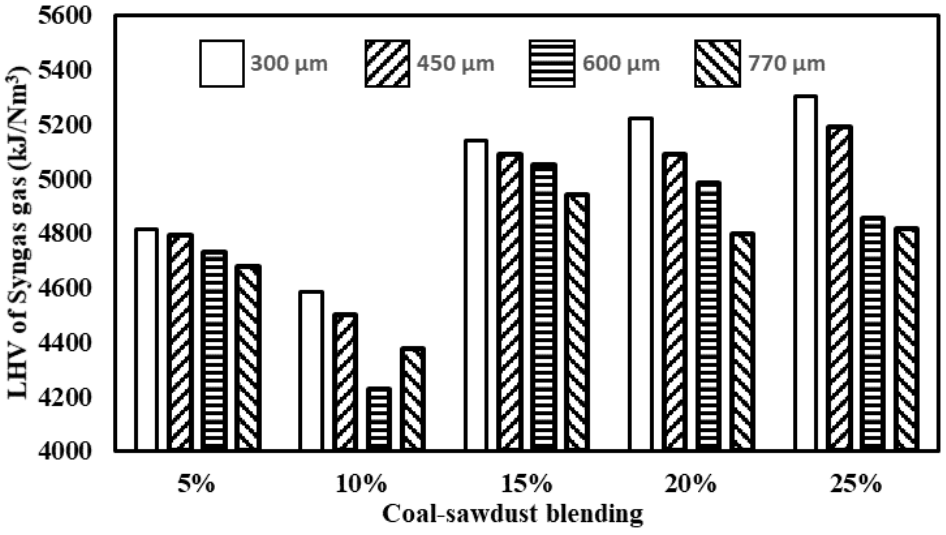

Fig. 7.23. Variation of LHV with coal-sawdust blends

As LHV is more susceptible to the change in CO concentration, therefore similar variation has also been reflected in the case of LHV which can be seen from Fig. 7.23. LHV is found to be decreasing with an increase in particle size from 300 to 770 µm. The decrement of LHV seems

to be minimal for 5% and 10% blending, while significant decrement in LHV is observed for 15 to 25% coal-sawdust blend. The higher value of LHV is evident for higher blending ratios for a particular particle diameter.

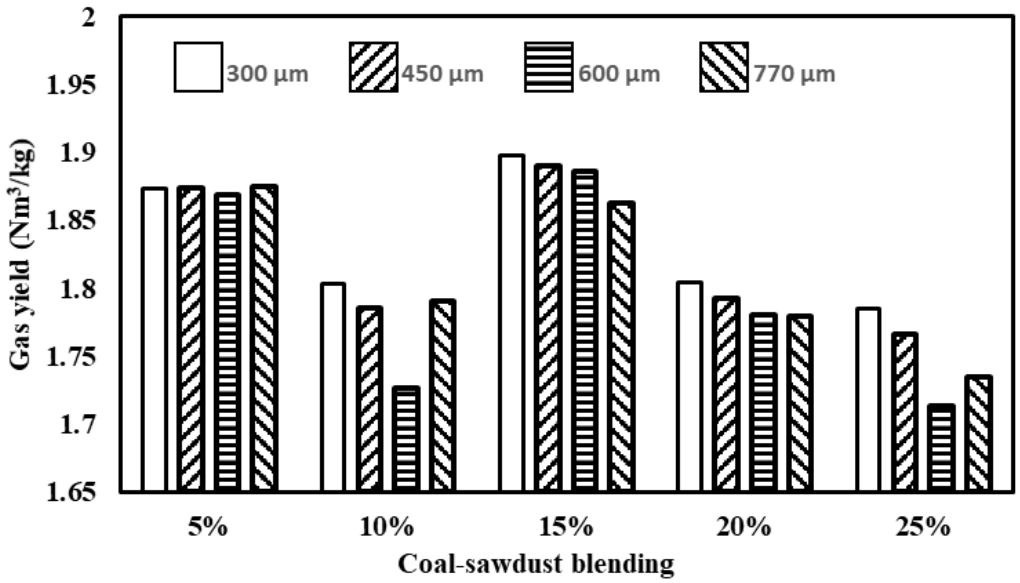

Fig. 7.24. Variation of dry gas yield with coal-sawdust blends

As it can be perceived from Fig. 7.24, the effect of particle size on dry gas yield is minimal for most of the blending ratios. The dry gas yield is almost constant as particle size increases from 300 to 770 µm, with the blending ratio being fixed. Some discrepancy is observed for 600µm particle diameter with 10% and 25% blending cases. The highest dry gas yield is found to be 1.89 Nm^3/kg for 300 µm of mean particle size and 15% coal-sawdust blending.

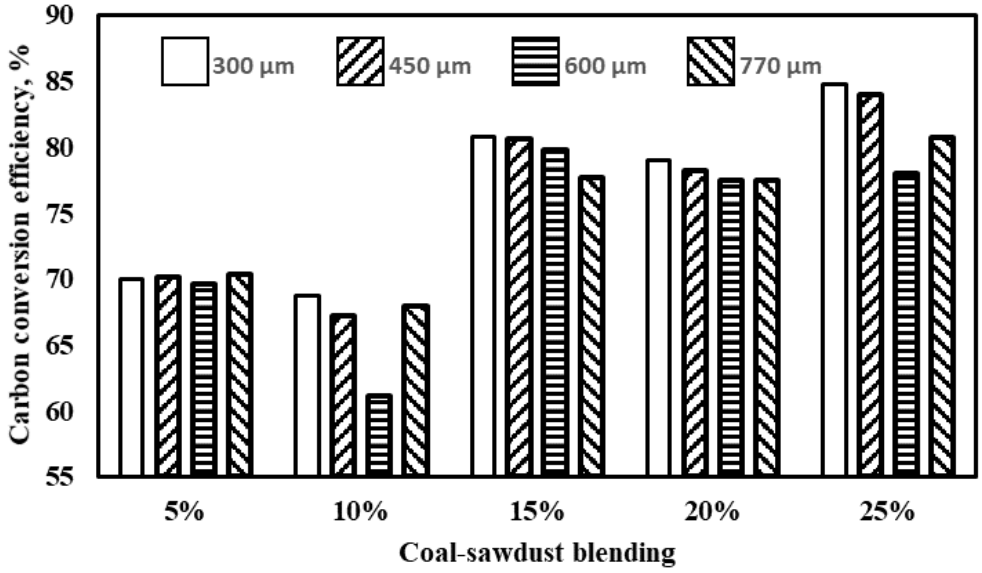

Fig. 7.25. Variation of CCE with coal-sawdust blends

The effect on CCE due to variation in the coal-sawdust blend, as well as the particle size, is presented in Fig. 7.25. The maximum value of CCE is found to be 84% for 25% blends with a mean particle size of 300 μm. For 5%, 15%, and 20% blend, the CCE is mostly invariant to the variation in particle size. It can be also concluded that the maximum value of CCE corresponding to a certain blending can be achieved through decrement of the particle diameter.

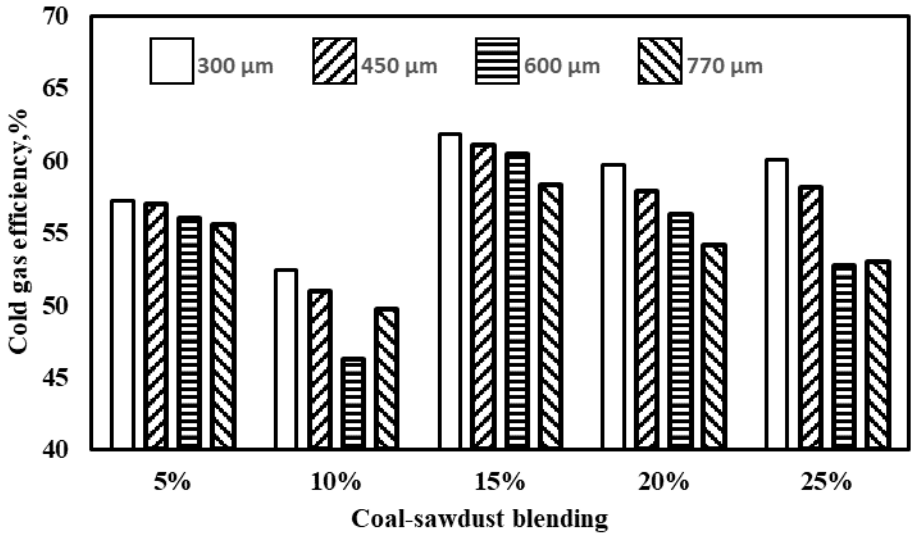

Fig. 7.26. Variation of CGE with coal-sawdust blends

In similar to CCE, as can be seen from Fig. 7.26, CGE for a particular blending ratio happens to be maximum for the lower particle size. Furthermore, as found in the previous studies, CGE also seems to be affected by the blending ratios for almost all the considered particle size. Nevertheless, the effect is predominant at higher blending ratios. The maximum CGE is found to be 62% for 300 μm with a 15% sawdust blend.

7.12 Summary

The blends of coal with sawdust under different pressure is gasified successfully. Out of all the four operating pressures 3 bar is preferred as an optimum pressure condition based on the highest LHV of the syngas. Effect of use of dolomite as a catalyst is also studied, and with the addition of dolomite, it was found that the rate of gas yield increases with decrease in tar yield. The effect of particle size is also studied and observed that particle size has minimal effect under these operating conditions; however, there is a small increase in LHV is found with the decrease in particle size for coal-sawdust blends. Chapter 8 presents the overall conclusions and scope for future work.

Chapter – 8

Conclusions and Scope for Future Work

8.1 Conclusions

In the present investigation, an attempt has been made to perform hydrodynamic, heat transfer and gasification studies in a PCFB gasifier. In this context, a numerical study has been performed for the hydrodynamic study followed by an in-house fabrication of a PCFB gasifier. The effect of operating parameters for the hydrodynamic and heat transfer is carried out. The gasification is carried out with low-grade coal and biomass such as sawdust, rice husk, and sugarcane bagasse. Finally, co-gasification with various blends of low-grade coal and sawdust has been studied. Chapterwise conclusions are presented in the following sub-sections:

8.1.1 Numerical Study

The numerical study is conducted using ANSYS FLUENT 14 for the 2D geometrical model. The operating pressure is varied from 1 to 10 bar. The key outcomes are presented below:

- The bed voidage is found to be decreasing with an increase in operating pressure and there is a phase shift that is observed with an increase in operating pressure.
- The suspension density is found to be increasing with an increase in operating pressure.
- The other profiles such as solid velocity, radial voidage, and axial velocity show a good agreement of flow-pattern as observed from literature.
- The bed temperature is found to be increasing with an increase in operating pressure.

From this study, it is concluded that operating pressure is a strong function of suspension density. The numerical study helped to validate the results available in the literature, and the same has helped in developing the PCFB unit subsequently.

8.1.2 Hydrodynamic and heat transfer experiments

In this section, the development of PCFB riser with operating pressure in the range of 1 to 4 bar due to limitation in the size of the compressor is performed. Additionally, a blower is used for feeding of air at a constant superficial velocity of the range of 3 to 5 m/s. Low-Grade coal and blends of coal and sawdust is considered as feed material. The outcome from the detailed study is presented below:

- S-shaped bed voidage profile is observed along with the height of the riser for pressure 2 bar and 4 bar for all the operating conditions, while at the atmospheric pressure, the voidage profile is found flatter.
- Suspension density increases with increase in operating pressure and decreases with superficial velocity, i.e., for 4 bar it decreases from 150 to 60 kg/m^3 for the increase in superficial velocity from 3 to 5 m/s hence, PCFB plays an important role with low velocity and high pressure for better heat transfer.
- Overall uncertainty of ± 3.25% was observed in case of suspension density.
- The solid circulation rate increases with an increase in inventory and operating pressure, whereas decreases with an increase in particle size. A significant increment of 64% is observed for 4 bar operating pressure concerning atmospheric conditions for 1000 g inventory at a velocity of 5 m/s.
- Overall uncertainty of ± 5.32% was observed in case of solid circulation rate.
- With the addition of sawdust along with coal as inventory, as the weight percentage of sawdust increases from 5 to 20%, bed voidage increases by a maximum value of 3.3% for 4 bar operating pressure.
- With the addition of sawdust along with coal as inventory, as the weight percentage of sawdust increases from 5 to 20%, the solid circulation rate increases from 17.96 to 19.84, 27.32 to 29.47, and 35.33 to 38.09 kg/m^2s for 1, 2 and 4 bar, respectively.
- The bed temperature is found to be increasing with an increase in operating pressure and a reduction in input power for sustaining the gasification reactions from 500^0C to 850^0C.

8.1.3 Gasification experiments

In this chapter low-grade coal, and biomass such as sawdust, rice husk, and sugarcane bagasse are considered as a feed material. All the feed materials are gasified successfully individually. The operating pressure for the experiments is considered in the range of 1 to 4 bar with a step increase of 1 bar. The outcomes from gasification study are presented below:

- With a rise in pressure from 1 to 4, bar CH_4 concentration is found to be increasing from 2.32 to 4.01 vol% for coal as a feed material. The increasing trend is also observed for sawdust and rice husk. An increment of 33 and 16 % are observed respectively for a rise in pressure 1 to 4 bar.

- The effect of pressure on gas composition is less significant for hydrogen. The concentration of H_2 slightly decreases with an increase in operating pressure from 1 to 4 bar. There is a decrement of H_2 concentration with 20%, 7.8% and 11% for coal, sawdust, and rice husk, respectively, with an increase in operating pressure from 1 to 4 bar.
- The lower heating value of the syngas is found to be increasing with an increase in operating pressure for coal and sawdust. An increment of 12% for both coal and sawdust is observed with an increase in pressure from 1 to 4 bar while for rice husk the LHV increases from 3693.77 to 3778.16 kJ/Nm^3 with an increase in pressure from 1 to 3 bar and then slightly decrease to 3634.67 kJ/Nm^3 from 3 to 4 bar.
- The cold gas and carbon conversion efficiency are also found to be increasing with an increase in operating pressure for all the feed materials. For considering coal as feed material, the CCE is found to be increasing from 64 to 97% with an increase in pressure 1 to 4 bar. A similar increment with 61 and 54% is also observed for sawdust and rice husk respectively. With a rise in pressure, CGE is also found to be increasing with 34, 51, 61% for rice husk, coal, and sawdust, respectively.

8.1.4 Co-gasification experiments

After successful gasification of all the selected feed materials individually, the co-gasification study is performed considering coal-sawdust blends such as 5%, 10%, 15%, 20%, and 25% (wt/wt) in the PCFB gasifier. As observed from the hydrodynamic study, it is seen that suspension density is found to be decreasing with an increase in the percentage of blending with reduction in residence time in the riser. The second challenge from the co-gasification study is the chocking of biomass inside the riser with increase in biomass percentage above 25% (wt/wt). The operating conditions for the co-gasification study are kept the same as the gasification study. The key points are highlighted below:

- With the increae in the percentage of blending, the concentration of H_2 increasees for any particular operating pressure. CO is found to be increasing, from 1 to 3 bar for all the coal-sawdust blends except 10% and 25% blends. With increase in operating pressure from atmospheric condition to 4 bar, the concentration of CH_4 is found to increase by 28.9%, 15.3%, 15.8%, 14.5% and 7.5% with 5%, 10%, 15%, 20% and 25% coal-biomass blends, respectively.

- The maximum LHV of 5051.3 kJ/Nm^3 is found for 15% coal-sawdust blend operating at a pressure of 3 bar.
- The maximum value of CCE and CGE are found to be 84% with 25% blends and 62% with 15% blends, respectively for mean particle size of 300 μm.
- Maximum tar content (5.97 g/kg of dry fuel) is observed for 1 bar and 25% coal-sawdust blends while the minimum value of 1.91 g/kg of dry fuel is detected for 4 bar with 5% coal-sawdust blends. A maximum of 38% decrement in tar content is observed for 25% sawdust blending.

8.2 Application Potential

The PCFB gasifier is successfully tested under laboratory conditions, and the same has a great potential to be used in the pilot-scale and commercial unit. The syngas obtained from the gasifier can directly be used in the gas engine for generation of power. However, proper scale-up study is essential to implement. The outcome of the present investigation will help the researchers to get a brief idea about fluidized bed gasifiers under pressurized conditions.

8.3 Scopes for Future Work

- The scale-up of the setup from laboratory scale to pilot and commercial scale can be carried out so as to improve its performance.
- 3D simulation can be carried out for improving the results obtained from the numerical study, and the same can be implemented for the scale-up of the unit. The numerical results can further be improved by considering different drag models.
- Geldart B type particles were considered in the present work. Further experiments may be carried out with other type of Geldart particles including pallets and briquettes as feed materials.

REFERENCES

Abdoulmoumine, N., Kulkarni, A. and Adhikari, S., (2014). Effects of temperature and equivalence ratio on pine syngas primary gases and contaminants in a bench-scale fluidized bed gasifier. *Industrial & Engineering Chemistry Research*, *53*(14), pp.5767-5777.

Adamczyk, W.P., Klimanek, A., Białecki, R.A., Węcel, G., Kozołub, P. and Czakiert, T., (2014). Comparison of the standard Euler–Euler and hybrid Euler–Lagrange approaches for modeling particle transport in a pilot-scale circulating fluidized bed. *Particuology*, *15*, pp.129-137.

Adeyemi, I., Janajreh, I., Arink, T. and Ghenai, C., (2017). Gasification behavior of coal and woody biomass: Validation and parametrical study. *Applied Energy*, 185, pp.1007-1018.

Aigner, I., Pfeifer, C. and Hofbauer, H., (2011). Co-gasification of coal and wood in a dual fluidized bed gasifier. *Fuel*, *90*(7), pp.2404-2412.

Almuttahar, A. and Taghipour, F., (2008). Computational fluid dynamics of a circulating fluidized bed under various fluidization conditions. *Chemical Engineering Science*, *63*(6), pp.1696-1709.

Ardila, Y., Figueroa, J., Lunelli, B., Maciel Filho, R. and Maciel, M.R.W., (2012), June. Syngas production from sugar cane bagasse in a circulating fluidized bed gasifier using Aspen Plus TM: Modelling and Simulation. on Computer Aided. In *Symposium on Computer Aided Process Engineering* (Vol. 17, p. 20).

Arenas, C., Leiva, C., Vilches, L.F. and Cifuentes, H., (2013). Use of co-combustion bottom ash to design an acoustic absorbing material for highway noise barriers. *Waste Management*, *33*(11), pp.2316-2321.

Aznar, M.P., Caballero, M.A., Sancho, J.A. and Francés, E., (2006). Plastic waste elimination by co-gasification with coal and biomass in fluidized bed with air in pilot plant. *Fuel Processing Technology*, 87(5), pp.409-420.

Barletta, M., (2009). Progress in abrasive fluidized bed machining. *Journal of Materials Processing Technology*, *209*(20), pp.6087-6102.

Basu, P. and Nag, P.K., (1987). An investigation into heat transfer in circulating fluidized beds. *International Journal of Heat and Mass Transfer*, *30*(11), pp.2399-2409.

Basu, P. and Nag, P.K., (1996). Heat transfer to walls of a circulating fluidized-bed furnace. *Chemical Engineering Science*, *51*(1), pp.1-26.

Basu, P., (2006). *Combustion and gasification in fluidized beds*. CRC press.

Basu, P., Cheng, L. and Cen, K., (1996). Heat transfer in a pressurized circulating fluidized bed. *International Journal of Heat and Mass Transfer*, *39*(13), pp.2711-2722.

Benyahia, S., Arastoopour, H., Knowlton, T. and Massah, H., (2000). Simulation of particles and gas flow behavior in the riser section of a circulating fluidized bed using the kinetic theory approach for the particulate phase. *Powder Technology*, *112*(1-2), pp.24-33.

Berrueco, C., Montané, D., Güell, B.M. and Del Alamo, G., (2014a). Effect of temperature and dolomite on tar formation during gasification of torrefied biomass in a pressurized fluidized bed. *Energy*, 66, pp.849-859

Berrueco, C., Recari, J., Güell, B.M. and Del Alamo, G., (2014b). Pressurized gasification of torrefied woody biomass in a lab scale fluidized bed. *Energy*, 70, pp.68-78.

Borodulya, V.A., Ganzha, V.L. and Kovenskii, V.I., (1982). Hydrodynamics and heat transfer in a fluidized bed under pressure. *Minsk: Science and Technology*.

Boskovic, S., Reddy, B.V. and Basu, P., (2002). Effect of operating parameters on sulphur capture in a pressurized circulating fluidized bed combustor. *International Journal of Energy Research*, *26*(2), pp.173-183.

Casleton, D.K., Shadle, L.J. and Ross, A.A., (2010). Measuring the voidage of a CFB through image analysis. *Powder Technology*, *203*(1), pp.12-22.

Chalermsinsuwan, B., Kuchonthara, P. and Piumsomboon, P., (2010). CFD modeling of tapered circulating fluidized bed reactor risers: hydrodynamic descriptions and chemical reaction responses. *Chemical Engineering and Processing: Process Intensification*, *49*(11), pp.1144-1160.

Cheng, L. and Basu, P., (1999). Effect of pressure on loop seal operation for a pressurized circulating fluidized bed. *Powder Technology*, *103*(3), pp.203-211.

Chitester, D.C., Kornosky, R.M., Fan, L.S. and Danko, J.P., (1984). Characteristics of fluidization at high pressure. *Chemical Engineering Science*, *39*(2), pp.253-261.

Daizo, K. and Levenspiel, O., (1991). Fluidization Engineering.

Das, M., Bandyopadhyay, A., Meikap, B.C. and Saha, R.K., (2008). Axial voidage profiles and identification of flow regimes in the riser of a circulating fluidized bed. *Chemical Engineering Journal*, *145*(2), pp.249-258.

Datta, S., Sarkar, P., Chavan, P.D., Saha, S., Sahu, G., Sinha, A.K. and Saxena, V.K., (2015). Agglomeration behaviour of high ash Indian coals in fluidized bed gasification pilot plant. *Applied Thermal Engineering*, *86*, pp.222-228.

De Jong, W., Andries, J. and Hein, K.R., (1999). Coal/biomass co-gasification in a pressurised fluidised bed reactor. *Renewable Energy*, 16(1-4), pp.1110-1113.

Del Valle-Zermeño, R., Chimenos, J.M., Giro-Paloma, J. and Formosa, J., (2014). Use of weathered and fresh bottom ash mix layers as a subbase in road constructions: environmental behavior enhancement by means of a retaining barrier. *Chemosphere*, *117*, pp.402-409.

Del Valle-Zermeño, R., Formosa, J., Prieto, M., Nadal, R., Niubó, M. and Chimenos, J.M., (2014). Pilot-scale road subbase made with granular material formulated with MSWI bottom ash and stabilized APC fly ash: environmental impact assessment. *Journal of Hazardous Materials*, *266*, pp.132-140.

Duan, F., Jin, B., Huang, Y., Li, B., Wu, Y. and Zhang, M., (2010). Results of bituminous coal gasification upon exposure to a pressurized pilot-plant circulating fluidized-bed (CFB) reactor. Energy & Fuels, 24(5), pp.3150-3158.

Ergun, S. and Orning, A.A., (1949). Fluid flow through randomly packed columns and fluidized beds. *Industrial & Engineering Chemistry*, *41*(6), pp.1179-1184.

Ersoy, L.E., Golriz, M.R., Koksal, M. and Hamdullahpur, F., (2004). Circulating fluidized bed hydrodynamics with air staging: an experimental study. *Powder Technology*, *145*(1), pp.25-33.

Fermoso, J., Arias, B., Gil, M.V., Plaza, M.G., Pevida, C., Pis, J.J. and Rubiera, F., (2010). Co-gasification of different rank coals with biomass and petroleum coke in a high-pressure reactor for H_2-rich gas production. *Bioresource Technology*, 101(9), pp.3230-3235.

Fermoso, J., Arias, B., Plaza, M.G., Pevida, C., Rubiera, F., Pis, J.J., García-Peña, F. and Casero, P., (2009). High-pressure co-gasification of coal with biomass and petroleum coke. *Fuel Processing Technology*, 90(7-8), pp.926-932.

Figueroa, J.J., Ardila, Y.C. and Maciel, M.R.W., (2014). Fluidized bed reactor for gasification of sugarcane bagasse: Distribution of syngas, bio-tar and char. *Chemical Engineering Transactions*.

Garcıa-Ibanez, P., Cabanillas, A. and Sánchez, J.M., (2004). Gasification of leached orujillo (olive oil waste) in a pilot plant circulating fluidised bed reactor. Preliminary results. *Biomass and Bioenergy*, *27*(2), pp.183-194. Han, L.,

Geldart, D., (1973). Types of gas fluidization. *Powder Technology*, *7*(5), pp.285-292.

Gibilaro, L.G., (2001). *Fluidization dynamics*. Elsevier.

Glicksman, L. R., (1988). Circulating fluidized bed heat transfer. In Circulating fluidized bed technology (pp. 13-29). Pergamon.

Grace, J.R., (1986). Heat transfer in circulating fluidized beds. In *Circulating Fluidized Bed Technology* (pp. 63-81). Pergamon.

Guan, J., Wang, Q., Li, X., Luo, Z. and Cen, K., (2007). Thermodynamic analysis of a biomass anaerobic gasification process for hydrogen production with sufficient CaO. *Renewable Energy*, *32*(15), pp.2502-2515.

Gül, S., Akgün, F., Aydar, E. and Ünlü, N., (2018). Pressurized gasification of lignite in a pilot scale bubbling fluidized bed reactor with air, oxygen, steam and CO2 agents. *Applied Thermal Engineering*, *130*, pp.203-210.

Gupta, A.V.S.S.K.S. and Nag, P.K., (2002). Bed-to-wall heat transfer behavior in a pressurized circulating fluidized bed. *International Journal of Heat and Mass Transfer*, *45*(16), pp.3429-3436.

Gupta, A.V.S.S.K.S. and Reddy, B.V., (2006). Effect of pressure on thermal aspects in the riser column of a pressurized circulating fluidized bed. *International Journal of Energy Research*, *30*(3), pp.149-162.

Gupta, S.K. and Berruti, F., (2000). Evaluation of the gas–solid suspension density in CFB risers with exit effects. *Powder Technology*, *108*(1), pp.21-31.

Gupta, S.K., Pugsley, T. and Berruti, F., (1999). A Process simulator for circulating fluidized bed chemical reactors. In *Circulating Fluidized Bed Technology* (Vol. 6, pp. 443-448).

Herman, A.P., Yusup, S., Shahbaz, M. and Patrick, D.O., (2016). Bottom ash characterization and its catalytic potential in biomass gasification. *Procedia Engineering*, *148*, pp.432-436.

Huang, J., Fang, Y., Chen, H. and Wang, Y., (2003). Coal gasification characteristic in a pressurized fluidized bed. Energy & Fuels, 17(6), pp.1474-1479.

IEA (2019) Coal information: overview, International Energy Agency.

Ismail, T.M., Ramos, A., Monteiro, E., El-Salam, M.A. and Rouboa, A., (2019). Parametric studies in the gasification agent and fluidization velocity during oxygen-enriched gasification of biomass in a pilot-scale fluidized bed: Experimental and Numerical Assessment. *Renewable Energy*.

Iyengar, R.K. and Haque, R., (1991). Gasification of high-ash Indian coals for power generation. *Fuel Processing Technology*, *27*(3), pp.247-262.

Jiang, W. and Roy, D.M., (1992). Hydrothermal processing of new fly ash cement. *American Ceramic Society Bulletin;(United States)*, *71*(4).

Ju, F., Chen, H., Yang, H., Wang, X., Zhang, S. and Liu, D., (2010). Experimental study of a commercial circulated fluidized bed coal gasifier. *Fuel Processing Technology*, *91*(8), pp.818-822.

Kalita, P., Mahanta, P. and Saha, U.K., (2014). Study of bed-to-wall heat transfer with twisted tape at the upper splash region of a pressurized circulating fluidized bed unit. *International Journal of Heat and Mass Transfer*, *78*, pp.260-266.

Kalita, P., Saha, U.K. and Mahanta, P., (2013a). Parametric study on the hydrodynamics and heat transfer along the riser of a pressurized circulating fluidized bed unit. *Experimental Thermal and Fluid Science*, 44, pp.620-630.

Kalita, P., Saha, U.K. and Mahanta, P., (2013b). Effect of biomass blending on hydrodynamics and heat transfer behavior in a pressurized circulating fluidized bed unit. *International Journal of Heat and Mass Transfer*, *60*, pp.531-541.

Karmakar, M.K. and Datta, A.B., (2011). Generation of hydrogen rich gas through fluidized bed gasification of biomass. *Bioresource Technology*, *102*(2), pp.1907-1913.

Khongprom, P., Aimdilokwong, A., Limtrakul, S., Vatanatham, T. and Ramachandran, P.A., (2012). Axial gas and solids mixing in a down flow circulating fluidized bed reactor based on CFD simulation. *Chemical Engineering Science*, *73*, pp.8-19.

Khurram, M.S., Choi, J.H., Won, Y.S., Jeong, A.R. and Ryu, H.J., (2016). Relationship between Solid Flow Rate and Pressure Drop in the Riser of a Pressurized Circulating Fluidized Bed. Journal of Chemical Engineering of Japan, 49(7), pp.595-601.

Kitzler, H., Pfeifer, C. and Hofbauer, H., (2011). Pressurized gasification of woody biomass—variation of parameter. Fuel Processing Technology, 92(5), pp.908-914.

Klimanek, A. and Bigda, J., (2018). CFD modelling of CO2 enhanced gasification of coal in a pressurized circulating fluidized bed reactor. Energy, 160, pp.710-719.

Kolar, A.K. and Sundaresan, R., (2002). Heat transfer characteristics at an axial tube in a circulating fluidized bed riser. *International Journal of Thermal Sciences*, *41*(7), pp.673-681.

Kong, L., Zhang, C. and Zhu, J., (2014). Evaluation of the effect of wall boundary conditions on numerical simulations of circulating fluidized beds. *Particuology*, *13*, pp.114-123.

Konstantinou, E. and Marsh, R., (2015). Experimental study on the impact of reactant gas pressure in the conversion of coal char to combustible gas products in the context of Underground Coal Gasification. *Fuel*, *159*, pp.508-518.

Kumabe, K., Hanaoka, T., Fujimoto, S., Minowa, T. and Sakanishi, K., (2007). Co-gasification of woody biomass and coal with air and steam. *Fuel*, 86(5-6), pp.684-689.

Kunii, D. and Levenspiel, O., (1991). A general equation for the heat-transfer coefficient at wall surfaces of gas/solid contactors. *Industrial & Engineering Chemistry Research*, *30*(1), pp.136-141.

Kunii, D. and Levenspiel, O., (1997). Circulating fluidized-bed reactors. *Chemical Engineering Science*, *52*(15), pp.2471-2482.

Kurkela, E., Kurkela, M. and Moilanen, A., (2006). Fluidised-bed gasification of high-alkali biomass fuels. *Proceedings of Science in Thermal and Chemical Biomass Conversion*, pp.662-676.

Lapuerta, M., Hernández, J.J., Pazo, A. and López, J., (2008). Gasification and co-gasification of biomass wastes: Effect of the biomass origin and the gasifier operating conditions. *Fuel Processing Technology*, *89*(9), pp.828-837.

Li, J., Li, F., Liu, W., Liu, Z., Zhan, H., Zhang, Y., Hao, Z., Cheng, Z., Huang, J. and Fang, Y., (2018). Influence of pressure on fluidized bed gasifier: Specific coal throughput and particle behavior. *Fuel*, 220, pp.80-88.

Li, K., Zhang, R. and Bi, J., (2010). Experimental study on syngas production by co-gasification of coal and biomass in a fluidized bed. *International Journal of Hydrogen Energy*, 35(7), pp.2722-2726.

Li, P., Lan, X., Xu, C., Wang, G., Lu, C. and Gao, J., (2009). Drag models for simulating gas–solid flow in the turbulent fluidization of FCC particles. *Particuology*, *7*(4), pp.269-277.

Li, Q., Zhang, M., Zhong, W., Wang, X., Xiao, R. and Jin, B., (2009). Simulation of coal gasification in a pressurized spout-fluid bed gasifier. *The Canadian Journal of Chemical Engineering*, 87(2), pp.169-176.

Li, X., Grace, J.R., Watkinson, A.P., Lim, C.J. and Ergüdenler, A., (2001). Equilibrium modeling of gasification: a free energy minimization approach and its application to a circulating fluidized bed coal gasifier. *Fuel*, 80(2), pp.195-207.

Liu, Z., Fang, Y., Deng, S., Huang, J., Zhao, J. and Cheng, Z., (2012). Simulation of pressurized ash agglomerating fluidized bed gasifier using ASPEN PLUS. *Energy & Fuels*, *26*(2), pp.1237-1245.

Louge, M.Y., Bricout, V. and Martin-Letellier, S., (1999). On the dynamics of pressurized and atmospheric circulating fluidized bed risers. *Chemical Engineering Science*, *54*(12), pp.1811-1824.

Luo, K., Wu, F., Yang, S., Fang, M. and Fan, J., (2015). High-fidelity simulation of the 3-D full-loop gas–solid flow characteristics in the circulating fluidized bed. *Chemical Engineering Science*, *123*, pp.22-38.

Mahapatro, A., Kalita, P., Mahanta, M., Saha, U.K. and Mallick, S.S., (2014), May. Numerical simulation of gas-solid flow in a pressurized circulating fluidized bed riser. In *Proceedings of the 11th International conference on Fluidized Bed Technology (CFB-11)* (pp. 323-328).

Mahmoudi, S., Baeyens, J. and Seville, J., (2011). The solids flow in the CFB-riser quantified by single radioactive particle tracking. *Powder Technology*, *211*(1), pp.135-143.

Mallick, D., Mahanta, P. and Moholkar, V.S., (2017). Co-gasification of coal and biomass blends: chemistry and engineering. *Fuel*, *204*, pp.106-128.

Mallick, D., Mahanta, P. and Moholkar, V.S., (2019). Co–gasification of coal/biomass blends in 50 kWe circulating fluidized bed gasifier. *Journal of the Energy Institute*.

Masnadi, M.S., Grace, J.R., Bi, X.T., Lim, C.J., Ellis, N., Li, Y.H. and Watkinson, A.P., (2015). From coal towards renewables: Catalytic/synergistic effects during steam co-gasification of switchgrass and coal in a pilot-scale bubbling fluidized bed. *Renewable Energy*, 83, pp.918-930.

Mayerhofer, M., Mitsakis, P., Meng, X., de Jong, W., Spliethoff, H. and Gaderer, M., (2012). Influence of pressure, temperature and steam on tar and gas in allothermal fluidized bed gasification. *Fuel*, 99, pp.204-209.

Miao, Q., Wang, C., Wu, C., Yin, X. and Zhu, J., (2011). Fluidization of sawdust in a cold model circulating fluidized bed: Experimental study. *Chemical Engineering Journal*, *167*(1), pp.335-341.

Monazam, E.R., Breault, R.W. and Shadle, L.J., (2016). Pressure and apparent voidage profiles for riser with an abrupt exit (T-shape) in a CFB riser operating above fast fluidization regimes. *Powder Technology*, *291*, pp.383-391.

Moon, H., Choi, S., Park, Y.K. and Cho, H.H., (2017). Thermal-fluid characteristics on near wall of gas-solid fluidized bed reactor. *International Journal of Heat and Mass Transfer*, *114*, pp.852-865.

Motta, I.L., Miranda, N.T., Maciel Filho, R. and Maciel, M.R.W., (2019). Sugarcane bagasse gasification: Simulation and analysis of different operating parameters, fluidizing media, and gasifier types. *Biomass and Bioenergy*, *122*, pp.433-445.

Nakamura, M., Hamada, Y., Toyama, S., Fouda, A.E. and Capes, C.E., (1985). An experimental investigation of minimum fluidization velocity at elevated temperatures and pressures. *The Canadian Journal of Chemical Engineering*, *63*(1), pp.8-13.

Neri, A. and Gidaspow, D., (2000). Riser hydrodynamics: simulation using kinetic theory. *AIChE Journal*, *46*(1), pp.52-67.

Niu, M., Huang, Y., Jin, B., Liang, S., Dong, Q., Gu, H. and Sun, R., (2019). A novel two-stage enriched air biomass gasification for producing low-tar high heating value fuel gas: Pilot verification and performance analysis. *Energy*, *173*, pp.511-522.

Padban, N., Wang, W., Ye, Z., Bjerle, I. and Odenbrand, I., (2000). Tar formation in pressurized fluidized bed air gasification of woody biomass. *Energy & Fuels*, 14(3), pp.603-611.

Pan, Y.G., Velo, E., Roca, X., Manya, J.J. and Puigjaner, L., (2000). Fluidized-bed co-gasification of residual biomass/poor coal blends for fuel gas production. *Fuel*, 79(11), pp.1317-1326.

Patil, R.S., Pandey, M. and Mahanta, P., (2011). Parametric studies and effect of scale-up on wall-to-bed heat transfer characteristics of circulating fluidized bed risers. *Experimental Thermal and Fluid Science*, *35*(3), pp.485-494.

Pellegrini, L.F. and de Oliveira Jr, S., (2007). Exergy analysis of sugarcane bagasse gasification. *Energy*, *32*(4), pp.314-327.

Peng, B., Xu, J., Zhu, J. and Zhang, C., (2011a). Numerical and experimental studies on the flow multiplicity phenomenon for gas–solids two-phase flows in CFB risers. *Powder Technology*, *214*(2), pp.177-187.

Peng, B., Zhang, C. and Zhu, J., (2011b). Numerical study of the effect of the gas and solids distributors on the uniformity of the radial solids concentration distribution in CFB risers. *Powder Technology*, *212*(1), pp.89-102.

Peng, W.X., Ge, S.B., Ebadi, A.G., Hisoriev, H. and Esfahani, M.J., (2017). Syngas production by catalytic co-gasification of coal-biomass blends in a circulating fluidized bed gasifier. *Journal of Cleaner Production*, 168, pp.1513-1517.

Pinto, F., Franco, C., André, R.N., Miranda, M., Gulyurtlu, I. and Cabrita, I., (2002). Co-gasification study of biomass mixed with plastic wastes. *Fuel*, *81*(3), pp.291-297.

Qin, Y., Huang, H., Wu, Z., Feng, J., Li, W. and Xie, K., (2007). Characterization of tar from sawdust gasified in the pressurized fluidized bed. *Biomass and Bioenergy*, 31(4), pp.243-249.

Rawat, J., (1993). Static analysis of cache performance for real-time programming. *Master's thesis, Iowa State University*.

Reddy, B.V. and Basu, P., (2001). A model for heat transfer in a pressurized circulating fluidized bed furnace. *International Journal of Heat and Mass Transfer*, *44*(15), pp.2877-2887.

Reddy, B.V. and Basu, P., (2001). Effect of pressure and temperature on cluster and particle heat transfer in a pressurized circulating fluidized bed. *International Journal of Energy Research*, *25*(14), pp.1263-1274.

Rongtao, F., Junguo, L., Libo, D., Zhenhua, H., Zhongren, B., Haijuan, Z. and Yitian, F., (2019). Gas-solid flow behaviors in a multi-stage circulating fluidized bed under elevated pressure. *Chemical Engineering Science*, 196, pp.1-13.

Sahoo, A. and Ram, D.K., (2015). Gasifier performance and energy analysis for fluidized bed gasification of sugarcane bagasse. *Energy*, *90*, pp.1420-1425.

Saikia, R. and Mahanta, P., (2017). Transient hydrodynamic and heat transfer behavior in a pressurized circulating fluidized bed. In *ISHMT Digital Library*. Begel House Inc.

Sánchez, C., Arenas, E., Chejne, F., Londoño, C.A., Cisneros, S. and Quintana, J.C., (2016). A new model for coal gasification on pressurized bubbling fluidized bed gasifiers. *Energy Conversion and Management*, *126*, pp.717-723.

Sarbassov, Y., Zayoud, A., Gu, S., Ranganathan, P., Mahanta, P. and Saha, U.K., (2015) Circulating Fluidized Bed Hydrodynamics Study at Elevated Pressure and Atmospheric O_2/CO_2 Environment.

Saxena, S.C. and Vogel, G.J., (1977). Segregation and fluidization characteristics of a dolomite bed with a range of particle sizes and shapes. *Chemical Engineering Journal (Lausanne, Switzerland: 1996)*, *14*(1), pp.59-63.

Seo, M.W., Goo, J.H., Kim, S.D., Lee, S.H. and Choi, Y.C., (2010). Gasification characteristics of coal/biomass blend in a dual circulating fluidized bed reactor. *Energy & Fuels*, 24(5), pp.3108-3118.

Shah, S., Myöhänen, K., Kallio, S., Ritvanen, J. and Hyppänen, T., (2015). CFD modeling of gas–solids flow in a large scale circulating fluidized bed furnace. *Powder Technology*, *274*, pp.239-249.

Shah, S., Ritvanen, J., Hyppänen, T. and Kallio, S., (2012). Space averaging on a gas–solid drag model for numerical simulations of a CFB riser. *Powder Technology*, *218*, pp.131-139.

Shahbaz, M., Taqvi, S.A., Loy, A.C.M., Inayat, A., Uddin, F., Bokhari, A. and Naqvi, S.R., (2019). Artificial neural network approach for the steam gasification of palm oil waste using bottom ash and CaO. *Renewable Energy*, *132*, pp.243-254.

Shahbaz, M., Yusup, S., Inayat, A., Patrick, D.O., Pratama, A. and Ammar, M., (2017). Optimization of hydrogen and syngas production from PKS gasification by using coal bottom ash. *Bioresource Technology*, *241*, pp.284-295.

Sharma, M., Attanoor, S. and Dasappa, S., (2015). Investigation into co-gasifying Indian coal and biomass in a down draft gasifier—Experiments and analysis. *Fuel Processing Technology*, *138*, pp.435-444.

Sidorenko, I. and Rhodes, M.J., (2003). Pressure effects on gas-solid fluidized bed behavior. *International Journal of Chemical Reactor Engineering*, *1*(1).

Sidorenko, I. and Rhodes, M.J., (2004). Influence of pressure on fluidization properties. *Powder Technology*, *141*(1-2), pp.137-154.

Sjöström, K., Chen, G., Yu, Q., Brage, C. and Rosén, C., (1999). Promoted reactivity of char in co-gasification of biomass and coal: synergies in the thermochemical process. *Fuel*, 78(10), pp.1189-1194.

Srinivas, T., Gupta, A.V.S.S.K.S. and Reddy, B.V., (2008). Parametric Exergy Analysis of Coal Gasifier and Gas Turbine Combustion Chamber with Emission Study. *International Energy Journal*, 9(1).

Srinivas, T., Gupta, A.V.S.S.K.S. and Reddy, B.V., (2009). Thermodynamic equilibrium model and exergy analysis of a biomass gasifier. *Journal of Energy Resources Technology*, 131(3), p.031801.

Statistics, B.P., (2016). Output Table Dynamic of the Central Bureau of Statistics.

Stairmand, C.J., (1951). The design and performance of cyclone separators. *Trans. Instn. Chem. Engrs.*, *29*, pp.356-383.

Stenberg, V., Sköldberg, V., Öhrby, L. and Rydén, M., (2019). Evaluation of bed-to-tube surface heat transfer coefficient for a horizontal tube in bubbling fluidized bed at high temperature. *Powder Technology*, *352*, pp.488-500.

Suksuwan, W., Wae-hayee, M. and Mel, M., (2018). Development of Mini Pilot Fluidized Bed Gasifier for Industrial Approach: Preliminary Study Based on Continuous Operation. *Journal of Advanced Research in Fluid Mechanics and Thermal Sciences*, *45*, pp.35-43.

Tawfik, M.H.M., Diab, M.R. and Abdelmotalib, H.M., (2020). Heat transfer and hydrodynamics of particles mixture in swirling fluidized bed. *International Journal of Thermal Sciences*, *147*, p.106134.

Tian, Y., Zhou, X., Yang, Y. and Nie, L., (2019). Experimental analysis of air-steam gasification of biomass with coal-bottom ash. *Journal of the Energy Institute*.

Toraldo, E., Saponaro, S., Careghini, A. and Mariani, E., (2013). Use of stabilized bottom ash for bound layers of road pavements. *Journal of Environmental Management*, *121*, pp.117-123.

Tremel, A., Haselsteiner, T., Kunze, C. and Spliethoff, H., (2012). Experimental investigation of high temperature and high pressure coal gasification. *Applied Energy*, *92*, pp.279-285.

Valin, S., Ravel, S., Guillaudeau, J. and Thiery, S., (2010). Comprehensive study of the influence of total pressure on products yields in fluidized bed gasification of wood sawdust. *Fuel Processing Technology*, *91*(10), pp.1222-1228.

Vélez, J.F., Chejne, F., Valdés, C.F., Emery, E.J. and Londoño, C.A., (2009). Co-gasification of Colombian coal and biomass in fluidized bed: An experimental study. *Fuel*, 88(3), pp.424-430.

Wang, Q., Feng, J.T., Sun, B.Z., Qi, Y.Q., Chen, D.F. and Luo, J.L., (2012). Numerical simulation research on gas-solid two phase flow in oil shale circulating fluidized bed. *Energy Procedia*, *17*, pp.851-860.

Wang, Q., Luo, Z., Rong, N. and Deng, G., (2013). H2 rich gas production via pressurized fluidized bed gasification of sawdust with in situ CO2 capture. *Applied Energy*, *109*, pp.36-43.

Wang, X., Liao, L., Fan, B., Jiang, F., Xu, X., Wang, S. and Xiao, Y., (2010). Experimental validation of the gas–solid flow in the CFB riser. *Fuel Processing Technology*, *91*(8), pp.927-933.

Wen, C.Y. and Yu, Y.H., (1966). A generalized method for predicting the minimum fluidization velocity. *AIChE Journal*, *12*(3), pp.610-612.

Wiman, J. and Almstedt, A.E., (1997). Hydrodynamics, erosion and heat transfer in a pressurized fluidized bed: influence of pressure, fluidization velocity, particle size and tube bank geometry. *Chemical Engineering Science*, *52*(16), pp.2677-2695.

Winaya, N.S. and Basu, P., (2001). Effect of pressure and carbon dioxide concentration on heat transfer at high temperature in a Pressurized Circulating Fluidized Bed (PCFB) combustor. *International Journal of Heat and Mass T ransfer*, *44*(15), pp.2965-2971.

Xiao, R., Zhang, M., Jin, B., Huang, Y. and Zhou, H., (2006). High-temperature air/steam-blown gasification of coal in a pressurized spout-fluid bed. Energy & Fuels, 20(2), pp.715-720.

Xiong, R., Dong, L., Yu, J., Zhang, X., Jin, L. and Xu, G., (2010). Fundamentals of coal topping gasification: Characterization of pyrolysis topping in a fluidized bed reactor. *Fuel Processing Technology*, *91*(8), pp.810-817.

Yates, J.G., (1996). Effects of temperature and pressure on gas-solid fluidization. *Chemical engineering science*, *51*(2), pp.167-205.

Yates, J.G., (1997). Experimental observations of voidage in gas fluidized beds. In *Non-invasive monitoring of multiphase flows* (pp. 141-160). Elsevier Science BV.

Yin, S., Jin, B., Zhong, W., Lu, Y., Shao, Y. and Liu, H., (2014). Gas-solid flow behavior in a pressurized high-flux circulating fluidized bed riser. Chemical Engineering Communications, 201(3), pp.352-366.

Yin, S., Jin, B.A.O.S.H.E.N.G., Zhong, W.E.N.Q.I., Lu, Y.O.N.G., Zhang, Y., Shao, Y.I.N.G.J.U.A.N. and Liu, H., (2012). Solids holdup of high flux circulating fluidized bed at elevated pressure. *Chemical Engineering & Technology*, *35*(5), pp.904-910.

Yin, S., Zhong, W., Jin, B. and Fan, J., (2014). Modeling on the hydrodynamics of pressurized high-flux circulating fluidized beds (PHFCFBs) by Eulerian–Lagrangian approach. *Powder Technology*, *259*, pp.52-64.

Yue, G., Lu, J., Zhang, H., Yang, H., Zhang, J., Liu, Q., Li, Z., Joos, E. and Jaud, P., (2005), May. Design theory of circulating fluidized bed boilers. In *18th International Fluidized Bed Combustion Conference* (pp. 18-21).

Zeng, J., Xiao, R., Zeng, D., Zhao, Y., Zhang, H. and Shen, D., (2016). High H2/CO ratio syngas production from chemical looping gasification of sawdust in a dual fluidized bed gasifier. Energy & Fuels, 30(3), pp.1764-1770.

Zhang, N., Lu, B., Wang, W. and Li, J., (2010). 3D CFD simulation of hydrodynamics of a 150 MWe circulating fluidized bed boiler. *Chemical Engineering Journal*, *162*(2), pp.821-828.

Zhang, Y., Lei, F. and Xiao, Y., (2018). The influence of pressure and temperature on gas-solid hydrodynamics for Geldart B particles in a high-density CFB riser. *Powder Technology*, *327*, pp.17-28.

Zhou, X., Gao, J., Xu, C. and Lan, X., (2013). Effect of wall boundary condition on CFD simulation of CFB risers. *Particuology*, *11*(5), pp.556-565.

Żogała, A., (2014). Equilibrium simulations of coal gasification–factors affecting syngas composition. *Journal of Sustainable Mining*, *13*(2), pp.30-38.

Zou, Z., Liu, W., Yan, D., Xie, Z., Li, H., Zhu, Q. and He, S., (2019). CFD simulations of tapered bubbling/turbulent fluidized beds with/without gas distributor based on the structure-based drag model. *Chemical Engineering Science*, *202*, pp.157-168.

Appendices

Appendix-I

Design of Cyclone Separator

Maximum gas flow rate, (Q_m):

$$Q_m = U_m \times A_b \tag{I.1}$$

$$Q_m = 7.5 \times \frac{\pi}{4} \times 0.1^2$$

$$Q_m = 0.0589\,\mathrm{m^3/s}$$

$$Q_m = 212\,\mathrm{m^3/hr}$$

Design gas flow rate, (Q_d) = 140 m^3/hr

= 2.33 m^3/min

Calculation of cyclone barrel diameter, D_c: The gas handling capacity of a Stairmand high efficiency cyclone is given by the following equation:

$$Q_d = K.D_c^2 \tag{I.2}$$

$$K = 91.2\,m/\mathrm{min}$$

$$2.33 = 91.2 \times D_c^2$$

$$D_c = 0.16\,m$$

$$= 160\,mm$$

Cyclone design ratios: using Stairmand (1951) designed data for high efficiency cyclone, the various dimensions ratios are written down from which the cyclone dimensions are arrived at:

$$\frac{B_c}{D_c} = \frac{1}{4} \tag{I.3}$$

$$\frac{H_c}{D_c} = \frac{1}{2} \tag{I.4}$$

$$\frac{D_e}{D_c} = \frac{1}{4} \tag{I.5}$$

$$\frac{Z_c}{D_c}=\frac{L_c}{D_c}=2 \tag{I.6}$$

$$\frac{S_c}{D_c}=\frac{1}{8} \tag{I.7}$$

$$J_c=\frac{D_c}{4} \tag{I.8}$$

Form the above equations, the values are calculated as $B_c=40\,mm$, $H_c=80\,mm$, $D_e=40\,mm$, $Z_c=320\,mm$, $L_c=320\,mm$, $S_c=20\,mm$, and $J_c=40\,mm$

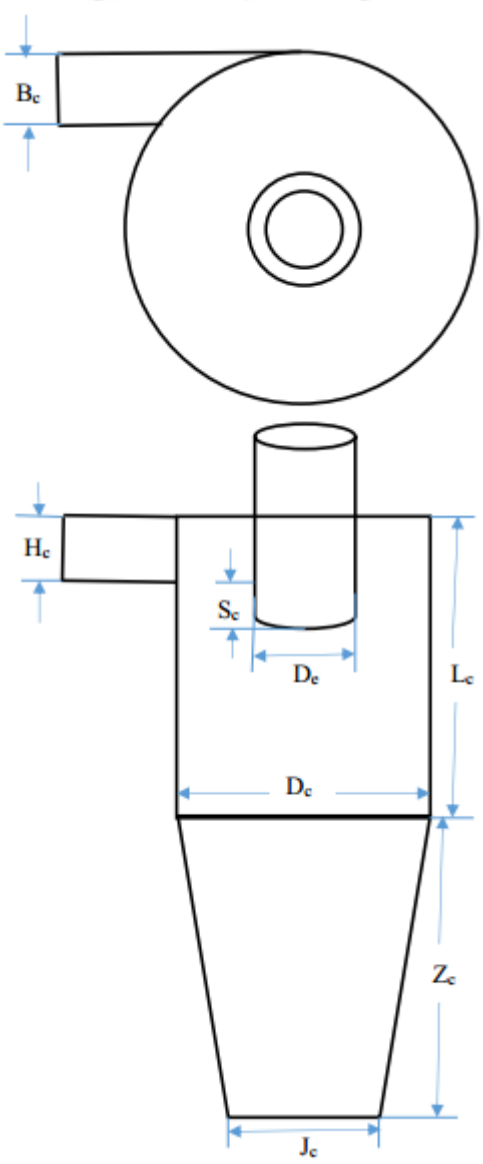

Fig. I.1 Schematic diagram of cyclone seperator

Appendix-II

Design of Distributor Plate

The distributor was fabricated based on the design procedure described by Kunii and Levenspiel 1991, and Basu 2006). It is a straight hole orifice type of distributor. The design considerations are given below:

Bed inventory, I = 1.5 kg

Operating velocity, U_{or} = 5m/s

Voidage at maximum fluidization, ε_{mf} = 0.5

Height of bed = 3000 mm

Cross sectional area of the bed, (A_b) = 0.007854 m^2

Density of the solid particle (Coal), ρ_s = 1350 kg/m^3

Density of air, ρ_g = 1.113kg/m^3

Acceleration due to gravity, g = 9.81 m/s^2

Height of the bed at minimum fluidization (H_{mf}):

$$H_{mf} = \frac{\Delta p}{\left(1-\varepsilon_{mf}\right)\times\rho_s\times g} = \frac{I\times g / A_b}{\left(1-\varepsilon_{mf}\right)\times\rho_s\times g} = \frac{I}{A_b\times\left(1-\varepsilon_{mf}\right)\times\rho_s} \qquad \text{(II.1)}$$

$$= 0.283 \text{ m}$$

Bed pressure drop (Δp_b):

$$\Delta p_b = \rho_s\times g\times H_{mf}\times\left(1-\varepsilon_{mf}\right) \qquad \text{(II.2)}$$

$$\Delta p_b = 1872 \text{ N/m}^2$$

Minimum distributor pressure drop for uniform distribution (ΔP_d): (Kunii and Levenspiel 1991)

$$\Delta P_d = 0.15\Delta P_b \qquad \text{(II.3)}$$

$$= 280.8 \text{ N/m}^2$$

Thickness of the distributor plate (t): t = 5 mm = 0.005 m

Orifice diameter (d_{or}) = 4 mm =.004 m

Orifice discharge coefficient (C_D):

$$C_D = 0.82 \times \left(t / d_{or}\right)^{0.13} \quad \text{(II.4)}$$

$$C_D = 0.923$$

Gas velocity through the Orifice (U_{or}):

$$U_{or} = C_D \times \left[2 \times \Delta p_D / \rho_g\right]^{1/2} \quad \text{(II.5)}$$

$$U_{or} = 20.73 \text{ m/s}$$

Number of orifice per square meter of distributor (N_{or}):

$$N_{or} = (U_{op} / U_{or}) \times (1 / A_{or}) = (U_{op} / U_{or}) \times (4 / (\pi d_{or}{}^2)) \quad \text{(II.6)}$$

$$N_{or} = 19193/m^2$$

Total number of holes on perforated distributor

$$N_{or} \times A_b \quad \text{(II.7)}$$

Total number of holes = 150.67

Pitch of orifice in the distributor

$$(1/ N_{or})^{1/2} \quad \text{(II.8)}$$

Pitch of orifice in the distributor = 7 mm

Open area in the distributor (m^2)

$$\pi/4 \times d_{or}{}^2 \times \text{No. of holes} \quad \text{(II.9)}$$

Open area in the distributor (m^2) = 1.89×10^{-3}

Percentage opening

$$\frac{\text{Open area in the distributor}}{A_b} \times 100\% \quad \text{(II.10)}$$

Percentage opening = 16.4%

Appendix-III

Calibration of Pressure Sensor

The calibration of the pressure sensor is done by fixing the pressure sensor in the machine. After fixing the sensor, deadweight pressure standards are mounted in the device, and electrical signals are recorded in mV (DC) by the help of the data accusation system. The electrical signals in terms of mV are recorded for both upscaling and downscaling from 1 bar to 10 bar and then 10 bar to 1 bar respectively by constantly adding a pressure weight of 0.5 bar. The calibration curve so obtained is presented in Figure.

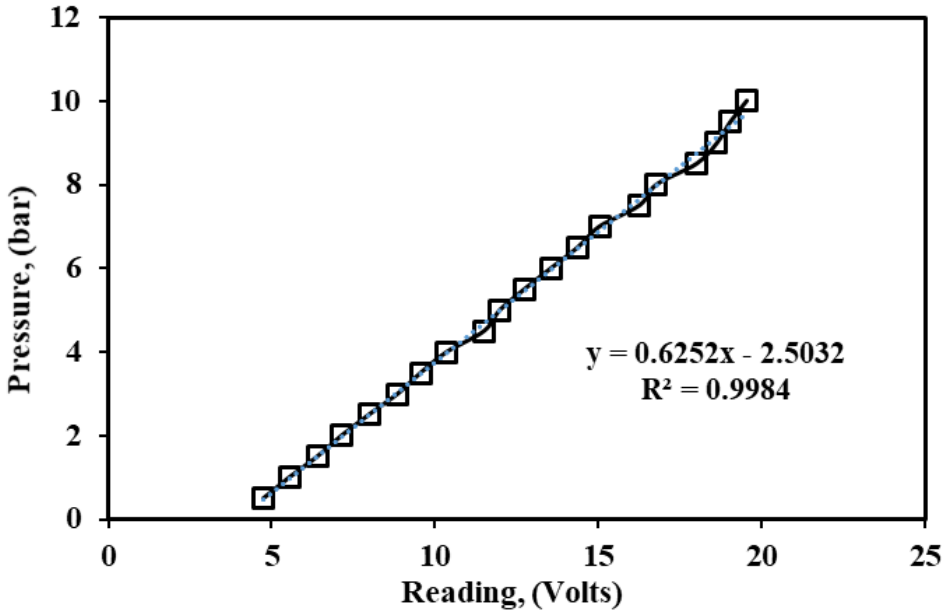

Fig. III.1 Calibration curve for pressure sensors

Appendix-IV

Calibration of Thermocouple

The K-type thermocouples are connected to the data acquisition (DAQ) system for displaying temperature. Before starting the experiments, the thermocouples are calibrated to minimize the error associated concerning the standard temperature readings obtained in a variable temperature water bath. The end of the thermocouple is immersed in the water bath and the temperature is varied in regular intervals of 5^0C while the other end of the thermocouple is connected to the data acquisition system. The reading obtained from the water bath and the readings from the data acquisition system are recorded and plotted for calibration. The calibration curve is presented below.

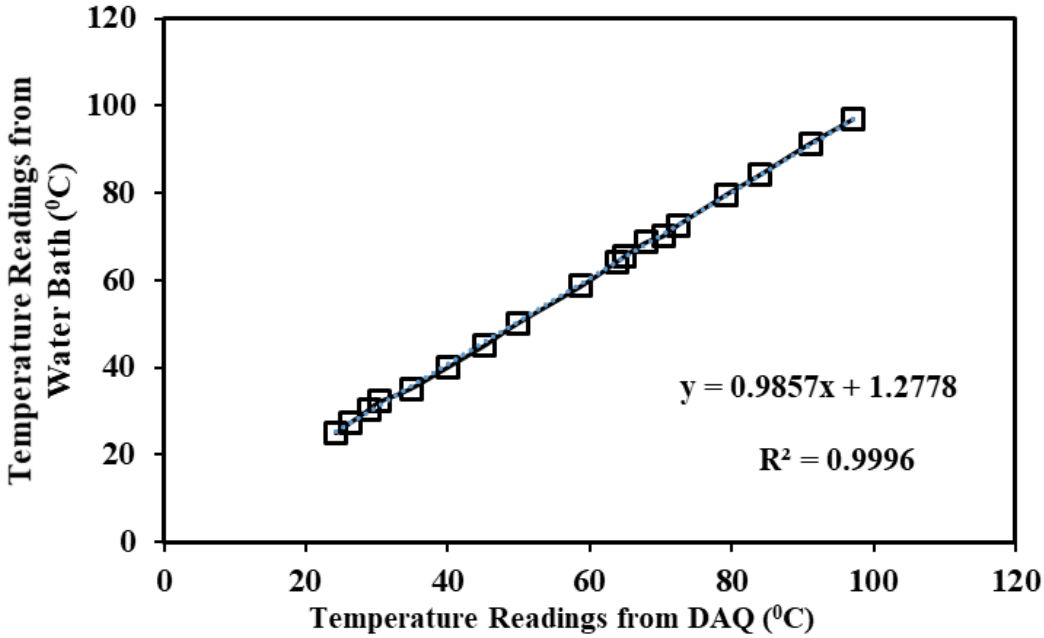

Fig. IV.1 Calibration curve for temperature readings

Appendix-V

List of Equipment/Instrument Used

List of the instrument used

- ✓ Data acquisition system: Agilent 34970A (Data acquisition switch unit with multiplexer)
- ✓ Twin Lobe Blower: Capacity-1275 M3/HP, pressure - 2000 MMWC, speed - 1300 rpm, motor for blower - 3 phase induction motor, 20 HP, 1400 rpm, 28.5 amp (Model:710)
- ✓ Compressor: Capacity - 225 liters, Maximum working pressure - 12.30 kg/cm^2, run by a 3 hp motor (manufacture by Ingersoll Rand (IR), Model: S-01480)
- ✓ Weighing balance: measuring range: max-15 kg, min-0.04 kg, error - 2 gm (Model: SP/p1s-15-FLP, manufactured by M/s. Shyaam Switchgears Pvt. Ltd.)
- ✓ Auto transformer (Make: VARIVOLT (0-270 V), 6 amp and 15 amp)
- ✓ Pressure guage (Make: Swagelok, Model: EN837-1)
- ✓ Pressure regulator (Make: Swagelok)
- ✓ Sieve machine for particle size measurement (manufactured by M/s. Scientific Engineering Corporation)
- ✓ Stopwatch, Ball valve, Gate valve, Butterfly valve, Flow control valve, Bye pass valve, Air control valve
- ✓ Water-tube manometer board – In-house fabrication
- ✓ Installation of Orifice plate with U-tube water-filled manometer - In-house fabrication
- ✓ Thermocouple sensor [Chromel-Alumel (K-type)]
- ✓ Non-contact type thermometer (infrared)
- ✓ Thermocouple calibrator with a constant temperature bath (Make: Julabo).
- ✓ Compressed air flowmeter: Make Testo. (Model: TESTO 6441) range 0.25 to 75 Nm^3/h, Accuracy ± 3% of measured value, ± 0.3% of final value.
- ✓ DC voltage supply: Model: Beetek-3005, Output voltage range: 0 to 30V, 5A.
- ✓ Gas Chromatograph (GC), (Model No.: CP-3800; Make: M/s Varian, Netherland)

Appendix-VI

Measurement of Mean Particle Size of Coal

To investigate the mean particle size the following procedure proposed by Kunii and Levenspiel (1991) is followed with the following assumptions

(1) The volume of the particles remains constant

(2) The surface area of the particles remains constant

Let there be:

n_1 : Particles of diameter d_1

n_2 : Particles of diameter d_2

n_3 : Particles of diameter d_3

and so on.

By using assumption no.1:

$$N \times \frac{\pi \bar{d}_p^3}{6} = n_1 \times \frac{\pi d_1^3}{6} + n_2 \times \frac{\pi d_2^3}{6} + n_3 \times \frac{\pi d_3^3}{6} + \ldots \quad \text{(VI.1)}$$

where N is the number of replaced, uniformly sized particles of diameters $\bar{d}_p$.

$$N \times \bar{d}_p^3 = n_1 \times d_1^3 + n_2 \times d_2^3 + n_3 \times d_3^3 + \ldots \quad \text{(VI.2)}$$

By using assumption no.2:

$$N \times \pi \bar{d}_p^2 = n_1 \times \pi d_1^2 + n_2 \times \pi d_2^2 + n_3 \times \pi d_3^2 + \ldots$$

$$\text{or, } N \times \bar{d}_p^2 = n_1 \times d_1^2 + n_2 \times d_2^2 + n_3 \times d_3^2 + \ldots \quad \text{(VI.3)}$$

Let X_1 be the weight fraction of the solids of diameter d_1

$$\text{Therefore, } X_1 = \frac{\frac{n_1 \times \bar{d}_1^3}{6} \times \rho_s}{\frac{N \times \bar{d}_p^3}{6} \times \rho_s} = \frac{n_1 \times d_1^3}{N \times \bar{d}_p^3} \quad \text{(VI.4)}$$

where ρ_s represents the density of coal

$$\text{Similarly, } X_1 = \frac{\frac{n_2 \times \bar{d}_2^3}{6} \times \rho_s}{\frac{N \times \bar{d}_p^3}{6} \times \rho_s} = \frac{n_2 \times d_2^3}{N \times \bar{d}_p^3}$$

Hence, $n_1 \times d_1^2 = X_1 \times N \times \bar{d}_p^3 / d_1$ and $n_2 \times d_2^2 = X_2 \times N \times \bar{d}_p^3 / d_2$

$$N \times \bar{d}_p^2 = n_1 \times d_1^2 + n_2 \times d_2^2 + n_3 \times d_3^2 + \ldots$$
$$= X_1 \times N \times \bar{d}_p^3 / d_1 + X_2 \times N \times \bar{d}_p^3 / d_2 + X_3 \times N \times \bar{d}_p^3 / d_3$$

$$\text{or, } \frac{1}{\bar{d}_p} = \frac{X_1}{d_1} + \frac{X_2}{d_2} + \frac{X_3}{d_3} + \ldots$$

$$\text{or, } \frac{1}{\bar{d}_p} = \sum \frac{X_i}{d_i}$$

$$\text{or, } \bar{d}_p = \frac{1}{\sum \frac{X_i}{d_i}} \qquad \text{(VI.5)}$$

Table-VI.1 Particle size measurement

Mesh (BSS)	Mean particle Size (d_i), μm	Weight in grams	Weight fraction $\left(X_i = \frac{W_i}{W}\right)$	X_i / d_i
18-22	751.3	256	0.307	3.7×10^{-4}
22-25	626.05	302	0.215	2.8×10^{-4}
25-30	510.18	95	0.087	1.4×10^{-4}
30-36	573.73	147	0.130	2.7×10^{-4}
36-44	376.07	64	0.071	2.1×10^{-4}
44-52	353.57	32	0.011	3.6×10^{-4}
52-60	234.08	47	0.035	1.7×10^{-4}
60-72	196.69	63	0.061	3.6×10^{-4}
72-Pan	174.8	78	0.060	3.2×10^{-4}

Hence, the mean particle size calculated based on the Eq. (VI.5) is found to be 300 μm.

Appendix-VII

Uncertainty Analysis

For overall uncertainty measurement consider the following quantities:

- Orifice : ± 0.5 mm
- Manometer : ± 0.2 mm
- Temperature : ± 0.5 °C
- Distributor plate : ± 0.6 % opening area
- Center to center pressure tappings: 1 mm (error)
- Pressure gauge error: ± 0.5
- Loss of inventory: ± 1 gm
- Error in calculating recirculation: ± 1 mm
- Visual Error : ± 0.5
- Bulk temperature calculation: ± 1°C
- Thermocouple temperature measurement error: ± 0.5 °C

Uncertainty in calculating suspension density

The experimental uncertainty is determined for suspension density by considering all the parameters. The parameters affect the suspension density are bed voidage and density of both air and sawdust. While calculating bed voidage the error during the measurement of pressure drop via pressure sensor also taken into consideration.

The overall uncertainty is calculated for suspension density for these set of experiments. The calculation is carried out as per the equations (1-6).

ρ_{sus} = suspension density in kg/m^3
ε = bed voidage
ρ_g = density of air in kg/m^3
ρ_s = density of solid in kg/m^3
L_m = distance between to pressure tappings
Δh = difference in pressure readings between two consecutive pressure tapping in bar

$$\rho_{sus} = \varepsilon.\rho_g + (1-\varepsilon)\rho_s \qquad \text{(VII.1)}$$

$$\varepsilon = 1 - \frac{10\Delta h}{\rho_s \times L_m} \times 1019.72 \tag{VII.2}$$

$$\rho_{sus} = \left(1 - \frac{10\Delta h}{\rho_s \times L_m} \times 1019.72\right) \times \rho_g + \left(\frac{10\Delta h}{\rho_s \times L_m} \times 1019.72\right) \rho_s \tag{VII.3}$$

$$\rho_{sus} = \rho_g - \frac{10 \times \Delta h \times \rho_g}{\rho_s \times L_m} \times 1019.72 + \frac{10\Delta h}{L_m} \times 1019.72 \tag{VII.4}$$

$$\rho_{sus} = f\left(\Delta h, \rho_s\right) \tag{VII.5}$$

$$\rho_{sus\_overall\,unceraanity} = \left[\left(\frac{\partial \rho_{sus}}{\partial(\Delta h)}\right)^2 (\Delta h)^2 + \left(\frac{\partial \rho_{sus}}{\partial \rho_s}\right)^2 (\Delta \rho_s)^2\right]^{1/2} \tag{VII.6}$$

The overall uncertainty in calculating suspension density is expressed as $\pm 3.25\%$.

Uncertainty in calculating solid circulation rate (G_s in kg m^{-2}s^{-1})

Individual uncertainties are:

$$\rho_s = 1350 \pm 5 \text{ kg}$$

$$L_a = 0.135 \pm 0.002 \text{ m}$$

$$d_D = 0.50 \pm 0.002 \text{ m}$$

$$d_B = 0.10 \pm 0.005 \text{ m}$$

$$t = 30 \pm 0.2 \text{ s}$$

Solid circulation rate is calculated by using the following expression,

$$G_s = \frac{\rho_s \times L_a \times A_D \times \left(1 - \varepsilon_{mf}\right)}{A_B \times t} \tag{VII.7}$$

or,

$$G_s = \frac{\rho_s \times L_a \times d_D^2 \times \left(1 - \varepsilon_{mf}\right)}{d_B^2 \times t} \tag{VII.8}$$

Differentiating the above equation with respect to ρ_s, L_a, d_D, d_B, and t, we have,

$$\frac{\partial G_s}{\partial \rho_s} = \frac{L_a \times d_D^2 \times \left(1 - \varepsilon_{mf}\right)}{d_B^2 \times t} \tag{VII.9}$$

$$\frac{\partial G_s}{\partial L_a} = \frac{\rho_s \times d_D^2 \times \left(1-\varepsilon_{mf}\right)}{d_B^2 \times t} \tag{VII.10}$$

$$\frac{\partial G_s}{\partial d_D} = \frac{2 \times \rho_s \times L_a \times d_D \times \left(1-\varepsilon_{mf}\right)}{d_B^2 \times t} \tag{VII.11}$$

$$\frac{\partial G_s}{\partial d_B} = -\frac{2 \times \rho_s \times L_a \times d_D^2 \times \left(1-\varepsilon_{mf}\right)}{d_B^3 \times t} \tag{VII.12}$$

$$\frac{\partial G_s}{\partial t} = -\frac{\rho_s \times L_a \times d_D^2 \times \left(1-\varepsilon_{mf}\right)}{d_B^2 \times t^2} \tag{VII.13}$$

The overall uncertainty in calculating solid circulation rate is expressed as,

$$U_{G_s} = \sqrt{\left(\frac{\partial G_s}{\partial \rho_s}\right)^2 \times (\Delta \rho_s)^2 + \left(\frac{\partial G_s}{\partial L_a}\right)^2 \times (\Delta L_a)^2 + \left(\frac{\partial G_s}{\partial d_D}\right)^2 \times (\Delta d_D)^2 + \left(\frac{\partial G_s}{\partial d_B}\right)^2 \times (\Delta d_B)^2 + \left(\frac{\partial G_s}{\partial t}\right)^2 \times (\Delta t)^2} = 0.0532 \tag{VII.14}$$

Overall Uncertainty is ± 5.32% (VII.15)

Relative error associated with individual variables.

Table: VII.1 Relative error

Independent variable	Relative errors
Diameter	1%
Temperature	1%
Velocity	3%
Pressure	2%
Density	1%
Gas chromatography	1%
Ultimate analysis	0.5%
Proximate analysis	2%
Heating value	0.5%
Mass flow rate of air	1%

List of Publications

Journals:

1. **Mahapatro, A**. and Mahanta, P., 2019. Gasification studies of low-grade Indian coal and biomass in a lab-scale pressurized circulating fluidized bed. Renewable Energy, Article in Press).
2. **Mahapatro, A.,** Mahanta, P. and Jana, K., 2019. Hydrodynamic study of low-grade Indian coal and sawdust as bed inventory in a pressurized circulating fluidized bed. Energy, p.116234.

Conferences:

1. **Mahapatro, A**., Kumar, A., Mahanta, P., 2019. Gasification studies of sugarcane bagasse in a pressurized circulating fluidized bed. 2nd International Mechanical Engineering Congress, November 29 – December 01, NIT-Tiruchirappalli, India.
2. **Mahapatro, A**. and Mahanta, P., 2019, Hydrodynamic and gasification studies of sawdust in a pressurized circulating fluidized bed, 5th International Symposium on Hydrogen Energy, Renewable Energy and Materials. (HEREM-2019), June 13-15, Bangkok, Thailand.
3. **Mahapatro, A**. and Mahanta, P., 2018, "Effect of distributor plate design on the hydrodynamics of a pressurized circulating fluidized," International Conference on Sustainable Energy and Environment Sensing (SEES-2018), June 18–19, Fitzwilliam College, University of Cambridge, Cambridge City, United Kingdom.
4. **Mahapatro, A**. and Mahanta, P., 2017, "Numerical investigation of hydrodynamics and heat transfer in a pressurized circulating fluidized bed," 12th International Conference on Fluidized Bed Technology (CFB-12), May 23-26, Krakow, Poland.